Unraveling Insulin Transport Across the Brain Endothelium

Sarah Marie Gray

Delton, MI

Masters of Science in Biological and Physical Sciences, University of Virginia, Charlottesville, VA

Masters of Science in Animal Science, The Pennsylvania State University, University Park, PA

Bachelors of Science in Animal Science, Michigan State University, East Lansing, MI

A Dissertation Presented to the Graduate Faculty of the University of Virginia in Candidacy for the Degree of Doctor of Philosophy

Department of Pharmacology

University of Virginia

May 2017

Eugene J. Barrett, M.D., Ph.D.
Michael M. Scott, Ph.D.
Norbert Leitinger, Ph.D.
Patrice G. Guyenet, Ph.D.
Richard J. Price, Ph.D.

ABSTRACT

Insulin acts on the brain and is transported across the blood-brain barrier (BBB). This route is the primary pathway for insulin's entry into the brain as opposed to entry via CSF circulation. However, little is known regarding how circulating insulin crosses the BBB's highly-restrictive brain endothelial cell (BEC). Here, the mechanisms regulating BEC insulin uptake, signaling, and BBB transcytosis and how transport is affected by high-fat diet (HFD) feeding and astrocyte activity was examined. At physiologic insulin concentrations, blocking the insulin receptor (IR)—not the IGF-1 receptor—inhibited BEC insulin uptake and downstream insulin signaling. Inhibiting lipid raft endocytosis inhibited insulin uptake while blocking the insulin signaling to PI3-kinase or MEK had no effect. Isolated BECs (iBECs) from rats fed four wk of HFD had decreased insulin uptake and increased NFκB nuclear binding activity compared to iBECs from rats a normal chow diet (ND). Insulin-stimulated Akt and MEK phosphorylation, IR expression, and insulin degrading enzyme expression were comparable in HFD and ND iBECs. Using an *in vitro* BBB with co-cultured astrocytes and iBECs, insulin was found to be intact following BEC transcytosis and stimulating astrocytes with L-glutamate increased and L-NAME decreased insulin transcytosis. Thapsigargin treatment of astrocytes increased insulin transcytosis, suggesting that L-glutamate increases were mediated by increased cytosolic calcium in the astrocyte. In aggregate, this dissertation provides evidence for IR-specific, vesicle-mediated transport of intact insulin across the BEC. The effects of HFD feeding, nitric oxide inhibition, and astrocyte simulation suggest unique regulatory mechanisms govern BEC insulin uptake and transcytosis.

ACKNOWLEDGEMENTS

I would like to express my utmost gratitude to everyone involved in the completion of this dissertation. I consider myself incredibly lucky to have conducted my graduate work at the University of Virginia.

I am immensely grateful for my adviser, Dr. Gene Barrett. I am thankful that he agreed to accept a graduate student on her last rotation with very minimal experience in molecular biology. Under his guidance, I gained exposure to multiple techniques that allowed me to thoroughly pursue the work described in this dissertation. When things did not work, he calmly and confidently encouraged me to continue asking scientific questions, which in turn gave me confidence that, eventually, things would work. He gave me the freedom to pursue my interests, both in regard to my project and professional development. My experimental ideas were met with thoughtful discussion and heartened support, which improved the project and my scientific aptitude immensely. Early on, he encouraged me to write in a variety of settings and under his guidance, I've vastly improved my abilities as an academic writer. Moreover, he allowed me to travel extensively to conferences large and small to present this project and gain valuable feedback. I am thankful for his mentorship, appreciate my time as a graduate student in his laboratory, and believe he has fully prepared my future scientific endeavors.

I am forever indebted to Kevin Aylor, who kindly took me under his wing and patiently taught me so many laboratory techniques. Without him, I would have been completely lost. He has been incredibly valuable for bouncing ideas off of and has provided me with countless helpful suggestions. I am thankful for his friendship and advice. Dr. Zhenqi Liu has been a critical component of our laboratory meetings and has

given thoughtful criticism on this project from the beginning. I've greatly appreciated his comments and insight over the past few years. I've had the privilege with numerous researchers in the lab. Dr. Rick Meijer worked on components of this project and his enthusiasm, scientific knowledge, and friendship were instrumental for my time at UVA. Drs. Lina Zhao, April Fu, and Yvo Kusters have provided me with company and guidance in the lab and their comradery has made this journey a pleasant one. Dr. Mike Scott has been a great support of my work at UVA, from teaching me more about neuroscience to assisting with my fellowship applications to giving me advice on pursuing a postdoctoral position. Additionally, his support for my research and advice for pursuing key experiments was incredibly helpful for moving my work forward.

I would also like to thank my committee members, Drs. Patrice Guyenet, Norbert Leitinger, and Rich Price for their support over the years. They have diligently listened to my scientific progress and provided me with considerate, constructive evaluations that have vastly improved my research project. My time on the Cardiovascular Research Training Grant was instrumental for helping me improve as a researcher on many levels—here, I learned how to present and discuss my work and gained exposure to excellent research. My experiences with the Metabolism Interest Group and the DERC Research in Progress also provided me with great feedback and a collegial environment. Dr. Susanna Keller has been a wonderful support—both scientifically and personally—and I am very grateful to have had the opportunity to work with her. I also want to thank Drs. Chien Li and Craig Nunemaker, who chaperoned my early rotations and taught me a great deal about molecular biology. I would also like to extend my appreciation to Drs. Paula Barrett and Thurl Harris for their work as directors of the pharmacology graduate

program. Additionally, the Department of Pharmacology and the Division of Endocrinology have provided institutional support for my work and I am very grateful for this. I was very fortunate to receive fellowships from the AHA and NIDDK and I am very grateful for the donations and taxpayer dollars that have supported my research.

I must also pay tribute to Dr. Michael Thorner, who was instrumental in my selecting UVA for graduate school and his perpetual support was key for keeping me here. His indomitable enthusiasm for science and relentless curiosity have been inspiring and his constant reminders that "If it were easy, it would have already been done," gave me faith during my times of struggle. I sought him out when I was finishing my MS degree and, much to my delight, he has been an active participant in my graduate work at UVA. He's offered helpful guidance throughout the pursuit of my PhD and as well as in my post-graduate school endeavors. I am so fortunate to have been able to work with him and have his support—words can't express my gratitude.

I am so thankful for my friends that have supported me throughout graduate school. I would like to acknowledge my wonderful friends from afar, especially Heather, Anna, and Laura. I am grateful for the friendship of numerous individuals here in Charlottesville—especially Laura, Kelley, Becky, Lauren, Ethan, Peter, as well as my kickball teammates and running partners over the years. Shashanka Murthy has been a steadfast supporter of me for as long as I've known him and I'm incredibly lucky to have him in my life.

Lastly, I would like to thank my family for their love and boundless support of my enterprises. No matter where I land—from Kuala Lumpur to Charlottesville—they enthusiastically encourage my pursuits and I am eternally grateful.

TABLE OF CONTENTS

LIST OF FIGURES

LIST OF TABLES

ABBREVIATIONS

AgRP	Agouti-related protein
AQP	Aquaporin
BBB	Blood–brain barrier
BEC	Brain endothelial cell
BISF	Brain interstitial fluid
CNS	Central nervous system
CPT-cAMP	8-(4-Chlorophenylthio)adenosine 3',5'-cyclic monophosphate
CSF	Cerebrospinal fluid
CVO	Circumventricular organs
DPM	Disintegrations per minute
EET	Epoxyeicosatrienoic acids
eNOS	Endothelial nitric oxide synthase
ERK	Extracellular signal-regulated kinase
F12	Ham's F12 medium
GCM	Glial culture medium
GFAP	Glial fibrillary acidic protein
hBEC	Human brain endothelial cell
HD	Heat-denatured
HFD	High-fat diet
iBEC	Isolated brain endothelial cell
ICV	Intracerebroventricular
IDE	Insulin degrading enzyme
IGF-1	Insulin-like growth factor 1
IR	Insulin receptor
IR-β	Insulin receptor, β subunit
L-NAME	N^{ω}-nitro-L-arginine methyl ester
LRP	Low density lipoprotein-related protein

MβCD	Methyl-β-cyclodextrin
MEK	Mitogen-activated protein kinase kinase/extracellular signal-related kinase
Mfsd2a	Major facilitator superfamily domain-containing protein 2
ND	Normal chow diet
NOS	Nitric oxide synthase
NSB	Non-specific binding
PI3K	Phosphoinositide-3-kinase
PGE_2	Prostaglandin E_2
POMC	Pro-opiomelanocortin
RBMVEC	Rat brain microvascular endothelial cell
RFU	Relative fluorescence units
RIA	Radioimmunoassay
SEM	Standard error of the mean
TEER	Transendothelial electrical resistance
VRS	Virchow–Robin space

CHAPTER 1 INTRODUCTION

1.1 Introduction and rationale

Insulin is secreted by the pancreas and is a key hormone for regulating blood glucose concentrations. In skeletal muscle and adipose tissue, insulin has direct effects to stimulate nutrient (e.g., glucose) storage. In the brain, insulin does not stimulate nutrient storage. Here, insulin affects numerous processes, including feeding behavior, hepatic metabolism, body weight and cognition, which are increasingly appreciated in health and in disease. However, there is no clear understanding of how circulating insulin crosses the restrictive blood-brain barrier (BBB) to reach neuronal tissue where it may exert its effects in the central nervous system (CNS).

The vasculature facilitates the delivery of substances in blood to every tissue in the body. For circulating insulin to reach tissues, it must first cross the vascular endothelium, the cellular layer that lines blood vessels, which has different characteristics in different body tissues. For example, the liver endothelium is fenestrated and discontinuous, allowing easy movement of circulating substances into the tissue. Antithetically, the brain vasculature is highly restrictive and has more regulated transendothelial transport. Muscle and adipose endothelial permeability are intermediate between the extremes of the liver and the brain. Mechanistic regulation of insulin transport across muscle and adipose vasculature has been studied and insulin resistance

and type 2 diabetes each delay insulin movement from blood to these tissues, rending the tissue less efficient at responding to insulin and storing nutrients.

There is a paucity of knowledge regarding insulin's physiological role in the brain and the mechanism(s) by which insulin produced by the pancreas crosses the restrictive vasculature of the BBB and whether these processes are affected by insulin resistance. By investigating the mechanisms by which insulin is transported across the BBB endothelium, how insulin enters the brain interstitial fluid (BISF), i.e., the pool through which insulin exerts its neuroregulatory properties in the brain, will be understood.

This literature review will first present the potential pathways for insulin entry into the brain by comparing cerebrospinal fluid (CSF) secretion and the vascular structure of the BBB. Then, insulin's various actions in the brain will be reviewed, along with the reported effects of high-fat diet (HFD) feeding and insulin resistance on insulin action in the brain. Finally, the most recent understanding of insulin transport into the brain will be discussed as a foundation for the studies that will be presented in this dissertation.

1.2 Pathways for insulin entry: fluid circulation in the brain

Blood borne chemicals enter the BISF by crossing the fenestrated endothelium and subsequent epithelium of the choroid plexuses to enter CSF circulation, or by crossing the endothelium of the BBB, or a combination of both. A considerable amount of what is known regarding fluid and solute movement in the brain is based in early studies, which were sometimes based in small sample number and limited technical approaches. Improved methods and models have advanced our understanding of CSF

and BISF movement in the brain and throughout its barriers; however, much remains to be studied and the work to date still relies on complex methodology and, may be complicated by interspecies variability in structure and function.

1.2.1 Blood—CSF barrier

Cerebrospinal fluid serves a variety of functions, from providing buoyancy for the brain within the skull to transporting nutrients throughout the brain to clearing waste. Its composition is similar to plasma except it has lower protein concentration[1]. Biological sampling of the CSF is often used as a surrogate for the BISF that bathes the neuronal tissue. Cerebrospinal fluid can flow into the BISF; however, as will be described below, they are not identical. This section will discuss movement of blood-borne substances into CSF secretion in the cerebral ventricles and flow of CSF throughout the brain.

1.2.1.1 Choroid plexus secretion of CSF

Cerebrospinal fluid is predominantly produced in the highly-vascularized choroid plexuses of the lateral, third, and fourth ventricles. Blood-borne substances can cross the fenestrated capillaries of the choroid plexus more easily than crossing the blood-brain barrier endothelium[2,3] and blood flow through the choroid plexus is considerably higher than that of the brain when normalized to tissue mass[4,5]. Within the villi of the choroid plexus, blood-borne substances and water move across the fenestrated endothelium and are then transported across the choroid plexus epithelial cell and secreted to form CSF within the ventricle[6] (Figure 1-1). In humans, the rate of CSF secretion is calculated at

0.37 ml/min[7], daily production at 500-600 ml/d, and total volume ranges from 90-150 ml[8,9]. Despite interspecies differences in CSF volume, secretion rate (mL/min) is approximately 0.5% of total CSF volume[4]. Water and electrolytes are actively transported from blood into the ventricle through various transporters and aquaporins (AQP) and fluxes of these substances drive the regulated secretion of CSF[1,10,11].

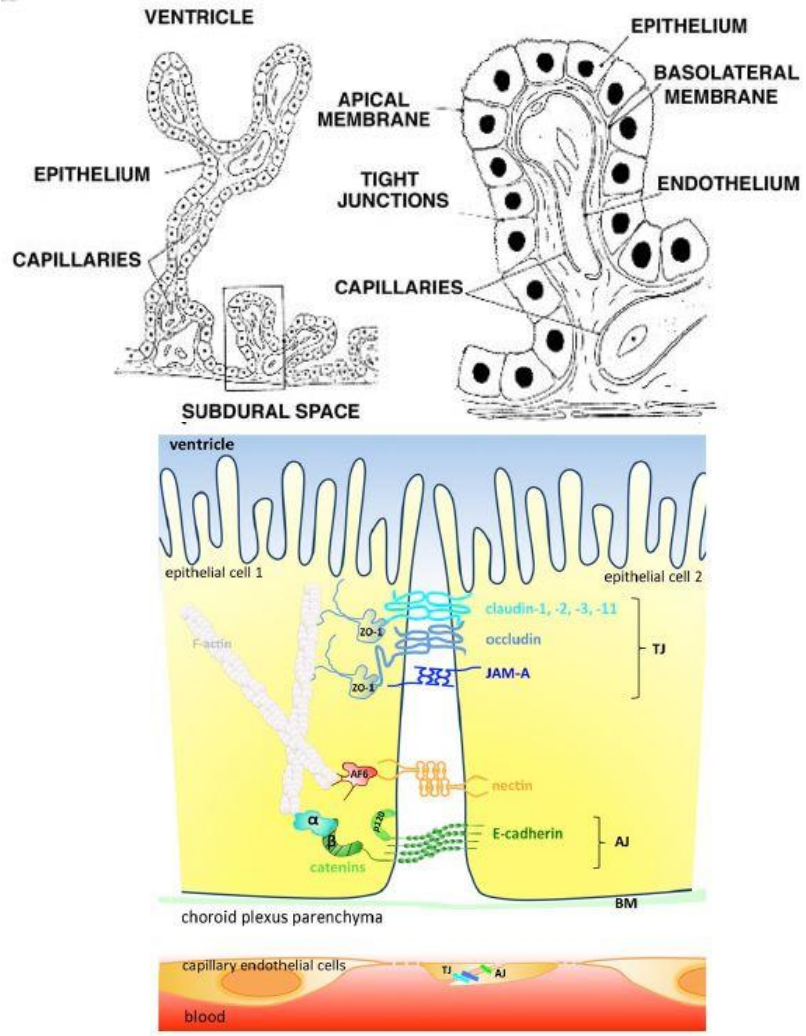

Figure 1-1 Blood-CSF barrier in the choroid plexus

Choroid plexus villi line the ventricle, with fenestrated capillaries allowing the flow of nutrients (upper left panel). Increased magnification (upper right panel) depicts structure of the villus. The blood-CSF barrier consists of a fenestrated capillary and secretion of CSF occurs from cuboidal epithelial cells with tight junctions (TJ) and adherens junctions (AJ) (lower panel). Active transport at both the basolateral and apical membranes of the cuboidal epithelial cells allows for the movement of blood-borne substances into the CSF within the ventricle. Image from Brown et al.[1] and Tietz and Engelhardt[12].

1.2.1.2 Protein secretion into CSF

Despite the lower protein concentrations in CSF compared to blood, select proteins and peptides are actively transported across the blood-CSF barrier and into CSF. Albumin and IgG are transported into CSF, though the mechanism by which these occur remains under debate[13-15]. Iron transport from plasma to the brain can occur across the blood-CSF barrier, with or without transferrin[16]. Circulating insulin-like growth factor-1 (IGF-1) can enter the brain through CSF[17,18]. Leptin is also transported across the choroid plexus and into CSF in a receptor-dependent manner[19,20]. The transport of these proteins is generally reported to be receptor-dependent, though low density lipoprotein-related proteins (LRP)-1 and -2 also contribute to IGF-1 and leptin transport into CSF, respectively[21,22]. To date, there is no evidence that LRP-1 or -2 facilitate insulin transport into the brain; however, LRP-2 (also known as megalin) has been implicated in insulin reabsorption in proximal tubules in the kidney[23]. Iron, leptin, and IGF-1 are also transported across the BBB, although at different rates[16-18,20], suggesting that peptide transport across the blood-CSF barrier and BBB may occur through different mechanisms.

1.2.1.3 Flow of secreted CSF

The routes and regulation of CSF flow have been investigated for nearly 100 years[24]. While this field has evolved considerably, much remains to be explored. Understanding of the CSF circulation continues to improve as imaging techniques and animal models provide more resolution.

Cerebrospinal fluid made by the choroid plexuses in ventricles flows from the lateral to the third and fourth ventricles before reaching the subarachnoid space (Figure 1-2). In vivo imaging with fluorescent tracers has elucidated the paravascular flow of cisternal CSF alongside penetrating arteries throughout the brain[25-28](Figure 1-3). At the penetrating arteries and arterioles, CSF flows parallel to the blood vessel in a perivascular space known as the Virchow-Robin space (VRS). At the capillary, the VRS becomes filled by basement membrane[29-32], though the terminology does not always reflect this, i.e. some sources report the VRS as present at the level of the capillary while others term this the perivascular space.

Obstacles for CSF flow alongside penetrating arteries and arterioles may exist. Some studies suggest that subarachnoid CSF must cross a pial sheath, which serves as a sieve, to gain entry to the perivascular/VR space of penetrating arteries in the cortex[31,32]. Pial sheaths lining the penetrating arteries were reported in human brain tissue. This cell layer became increasingly fenestrated in the penetrating arterioles and ultimately disappeared at the capillary[29]. However, pial sheaths have not been detected in rodents[25,32], which may be reflective of improved imaging techniques or species variations. It is not clear whether pial sheaths are of physiological importance; however, if present, they may provide additional regulation to CSF flow throughout the brain.

Regardless of the debate surrounding CSF flow, these studies have collectively made it clear that CSF is a distinct pool, different from the BISF that bathes neuronal tissue. Substances that cross the brain endothelium mix with paravascular CSF in the VR/perivascular space and components of this admixture may cross the astrocyte endfeet to reach the BISF.

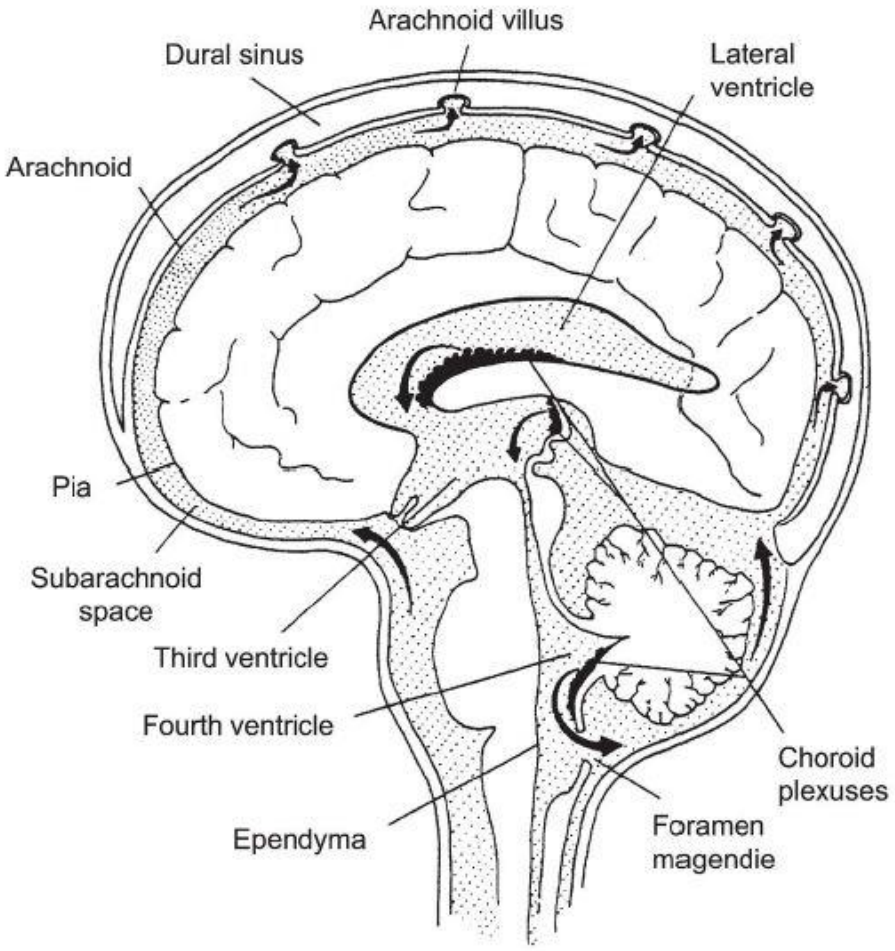

Figure 1-2 Cerebrospinal fluid flow through the ventricles and subarachnoid space

CSF is secreted from the choroid plexuses (black structures) in the lateral, third, and fourth ventricles. CSF flows from the lateral to the third and fourth ventricles. After leaving the fourth ventricle, CSF gains access to the subarachnoid space. Human brain is depicted above, image from Brown et al.[1]

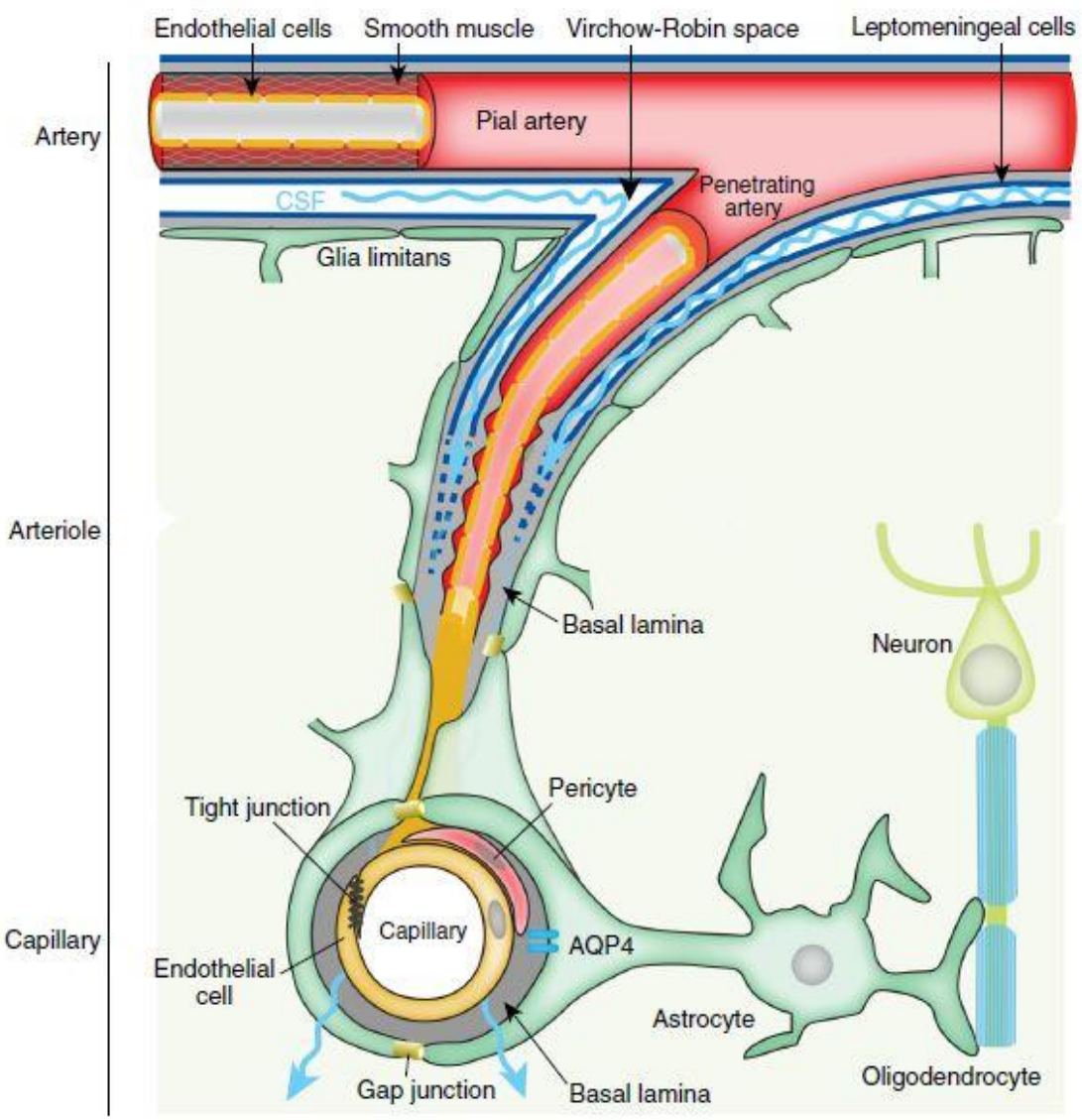

Figure 1-3 Cerebrospinal fluid flows parallel to blood vessels

CSF flows parallel to the pial arteries and continues to flow along penetrating arterioles and capillaries within the brain. Blood-borne substances that cross the brain endothelial cell can mix with CSF in the perivascular space before crossing the astrocyte endfeet and reaching the brain interstitial fluid. Image from Jessen et al.[28]

1.2.2 Blood—brain barrier

As discussed previously, CSF may mix with substances crossing the brain endothelium before ultimately reaching the BISF. To cross the BBB, substances must transit across the brain endothelium, pericytes, and subsequently astrocytic endfeet to reach BISF. This BBB transport can either complement entry via CSF secretion or provide an alternative pathway to reach BISF. Given the rate of CSF secretion, transport across the BBB provides a quicker way for blood-borne substances to reach the BISF.

The BBB consists of numerous barriers that restrict entry of substances in to the brain. At the forefront of this barrier is the brain endothelial cell (BEC), the abluminal side of which is covered partly (~30%) by pericytes. Beyond the pericyte is the VRS, which is surrounded by astrocyte endfeet, which cover 99% of the endothelium and pericytes (Figure 1-3, Figure 1-4). At the capillary, the VRS is synonymous with the basement membrane of the brain endothelium (Figure 1-4). Recent imaging studies estimated the distance between the endothelium and the astrocytic endfeet to be 6-8 μm at the capillary level[33]. Cellular components of the blood-brain barrier and their interplay in neurovascular coupling will be discussed.

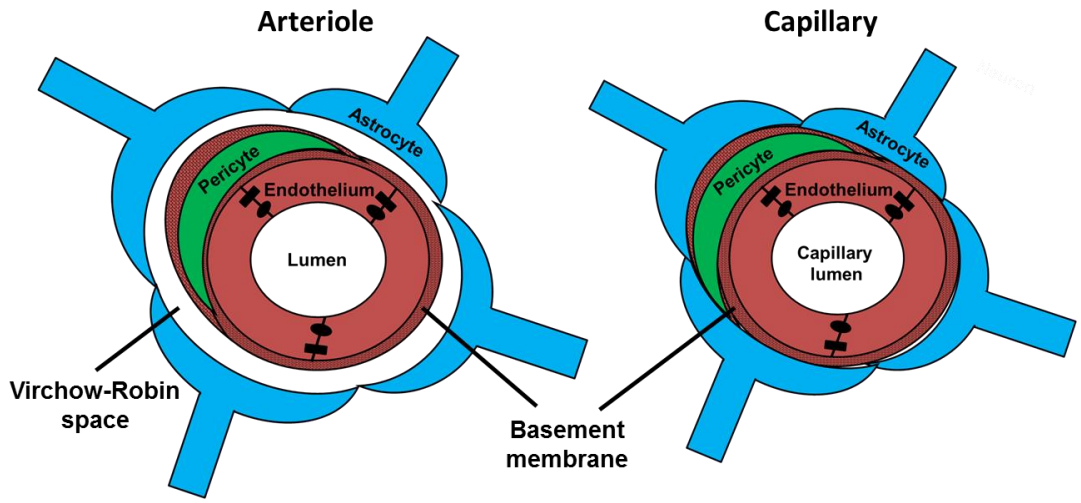

Figure 1-4 Cross section of blood—brain barrier arteriole and capillary

The brain endothelial cells have adherens junctions (rectangle) and tight junctions (ovals) creating a robust barrier. CSF flows in the VR/perivascular space along the brain arteries and arterioles and this space becomes synonymous with the basement membrane in the brain capillaries. Pericytes cover ~30% of the endothelium, with astrocytes ensheathing the blood vessel and providing the final barrier in the blood-brain barrier.

1.2.2.1 Brain endothelial cells

The BEC is the first obstacle of the BBB faced by substances in the blood. Brain endothelium is more restrictive than peripheral vasculature by virtue of its tight junctions and adherens junctions[34,35]. Trans-endothelial electrical resistance (TEER) is often reported as a measure of endothelial barrier integrity. In muscle, TEER values are approximately 30 $\Omega \times cm^2$ [36], while brain endothelium is considerably higher at >1,800 $\Omega \times cm^2$ [35]. Radio- or fluorescently-labeled tracers have also demonstrated the brain vasculature is less permeable than in the periphery.

Paracellular movement between BECs is prevented by tight and adherens junctions. Additionally, within the BEC, angulin and tricellulin are expressed at tricellular junctions to further restrict paracellular movement and maintain barrier integrity[37]. Interestingly, expression of these proteins was not detected in the choroid plexus vasculature or the circumventricular organ, consistent with the more fenestrated endothelium reported in these structures (Section 1.2.2.5). Tight junctions and adherens junctions occur between two endothelial cells, with the former located toward the vessel lumen and the latter located closer to the VR/perivascular space (Figure 1-5). Claudin-3,5, and 12; occludin; and junction adhesion molecules (JAM) A, B, and C are classified as tight junction proteins and are associated with scaffolding protein zona occludens-1 protein intracellularly. Adherens junctions are designated by VE-cadherin, which employs catenins as an intracellular scaffold[12]. Understanding of tight and adherens junction functions in the brain endothelium is limited, though they likely have a role in cell-to-cell communication, trafficking membrane proteins and/or molecules across the BEC, and intracellular signaling.

In addition to restrictive junctions, efflux pumps are highly expressed in the BEC and serve to limit entry and transport across the cell. These efflux pumps are in the ATP binding cassette (ABC) family and efficiently and effectively remove foreign substances, preventing the delivery of both harmful and therapeutic substances into the brain tissue. Thus, while offering a clear protective role, efflux pumps are an obstacle for delivering therapeutics into the brain tissue. Multiple forms of efflux pumps act at the luminal aspect of the BEC, though some are present abluminally[38]. The wide expression of these transporters and their ability to quickly increase expression in response to environmental factors is a challenge for drug delivery to the brain[39]. These pumps have been targeted to improve transport of drugs into the brain; however, the ability for some pumps to compensate for others makes this a challenging endeavor.

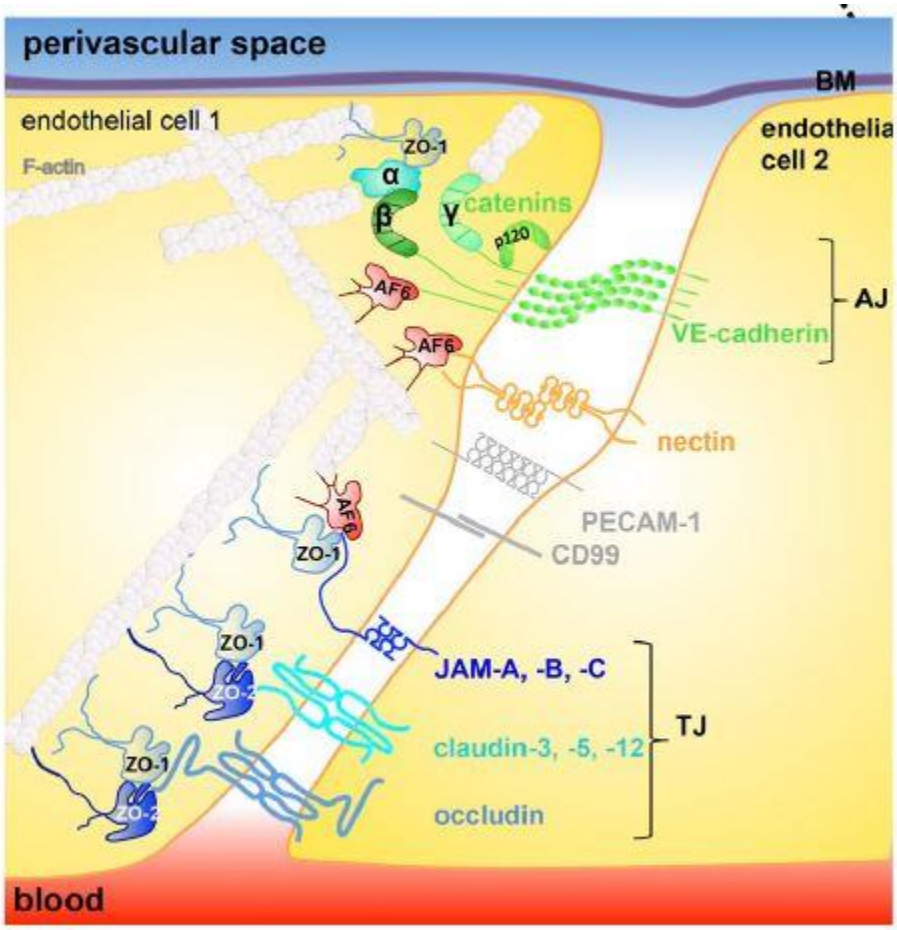

Figure 1-5 BEC intercellular junctions

Brain endothelium has tight junctions (TJ) and adherens junctions (AJ) connecting adjacent endothelial cells. This scaffolding restricts paracellular movement and may be involved in regulated cellular trafficking of substances across the BEC. Image from Tietz and Engelhardt[12].

1.2.2.2 Pericytes

Pericytes cover approximately 30% of the capillary endothelium[40] and assist with barrier integrity, support angiogenesis, and regulate blood flow[41-43]. Pericytes express similar cellular markers to smooth muscle (e.g., PDGF-β and α-smooth muscle actin) and may act in response to neurons or astrocytes to affect blood flow through the capillary. Given the lack of smooth muscle at the capillary level, pericytes may affect capillary dilation and constriction[41]. Exactly how pericytes regulate vessel diameter in the brain remains an area of active research. Pericyte morphology differs throughout the vasculature[44] and researchers have proposed that pericytes be separated into subtypes, depending on their location in the vasculature (i.e., artery, capillary, vein)[45]. This differential morphology may have implications for the pericyte's role in BBB function and improved terminology may refine our understanding of their role in the blood-brain barrier and neurovascular coupling.

In the retina, pericyte death is an early manifestation of microvascular damage during diabetes[43] and whether similar ramifications occur at the BBB is unknown. Pericyte loss is also implicated for breakdown of blood-brain barrier function and defects in neurovascular coupling and blood flow[46].

1.2.2.3 Astrocytes

Astrocyte endfeet form the lateral boundary of the BBB and encapsulate the endothelium and pericytes. Electron microscopy studies indicated that along a vessel, the endfeet of astrocytes interlock to form a tight barrier with some small clefts of ~20 nm,

which amount to ~50 nm per capillary cross section[40]. Astrocyte density varies throughout the brain vasculature, with arteries and arterioles having more astrocytic processes on the basis of length than capillaries or veins[33]. Gap junctions between astrocytes may allow for signal propagation throughout the astrocyte sheath of the vasculature. Recent work investigating the flow of CSF through the 'glymphatic' pathway demonstrates that larger tracers (either fluorescent or gadolinium) move more slowly than smaller molecules, supporting the idea that the astrocytic endfeet may regulate solute movement from the CSF to the BISF[25,47].

1.2.2.4 Neurovascular coupling

The interplay of neurons with astrocytes, pericytes, and endothelial cells to coordinate physiological processes related to the brain vasculature is known as neurovascular coupling. Neurovascular coupling has been implicated in vasodilation, vasoconstriction, and movement of substances from blood into the brain interstitial fluid. The current model for neurovascular coupling proposes a feed-forward mechanism, whereby neuronal activation increases cerebral blood flow, which then provides nutrients, such as oxygen and glucose, to the area[48].

Early investigations into neuronal metabolite utilization deduced that neuronal activation spurred glycolysis in astrocytes that released lactate, which shuttled back to neurons[49]. This suggested a major role for astrocytes during imaging fluorodeoxyglucose metabolism (via positon emission tomography) as a proxy measure for neuron metabolism. Neuronal nutrient metabolism and the lactate shuttle are still debated[50,51].

Regardless, the involvement of neurovascular coupling in moving substances from blood into neuronal tissue remains clear.

Neurovascular coupling research has focused on the interplay between neurons and astrocytes and subsequent effects on the endothelium. To date, the majority of the literature has focused on the penetrating arteries and arterioles in the brain, likely due to technical difficulties in imaging at greater depths in vivo. However, given the similarities in cell architecture at the capillaries (Figure 1-4), these smaller vessels may have a role in neurovascular coupling[33].

Glutamate is a key regulator of neurovascular coupling and is secreted from pre-synaptic neurons[52]. Glutamate can act via NMDA receptors on neurons to elicit nNOS activity and release NO, which dilates the smooth muscle cell, and act on astrocytes to influence neurovascular coupling. Astrocytes provide a barrier between the endothelium and the BISF, which bathes neurons (Figure 1-4) and their signaling may coordinate activity between these areas. In response to neurotransmitters (e.g., glutamate via metabotropic glutamate receptors), Ca^{2+} is released from the endoplasmic reticulum to increase soma calcium or enters from extracellular space via the Na+/Ca+ exchanger or TRPA1 channels in endfeet processes[53]. Calcium elevations induce the secretion of factors termed “gliotransmitters” that can act on neighboring neurons and BBB cells[53,54](Figure 1-6). These gliotransmitters may include ATP, glutamate [55-57], arachidonic acid[58], and other factors [53,59-61]. Arachidonic acid action on smooth muscle lining the endothelium causes vasoconstriction[58]. Alternatively, within the astrocyte, arachidonic acid may be converted to prostaglandin E_2 (PE_2) or epoxyeicosatrienoic acids (EET), which can cause vasodilation via smooth muscle cell relaxation[48].

While smooth muscle is necessary for neurovascular coupling at the level of the arteries and arterioles, smooth muscle is not present at the capillaries. In contrast to larger vessels, pericytes and astrocytes of the capillaries have been implicated for coordinating neuronal activity with vasodilation. Early studies examining morphology of neurons and the brain vasculature indicated that capillaries are indeed closer to neurons than arterioles[62]. Given the proximity of the pericyte to the endothelium, astrocytic endfeet, and neurons, its contractile ability and signaling capabilities could have a role in physiology and pathology[43,57]. Recent studies found that glutamate is able to dilate capillaries through the pericyte action, causing retrograde dilation in the penetrating arterioles[42]. Few studies have investigated neurovascular coupling at the capillary level and many questions remain regarding the involvement of neurons, astrocytes, and pericytes during this process.

While neurovascular coupling is generally considered to be a mechanism to increase the availability of oxygen and nutrients in active brain regions, it may have additional roles for facilitating the movement of hormones and peptides across the BBB. Neuronal activity and subsequent increased neurovascular coupling increases transport of IGF-1 across the BEC[22]. Whether this extends to other circulating hormones, including insulin, remains an outstanding question.

The interactions between cell types in the blood-brain barrier are complex and one must be cautious of attributing neurovascular coupling to a single cell type, as it is clear that neurons, astrocytes, pericytes, smooth muscle cells (at the arteriole), and endothelial cells collaboratively maintain barrier function and neurovascular coupling capabilities. It

is possible that the regulation of neurovascular coupling varies along the vasculature tree, throughout areas of the brain, and in response to various neuronal stimuli.

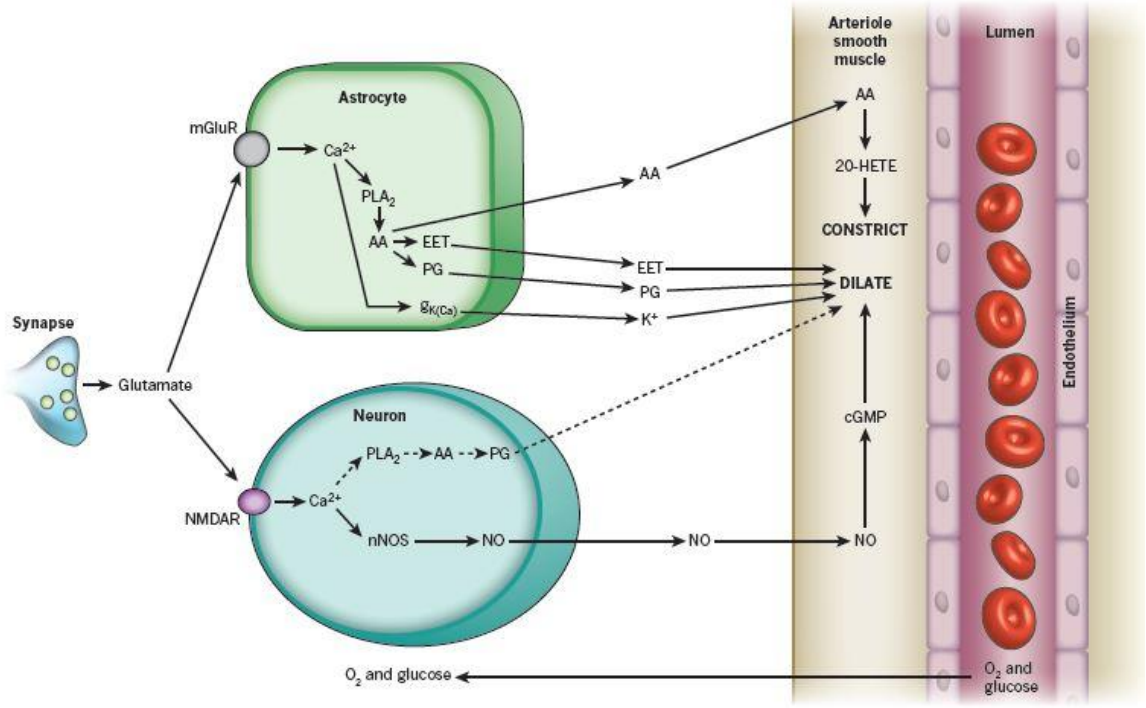

Figure 1-6 Neurovascular coupling at the arteriole

Simplified model for neurovascular coupling at the arteriole demonstrates that glutamate released from neurons can act on other neurons through NMDA receptor or on the astrocyte through metabotropic glutamate receptor (mGluR). Increased calcium (Ca^{2+}) in the neuron increases nNOS and subsequent NO release to elicit dilation. Neuronal increases in Ca^{2+} can (dotted line) increase phospholipase A_2 (PLA_2), driving production of arachidonic acid (AA) and prostaglandin (PG) to cause dilation. At the astrocyte, increases in Ca^{2+} may drive dilation through K^+ release via Ca^{2+}-gated K^+ channels or though PLA_2 increases in AA to cause release of EET and PGE_2. Astrocytes may secrete AA, which is converted to 20-hydroxy-eicosatetraenoic acid (20-HETE) in the smooth muscle, causing constriction. Whether similar pathways predominate at the capillary, where smooth muscle is absent and pericytes are present, is unknown. Image from Attwell et al.[48]

1.2.2.5 Areas with incomplete BBB

Despite the highly-restrictive qualities of the BBB, some areas of the brain have a more permissive, fenestrated BBB and allow substances to cross more freely from the blood into the BISF. These circumventricular organs (CVO) are anatomical landmarks and include the neurohypophysis, vascular organ of the lamina terminalis, subfornical organ, subcommissural organ, pineal gland, median eminence, and area postrema, line the third and fourth ventricles[63]. These various CVO are sensory organs and allow blood-borne substances to directly affect the brain tissue or secretory and release neuropeptides and hormones into the blood[63]. Early investigations into insulin transport in the brain found blood-borne radiolabeled insulin in the median eminence, arcuate nucleus, area postrema, and other CVOs[64-66].

The arcuate nucleus of the hypothalamus has fenestrated capillaries, leading some to state it qualifies as a CVO[67,68]. Insulin's anorectic role in the arcuate is well established (Section 1.3.1, 1.3.2), though exactly how it, and other hormones, reaches the arcuate from the blood is debated. Substances may reach the arcuate by 1) crossing this fenestrated capillary endothelium, entering the median eminence, then the third ventricle before gaining access to the arcuate nucleus, or 2) through a proposed route through the subependymal plexus, vasculature present between the third ventricle, median eminence, and arcuate nucleus[67,69]. Specialized hypothalamic cells, called tanycytes, form a barrier between the median eminence and the arcuate nucleus and may regulate transport of substances between blood-borne substances in the fenestrated capillaries, cerebrospinal fluid, and the brain tissue within the median eminence and arcuate nucleus of the hypothalamus[70-72] (Figure 1-7). Subsets of tanycytes (β1 and β2) possess endocytotic

machinery (caveolae and clathrin-coated pits) and have the capacity to transport fluid and hormones by receptor-mediated transport[73]. It is unknown whether tanycytes are able to transport insulin through these pathways.

Substances injected into CSF are able to enter the arcuate nucleus but not the median eminence, and intravenously-injected substances can enter the median eminence but not the arcuate nucleus[70]. These findings suggest the BBB is intact in the arcuate nucleus and fenestrated capillaries are present in the median eminence alone. Recent work has highlighted the dynamic qualities of the fenestration of the median eminence and the arcuate nucleus in response to fasting, which was mediated by hypoglycemia-induced VEGF-A expression in tanycytes[74]. During fasting, the arcuate nucleus is subjected to greater diffusion of blood-borne substances, whereas in the fed state, this diffusion is limited to the median eminence alone[74]. These studies highlight the plasticity of this system and exquisite regulation of the brain vasculature in the hypothalamus.

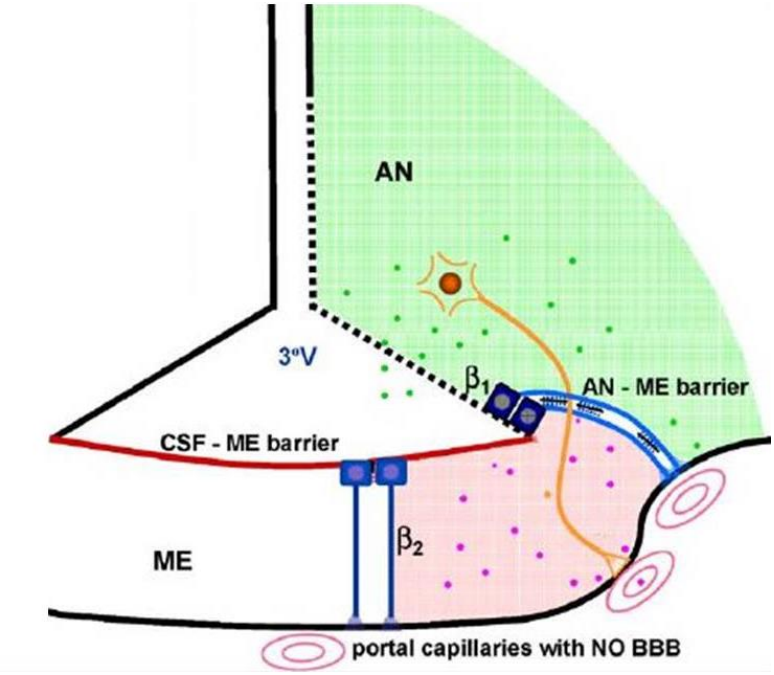

Figure 1-7 Arcuate nucleus and median eminence anatomy

The median eminence (pink, ME) of the hypothalamus has fenestrated capillaries and the arcuate nucleus (green, AN) is open to the third ventricle (dotted line). The CSF-ME barrier (red line) is composed of β_2 tanycytes, while the β_1 tanycytes form the AN-ME barrier. The differences between β_1 and β_2 tanycytes are beyond the scope of this review, but this image illustrates the blood and CSF flow in these areas of the hypothalamus. Image from Rodriguez et al.[71]

1.3 Insulin action and insulin resistance in the brain

Insulin's role in the brain differs from that in the periphery, as glucose uptake in the brain is insulin independent. Insulin receptor (IR) mRNA expression is highest in the olfactory bulb, followed by the cortex, hypothalamus, hippocampus, and cerebellum[75]. While IR protein expression has not been confirmed, insulin signaling has been implicated for numerous actions in the brain. Centrally-acting insulin may communicate short- and long-term nutrient status to, in turn, modulate metabolic processes[76]. Insulin's promotes satiety[77-79] and reduces body weight gain[80,81]; this effect is blunted by HFD feeding and obesity[82,83]. More recently, an effect of insulin to augment learning, cognition, and memory has been described[84-86].

Most studies examining insulin action in the brain have infused insulin directly into CSF. Most of these studies have focused on insulin's ability to affect feeding behavior, body weight, and hepatic metabolism may occur through its signaling in the hypothalamus. Insulin action in the brain may also affect cognitive function and prevent the biochemical and memory changes that occur with Alzheimer's disease. These effects of insulin are attributed to its actions in the cerebral cortex and hippocampus and have been observed after peripheral insulin dosage as well as intranasal insulin administration.

This section will review insulin action in the brain, as well as the reported effects of HFD feeding or insulin resistance. Additionally, the limited reports of insulin production within the brain will be discussed.

1.3.1 Hypothalamic insulin action on feeding behavior

Insulin's actions on feeding behavior and body weight described above are generally believed to result from hypothalamic signaling. Peripherally-injected radiolabeled insulin binds to the median eminence and arcuate nucleus in the hypothalamus[65] and acts on Agouti-related protein (AgRP) or pro-opiomelanocortin (POMC) neurons[75,87]. Insulin reduces the transcription of orexigenic peptides in AgRP neurons while increasing expression of anorexigenic peptides in POMC neurons, which in turn reduces food intake (Figure 1-8). Insulin and leptin both signal through phosphoinositide 3-kinase (PI3K) and elicit similar effects on feeding behavior[87]; however, they act in distinct hypothalamic POMC neuron populations[88]. Hypothalamic BBB differs from the rest of the brain (Section 1.2.2.5) and, while there is some debate as to the permeability of the arcuate, it is likely that insulin access to the hypothalamus is more permissive than in the remainder of the brain.

To investigate insulin action on feeding behavior, researchers commonly infuse insulin directly into CSF, which bypasses the restrictive brain endothelium and may gain access to the BISF more readily than insulin that crosses the BBB. Given the slow secretion of CSF, acute, post-prandial increases in insulin may more readily access the BISF by crossing the BBB as opposed to entering the CSF. Thus, insulin infusion into CSF may not represent the physiological route of insulin. Regardless, this route of insulin administration has been consistently employed in a variety of model systems and experiments. Based on an estimated CSF volume of 0.156 mL in the rat[9], estimates of the final CSF insulin concentration ranged from 1-460 nmol/L, suggesting pharmacologic insulin doses have been employed. Experiments in large animals, such as baboons or

sheep, resulted in estimated CSF insulin concentrations ranging from 0.1-10 nmol/L. These calculations are shown in Table A-1Table A-2. Despite these caveats, across species, insulin consistently reduces food intake.

In both baboons and rats, insulin's ability to reduce food intake appears dose-dependent, with higher concentrations exerting a greater reduction in feeding behavior and weight[79,89]. In baboons, changes in food intake accounted for the full effect of insulin-induced weight loss[79]. In contrast, the decrease in rat body weight was greater than anticipated based on the changes in food intake[89]. The ability of insulin to reduce food intake is sustained in *ad libitum* fed and food-deprived rats upon refeeding[90]. Additionally, insulin administration into CSF can alter macronutrient intake, with insulin decreasing in *ad libitum* fat intake compared to carbohydrate or protein[91]. Insulin administration into the ventricles of sheep robustly decreased food intake and body weight[92] and, curiously, stimulated increases in circulating insulin, suggesting ability of brain insulin action to affect pancreatic insulin secretion.

Central insulin action is affected by HFD feeding and in obesity-prone rodent models. Consistently, the ability of intraventricular insulin to decrease food is blunted in rats receiving moderate- or high-fat diet[82,83,91,93]. Intraventricular insulin increased hypothalamic POMC mRNA in rats fed a low-fat diet while this change was not detectable in those fed a HFD[83]. Interestingly, central insulin action was restored by reversing diet-induced obesity[94]. The genetically obese, leptin-receptor deficient, (*fa/fa*) Zucker rat is less sensitive to the anorectic effect of ventricular insulin administration than their lean, heterozygous counterparts[95]. Intracerebroventricular (ICV) administration of an IR anti-sense oligodeoxynucleotides downregulated IR in the arcuate nucleus and

these mice increased food intake and had increased expression of orexigenic peptides[81]. The neuronal IR knock-out mouse has a metabolic phenotype, including increased food intake and peripheral effects that will be discussed in the next section[80]. Collectively, these studies report hypothalamic insulin action through IR decreases food intake and this effect is reduced in HFD fed animals. However, as previously stated, in these studies, insulin was infused directly into CSF at the high concentrations, which allows insulin to bypass the brain endothelium to gain access to the paravascular space and neuronal tissue. Thus, these studies do not evaluate the potential role of the brain endothelium in regulating insulin transport, or how this component of the BBB may be affected by HFD feeding.

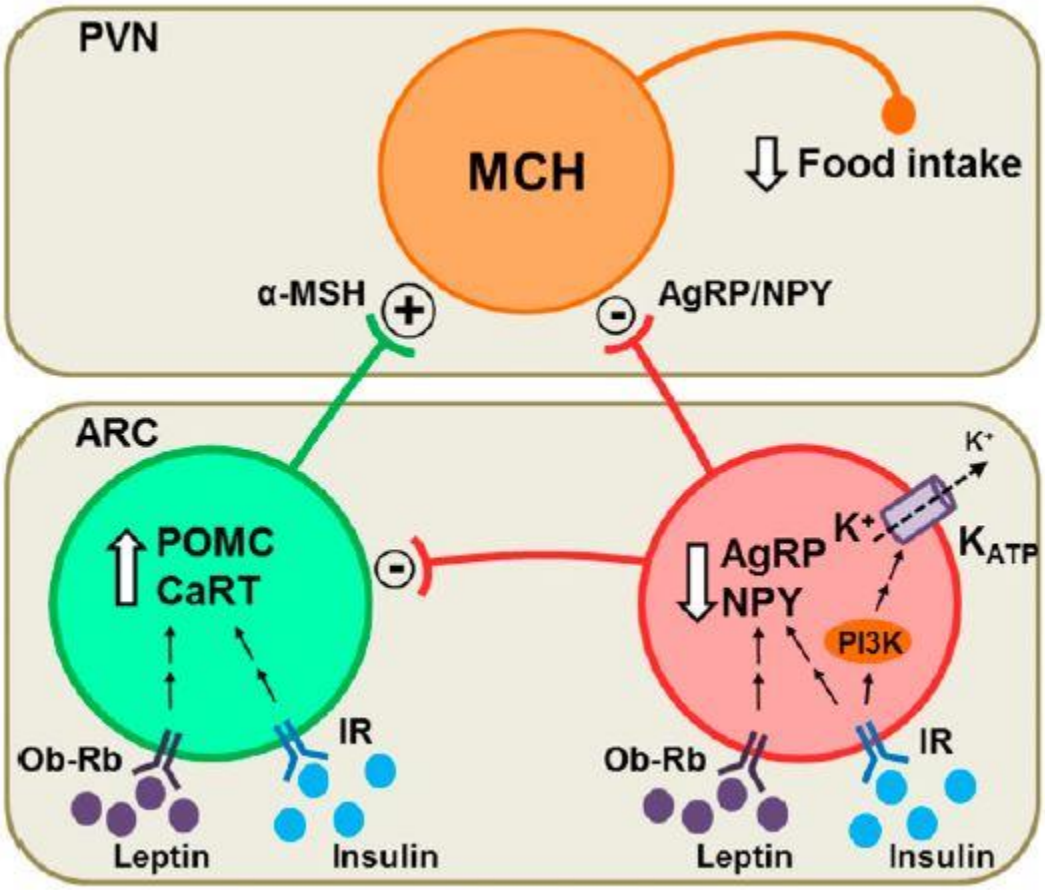

Figure 1-8 Insulin signaling in the hypothalamic arcuate nucleus (ARC) and paraventricular nucleus (PVN)

Insulin directly and indirectly decreases food intake through signaling in the hypothalamic ARC and PVN. Insulin binding to IR on POMC neurons (green) to increase expression of orexigenic peptides POMC and cocaine- and amphetamine-regulated transcript (CaRT), which in turn activate α-melanocyte-stimulating hormone (α-MSH) neurons in the paraventricular nucleus (PVN) to decrease food intake. Additionally, insulin binding to IR on AgRP neurons (red) decreases anorexigenic peptides AgRP and neuropeptide Y (NPY), which reduces the inhibitory tone on AgRP neurons and α-MSH and also contributes to decreased food intake. Image from Kleinridders et al.[75]

1.3.2 Hypothalamic insulin action on hepatic glucose production

Investigations into central insulin's effects on hepatic glucose production have been conducted in rodents, dogs, and humans. Variation in the techniques precludes any clear cross-species mechanisms and whether central insulin affects hepatic glucose metabolism remains an open question[96,97].

In rodents, CNS administration of insulin decreases hepatic glucose production by increasing vagal nerve efferent activity[98]. Rats given IR anti-sense oligodeoxynucleotides in the hypothalamus to block insulin signaling had greater hepatic glucose production than controls during a hyperinsulinemic-euglycemic clamp, suggesting hypothalamic IR action reduces hepatic glucose production[81]. The ability of insulin (ICV) to suppress hepatic glucose production was blocked by co-infusion with anti-insulin antibodies, pharmacological blockade of PI3K, or sulfonylureas (to block K_{ATP} channel activation)[99]. This suggests a role for insulin in suppressing hepatic glucose production, but these mice also received somatostatin infusions to block pancreatic hormone secretion and did not receive replacement of glucagon. Somatostatin infusion allows for isolation of central insulin from peripheral hormone action, but it also creates an artificial environment. Mice with a genetic mutation that induced >90% reduction of IR in the arcuate nucleus, have increased hepatic glucose production[100]. Selective reintroduction of IR into AgRP or POMC neurons decreased and increased hepatic glucose production, respectively[100]. Collectively, these rodent studies suggest central insulin influences hepatic insulin sensitivity.

In dogs, central insulin has a less substantial effect on hepatic glucose metabolism. In these studies, insulin was administered ICV and through head arteries at

far lower concentrations (i.e. 1.4 μmol/L in rats compared to 0.5 nmol/L in dogs) and found far more modest effects[101,102]. Insulin administration into the brain (either through ICV or through infusion into head arteries) increased hypothalamic insulin signaling and liver gluconeogenic and glycogenic gene expression[102]. In further studies, investigators found that when they increased portal vein insulin concentrations to reflect physiological conditions, increasing central insulin did not affect hepatic glucose output; however, central insulin increased glycogen synthase kinase 3β expression[96,103]. Such discrepancies between rodents and dogs may reflect methodological or species differences.

In humans, recent investigations into the peripheral effects of central insulin action have used intranasal insulin administration. Here, it is difficult to estimate insulin concentrations in CSF, as intranasal insulin may bind to IR in the olfactory bulb or may enter directly into CSF[104]. Intranasal insulin increased functional magnetic resonance signal in the hypothalamus and striatum[105,106], which may have implications for feeding behavior and metabolism. Fasted healthy individuals had increased peripheral insulin sensitivity after intranasal insulin[105]. Following intranasal insulin, lean male subjects required greater insulin infusion rates during a hyperinsulinemic-euglycemic clamp compared to obese men; however, hepatic glucose production was not reported and there was no control for spillover of intranasal insulin into blood[107]. Dash and colleagues accounted for spillover of intranasal insulin into blood and found intranasal insulin suppressed endogenous glucose production 3 hr after administration[108]. Intranasal insulin did not reduce endogenous glucose production in fasted lean or obese individuals; however, both lean and obese subjects had increased hepatic ATP and lean subjects had reduced liver fat[109]. While there is debate over whether spillover of nasal insulin into the

blood must be accounted for in these studies to clearly separate central from peripheral insulin action, recent work suggests that spillover of intranasal insulin does not substantially alter peripheral glucose metabolism[106]. Additionally, this recent publication found intranasal insulin suppressed endogenous glucose production and required a moderate increase in glucose infusion during a hyperinsulinemic-euglycemic clamp in lean compared to obese men[106].

1.3.3 Cognitive effects of insulin

Beyond its metabolic actions, insulin in the brain may also affect learning, memory, and cognition. Type 2 diabetes correlates with dementia and Alzheimer's disease[110,111] and diabetic individuals have a 60% greater risk of developing dementia[112]. Intranasal insulin administration slows cognitive decline[84,86,113]. Unlike the potentially fenestrated vasculature of the hypothalamus, the BBB is intact in the areas of the brain associated with cognition. Thus, investigation of insulin transport across the BBB is of consequence for insulin's cognitive effects.

Studies in both post mortem brain samples and rodent models support the hypothesis that diet-induced insulin resistance may have detrimental effects on cognition and augment Alzheimer's disease progression. Insulin treatment of post mortem brain sections induced canonical insulin signaling through PI3K and this was decreased in the cerebral cortex and hippocampus in patients with Alzheimer's disease[114]. Mice fed a HFD had decreased insulin-stimulated PI3K signaling in the cortex, dendritic spines, and spatial memory[115]. Mice that had Alzheimer's disease neuropathology (3xTg-AD) fed

HFD had increased diabetic pathology in the pancreas compared to wildtype controls and increased brain amyloid content compared to 3xTg-AD mice fed a normal diet[85]. In these mice, a single dose of insulin administered intraperitoneally reportedly restored memory function and reduced soluble amyloid β in the cortex and hippocampus. Rats fed a high-calorie diet (a combination of HFD and high-fructose corn syrup in drinking water) became insulin resistant and had impaired hippocampus-dependent spatial learning and reduced dendritic spine density[116]. These biochemical changes in insulin signaling, anatomical changes in neuron dendrite morphology, and behavioral changes in learning and cognition strongly support a role for diet and insulin action in affecting brain function over time. Given the relatively late-in-life onset of both type 2 diabetes and dementia, deconvoluting the contribution of one to the other is difficult and will continue to require careful study and continued analysis[117]. However, the studies presented here emphasize the potential importance of insulin action in the brain for these diseases.

1.3.4 Insulin production in the brain

In the early days of radioimmunoassay (RIA) development and use, insulin and IR were detected in the brain[118]. Later studies contested the amount of insulin present in the brain, with subsequent studies continually reporting lower concentrations[119]. The presence of insulin receptors in the brain has been supported[75], however insulin production in the brain continues to be questioned[120]. Recently, insulin transcripts were detected by single-cell PCR in GABAergic neurogliaform cells in the cortex[121]. Using an IR antagonist (S-961), these investigators prevented these specific cells from exciting

neighboring neocortical neurons, supporting the notion that insulin may be synthesized and secreted within the brain. While numerous hormones are made in the brain (e.g., IGF-1), it is unclear what the physiological role of neuronal-derived insulin may be and whether it may be impacted by peripheral insulin movement across the BBB.

1.4 Insulin transport across the vasculature

The bulk of work investigating insulin transport across the endothelium has focused on peripheral tissues such as muscle and adipose. Whether the mechanisms governing insulin movement across peripheral vasculature are conserved in the restrictive brain vasculature is unknown. This section will review receptor-mediate endocytosis, the current model for insulin transendothelial transport in the periphery, and summarize the limited work investigating this process in the brain.

1.4.1 Receptor-mediated endocytosis

Insulin transport across the peripheral vasculature and into muscle is mediated by its binding to IR. Endothelium throughout the body is heterogeneous, with the liver having discontinuous endothelium that allows for free movement of solutes, while the skeletal muscle endothelium is continuous and non-fenestrated[122]. Thus, the vasculature in skeletal muscle is less restrictive than the brain, yet more restrictive than that of liver. Receptor-mediated endocytosis and transcytosis requires dynamic movement of the cellular plasma membrane to facilitate endocytotic vesicle budding and trafficking.

Multiple cellular processes have been implicated for receptor-mediated transport, though they are generally broken into clathrin-dependent or -independent pathways[123,124].

Clathrin-coated pits utilize the curved triskelion structure of the clathrin trimer to form a lattice that facilitates endocytosis[125]. Beyond the clathrin protein, these pits contain membrane lipids and adaptor proteins that serve to mediate vesicle formation and budding. These pits have a diameter of ~150 nm and vesicles are generally destined for early endosomes and eventually, lysosomes[126]. Clathrin-coated pits likely facilitate endocytosis of low-density-lipoprotein receptor, transferrin receptor, and epidermal growth factor receptor transport[125,126].

Clathrin-independent endocytosis can occur through caveolae-dependent and clathrin- and caveolae-independent pathway[126]. Within the EC, caveolae are the primary facilitators in transcytosis[127]. Caveolae are lipid rafts approximately 50-100 nm wide, which consist of cholesterol, sphingolipids, and oligomers of caveolin proteins that act as scaffolding proteins. Internalization of caveolae vesicles is catalyzed by phosphorylation of caveolin-1, a structural component of caveolae, by Src kinase[128]. After caveolae bud from the plasma membrane, dynamin cleaves the vesicle[129]. Caveolae vesicles can be targeted to endosomes, lysosomes, or may be used for transendothelial transport. Caveolae associate with endothelial nitrous oxide synthase (eNOS) at the plasma membrane[130]. The association of eNOS with caveolin-1 may facilitate insulin transport across the peripheral EC to act in tissue[131,132].

In both clathrin- and caveolae-mediated endocytosis, the GTPase dynamin pinches the budding vesicle from the plasma membrane and allows endocytosis[124]. Given the redundancy of dynamin and use of actin remodeling in both pathways, it is difficult to

independently inhibit clathrin or caveolae using pharmacologic methods[133]. Additionally, alternate endocytotic machinery may compensate when one pathway is genetically inhibited. Genetic models also pose issues for elucidating endocytosis processes. For example, the caveolin-1 knockout mouse exhibits decreased albumin transendothelial transport in the lung and aorta[134] and has increased vascular permeability due to overactive eNOS[135]. Insulin transcytosis across the vasculature of various tissues is somewhat understood, but the mechanisms regulating insulin transcytosis in the brain vasculature are unclear.

1.4.2 Insulin transport across peripheral endothelium

Insulin transport across the vasculature is saturable and is the rate-limiting step for its action on muscle[136-138]. Endothelial cells concentrate and transcytose insulin[139,140]. In muscle and aortic endothelium, insulin transendothelial transport is necessitates insulin binding to IR on the endothelial cell and subsequent signaling through PI3K. Ultimately, the downstream generation of nitric oxide induces caveolae-mediated endocytosis and transcytosis[132,141-144]. Mice fed HFD had impaired muscle endothelium insulin signaling and insulin transport across muscle vasculature[145].

Some discrepancies in this process have been reported. For example, in adipose tissue microvasculature, insulin transcytosis may be mediated by clathrin, not caveolae[146]. These disparities may be due to differences in the endothelium in large vessels compared to capillaries, and methodological differences. Caveolae contribute to

endocytosis in muscle and aortic endothelium, but their role in the brain endothelium is unknown.

1.4.3 Insulin transport across the brain vasculature

As discussed earlier in this chapter, CSF has been used as a surrogate BISF to quantify insulin movement from blood into the brain. The first paper to demonstrate transport of intravenously-injected insulin into cerebrospinal fluid reported low concentrations (~25% lower than in plasma) that took 3-4 hr to stabilize[147]. Despite improvements in insulin assays and refinement of techniques, studies continue to report similar metrics in a variety of circumstances. Recent results confirm that CSF insulin concentrations are substantially lower than those measured simultaneously in plasma[94,148,149]. The CSF/plasma ratio is inversely related to obesity[150] and directly related to insulin sensitivity[149], suggesting insulin resistance at the brain endothelium of the choroid plexus, where CSF is produced.

Real-time comparisons of plasma and CSF insulin concentrations in dogs found that despite a rapid and sustained increase in plasma insulin, CSF insulin rose slowly and gradually, peaking at values <10% of that achieved in plasma[151]. In humans, similarly low CSF concentrations were observed during an insulin infusion (600 μIU/ml in blood, 0.9-2.8 μIU/ml in CSF)[152]. Schwartz and colleagues also found that CSF insulin concentrations increased as plasma insulin concentrations rose during an insulin clamp, indicating a dose-dependency of insulin transport into the CSF[151]. Mathematical modeling of this insulin movement postulated that BISF was the intermediate

compartment between plasma and CSF[153]. This has not been confirmed *in vivo*, as BISF is difficult to sample without causing tissue damage.

An early paper investigating insulin transport across bovine brain endothelial cells claimed that insulin transcytosis was receptor-mediated; however, this was based on the observation that the bulk of insulin transcytosed was intact as assayed by TCA precipitation[154]. The weaknesses of this paper are many. The use of TCA precipitation may overestimate intact protein[155]. Moreover, the barrier integrity was not reported through use of a permeability marker (e.g., sucrose, inulin, sodium fluorescein) or trans-endothelial electrical resistance (TEER) measurements. Ultimately, it is difficult to resolve whether the studies described by Miller et al. maintained an intact endothelial barrier and whether the results mimic physiology or are an artifact of a flawed barrier.

Other studies have also examined insulin uptake and binding in brain vessels within brain sections and in isolated brain capillaries. Early studies employed autoradiography and found radiolabeled insulin bound to blood vessels in brain sections[64]. Isolated human and bovine brain microvessels bound and endocytosed radiolabeled insulin[156,157]. Attempts to determine insulin degradation in brain capillaries are difficult to interpret, given that microvessel isolations may induce capillary damage and cause insulin degradation[157]. Thus, whether brain capillaries degrade insulin remains an open question. These studies should be interpreted with caution as 1) the use of isolated capillaries does not allow insulin loading from the luminal aspect and is unable to discriminate insulin uptake and transport from the abluminal vs the luminal surface, and 2) the temporal resolution of these studies in limited, i.e. capillaries were loaded with

radiolabeled insulin for 45-60 min before determining exocytosis and this timeframe may be less applicable to the *in vivo* movement of insulin across the BBB.

Autoradiography of intravenously-injected radiolabeled insulin in rabbit brain sections indicated that insulin was present in blood vessels and perhaps in brain tissue[158,159]; however, these studies were unable to resolve whether radiolabeled insulin remained intact or whether insulin was bound to the luminal aspect of the brain endothelium or whether it had successfully crossed the blood-brain barrier. To date, there has not been clear elucidation of blood-to-brain movement of insulin.

1.5 HFD Effects on BBB Function and Structure

Structural changes in the BBB following HFD feeding or type 2 diabetes have not been reported. In contrast, rodent models of type 1 diabetes that receive streptozotocin have reported increased barrier permeability to albumin, thickened basement membrane, and altered tight junctions[160,161]. Streptozotocin-induced diabetes is an extreme affront to the body and these findings should be interpreted with caution. In humans, a small post-mortem comparison of patients with diabetes (type 1 or 2) with healthy controls did not find any difference in BBB permeability[162].

The effect of diet on the BBB has been examined in rodents only. Long-term (90 d) consumption of high-energy diet (40% fat) in mice had slightly reduced tight junction gene expression in brain capillaries and increased hippocampal permeability compared to standard chow[163]. Thus, high-energy diet may increase BBB permeability via down regulation of junctional proteins. In regard to insulin signaling, cerebral arteries isolated

from Zucker obese rats, which lack leptin receptor, had increased insulin-induced ERK signaling and decreased Akt/eNOS signaling and increased reactive oxygen species generation compared to lean controls[164]. This is similar to what has been observed in large peripheral vessels, but may not accurately reflect changes in the smaller arterioles and capillaries.

Limited studies into HFD effects on BBB cellular components and neurovascular coupling have been reported. Short (1 wk)- and long (16 wk)-term HFD in mice can increase brain inflammatory markers and astrocyte glial fibrillary acidic protein (GFAP) expression[165,166]. Interestingly, as little as 3-7 d of HFD increased astrocyte caspase-3 in the arcuate nucleus and cortex, which decreased back to baseline after 2 wk[167]. Eight wk of HFD reduced whisker-stimulated increases in cerebral blood flow in male rats[168]. Interestingly, tanycytes structure[169] and astrocyte function[170,171] may be affected by HFD feeding and insulin resistance. These findings suggest a role for each component of the blood-brain barrier in regulating insulin transport and diabetes pathology.

Ultimately, much remains unknown about insulin movement from circulating plasma into the BISF. Insulin's role in the brain is clearly important—from feeding behavior to hepatic metabolism to cognition. However, whether this occurs under physiologic conditions is difficult to know given the use of ICV insulin at non-physiologic doses and flawed methodologies to analyze insulin transport across the BBB. Given the inadequacy of CSF as a surrogate for insulin reaching BISF, there is a strong impetus for examining insulin transport across the BBB. Understanding the mechanisms that govern this transport and how they may be altered during HFD feeding will progress our understanding of BBB transport during health and disease. Improving insulin

transport to the brain could prove beneficial for numerous health conditions, such as insulin resistance, diabetes, and dementia.

CHAPTER 2 MATERIALS AND METHODS

2.1 Cell culture

Three preparations of BECs were used: commercially-available rat brain microvascular endothelial cells (RBMVECs, Cell Applications, San Diego, CA), freshly isolated rat brain endothelial cells (iBECs), and human brain endothelial cells (hBEC). Isolated astrocytes were employed in a transwell co-culture system.

2.1.1 Rat brain microvascular endothelial cells (RBMVECs)

RBMVECs, passages 5-10, were cultured per manufacturer's recommendations.

2.1.2 Isolated rat brain endothelial cells (iBECs)

Male Sprague Dawley rats were purchased from Charles River (Wilmington, MA, USA) and brains were harvested using previously established methods[172]. Brain stem, pial blood vessels, and meninges were removed. The remaining cortical tissue was mechanically digested in BEC isolation buffer (15 mmol/l HEPES, 5.6 mmol/l NaCl, 5.6 mmol/l KCl, 1.74 mmol/l $CaCl_2$, 1.22 mmol/l $MgCl_2$, 1% BSA, pH 7.4) by dicing with a scalpel and pipetting repeatedly with a glass Pasteur pipet. Enzymatic digestion was done by incubating tissue at 37°C with collagenase (Worthington, Lakewood, NJ, USA), dispase (Worthington), and DNase (New England Biolabs, Ipswitch, MA, USA). Digestion was stopped with ice-cold BEC isolation buffer and myelin was removed by

centrifuging with 25% BSA. Pelleted cells were washed in BEC isolation buffer and then plated onto collagen IV-coated plates in BEC media (DMEM [1% glutamate, 4.5 g/l glucose], 10% FBS, Anti-Anti [1X, 50 unit/ml penicillin, 50 µg/ml streptomycin, 125 ng/ml fungizone; Thermo Fisher, Waltham, MA, USA]) supplemented with puromycin (4 µg/ml, decreasing to 2 µg/ml after 3 d) for 5 d to remove contaminating cells[173]. After 5 d in culture, iBECs were in puromycin-free media. Resulting cells (iBECs) were 98% CD31+ by flow cytometry, expressed claudin-5, and had increased Akt phosphorylation in response to insulin stimulation (Figure 2-1).

For experiments investigating the effect of HFD feeding, iBECs were isolated from 12-wk old SD rats after 4 wk of HFD or normal chow. For transwell experiments, iBECs were isolated from 3-4-wk-old male Sprague Dawley rats.

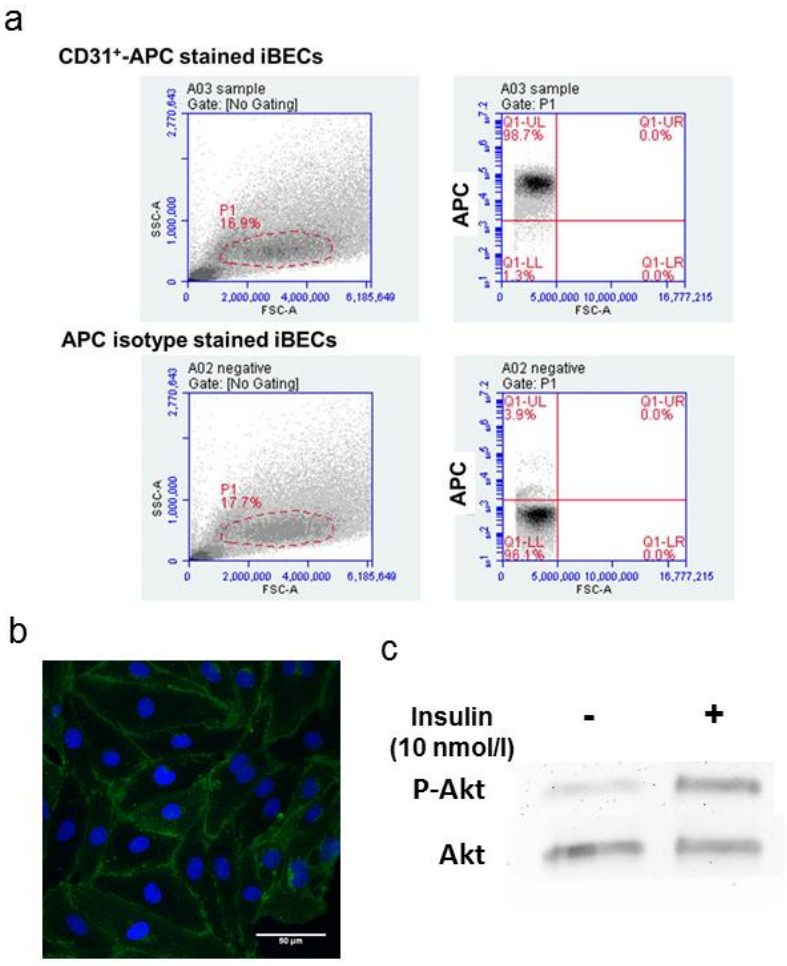

Figure 2-1 Characterization of iBECs

iBECs are 98% $CD31^+$ based on flow cytometry analysis (**a**). Left panels show forward and side scatter with gating (P1). Right panels show APC signal within P1. CD31-APC stained iBECs showed ~98% $CD31^+$ staining compared to APC isotype stained iBECs (lower panels). iBECs show endothelial morphology and immunofluorescent staining for claudin-5 (tight junction protein, green) and DAPI nuclear staining (blue) (**b**). In response to 15 min of 10 nmol/l insulin stimulation, iBECs had increased Akt^{Ser473} phosphorylation compared to vehicle control, indicating the PI3K/Akt pathway was intact (**c**).

2.1.3 Human brain endothelial cells (hBECs)

hBECs were a gift from Dr. John Catravas and were 99% positive for DiI-Ac-LDL (acetylated DiI-labelled LDL) uptake and eNOS expression[174]. hBECs were cultured in DMEM/F12 with HEPES and L-glutamine, 10% FBS, endothelial cell growth supplement (Corning, Corning, NY), heparin (Sigma-Aldrich, St. Louis, MO), and Anti-Anti[175].

2.1.4 Isolated astrocytes

Astrocytes were isolated from Sprague Dawley rat pups at postnatal day 3-10 per established protocols[176]. Astrocytes were positive for GFAP by immunofluorescence (Figure 2-2) and western blot. Astrocytes were cultured in glial culture media (GCM), which was DMEM [1% glutamate, 4.5 g/l glucose], 10% FBS, Anti-Anti (1X).

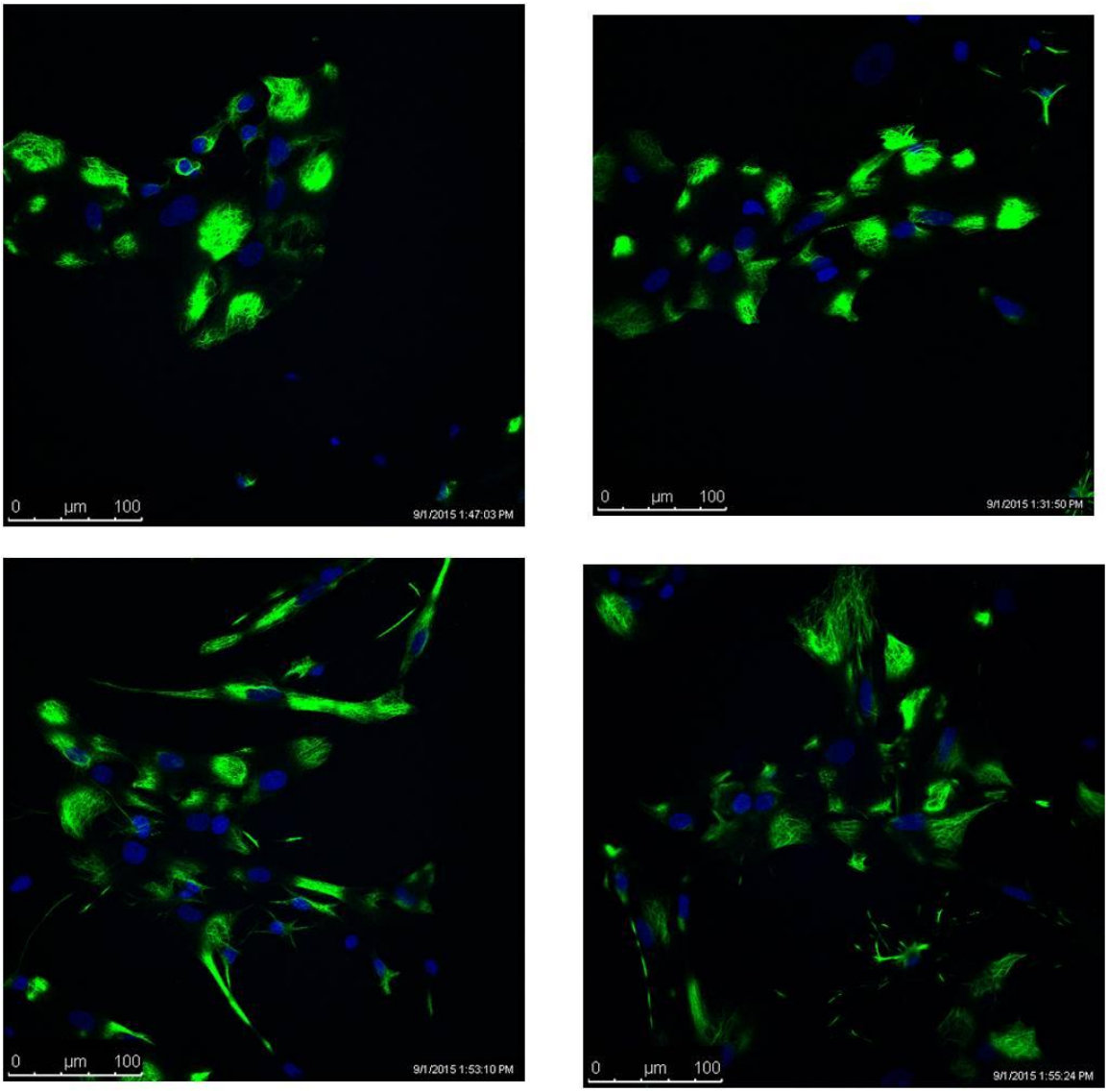

Figure 2-2 Characterization of astrocytes

Isolated astrocytes are GFAP positive. Isolated astrocytes were stained for GFAP (green) and show DAPI nuclear staining (blue). Four separate fields are shown.

2.2 Animals

Sprague Dawley rats were purchased from Charles River (Wilmington, MA, USA) and housed at 22°C on a 12-hr light-dark cycle and fed standard laboratory chow or HFD where specified, and water ad lib. Rats were group housed in accordance with institutional recommendations on corn cob bedding and received environmental enrichment.

To test whether HFD affected iBEC insulin uptake and signaling, male Sprague Dawley rats (Charles River, Wilmington, MA) aged 8 wk were fed a normal chow diet (ND) or HFD (60% lipid, Research Diets, New Brunswick, NJ) for 4 wk before BEC isolation. Prior to tissue collection, rats were weighed and trunk blood collected for non-fasting body weights and serum insulin concentrations. In total, 44 animals were used (21 ND/23 HFD).

2.3 Experimental assays

2.3.1 Flow cytometry

iBECs were cultured for 7 days, trypsinized, resuspended in MACS buffer (Miltenyi Biotec, San Diego, CA, USA) and 1 x 10^6 cells were counted for each condition: iBECs only, iBECs with $CD31^+$ antibody (anti-rat CD31/PECAM-1 APC-conjugated antibody, R&D Systems, Minneapolis, MN, USA, FAB3628A-025), iBECs with antibody control (Goat APC, R&D Systems, IC108A). 100,000 events were counted per condition on BD Accuri C6 flow cytometer (BD Biosciences, Franklin Lakes, NJ,

USA) and analyzed with CFlow Software. iBECs were gated based on forward scatter to detect intact cells versus cellular debris.

2.3.2 Immunofluorescence

iBECs were fixed in 4% PFA, permeabilized in 0.1% triton X, blocked in 10% donkey serum before overnight incubation with primary claudin-5 antibody (Cell Signaling, 1:100), and subsequent secondary antibody anti-mouse Alexa Fluor 488-conjucated secondary antibody (Jackson Immunoresearch 715-545-151, West Grove, PA, USA) and mounted in DAPI mounting media (Vectashield, Burlingame, CA, USA). Images were taken on Zeiss 780 confocal microscope. Astrocytes were fixed in 4% PFA, permeabilized and blocked in 0.1% triton X/5% donkey serum, before overnight incubation with primary GFAP antibody (Cell Signaling 3670, 1:800). Astrocytes were washed with PBS then incubated with anti-mouse, Alexa Fluor 488-conjucated secondary antibody and mounted with DAPI mounting media. Images were taken on a Leica SP5 confocal microscope.

2.3.3 ^{125}I-TyrA14-insulin uptake assay

When 90-95% confluent, cells were serum starved for 4, 2, or 1 hr (RBMVEC, iBEC, hBEC, respectively) then incubated with 200 pmol/l ^{125}I-TyrA14-insulin (Perkin Elmer, Waltham, MA) for 15 min in HEPES binding buffer (HBB) and uptake measured as previously described[140]. ^{125}I-TyrA14-insulin uptake assay was performed as previously described[140,177]. Cells were serum starved and treated with 200 pmol/l ^{125}I-TyrA14-

insulin for 15 min in HEPES binding buffer (HBB; 100 mmol/l HEPES, 120 mmol/l NaCl, 1.2 mmol/l $MgSO_4$, 5 mmol/l KCl, 8 mmol/l glucose, 1% BSA, pH 7.8). In pharmacological experiments, drugs were added in HBB 30 min prior to ^{125}I-TyrA14-insulin addition. Uptake was stopped by placing the cells on ice. Non-specific binding (NSB) was estimated either as ^{125}I-TyrA14-insulin uptake at 4°C for time course experiment or uptake after 30 min pretreatment with IR blocker S-961 (10 nmol/l, NovoNordisk, Copenhagen, Denmark). Cells incubated in cold acid wash buffer (0.5 mol/l NaCl, 0.2 mol/l acetic acid, pH 2.5) for 6 min and washed twice more to remove ^{125}I-TyrA14-insulin bound to the cell exterior. Cells were lysed in 1N NaOH. Radioactivity was quantified with a gamma counter, adjusted for efficiency (80%), and NSB subtracted. Protein was quantified with Bradford reagent and final results are expressed as disintegrations per minute (DPM) per mg protein.

For pharmacologic studies, cells were pretreated with drug 30 min prior to insulin addition.

2.3.4 Cell viability assay

Cell Titer Blue Cell Viability Assay (Promega) was used to assess cell viability per manufacturer's instructions. This assay is based on live cells retaining reducing capacity. RBMVECs were serum-starved for 4 hr then incubated for 30 min in HBB with vehicle or 10 mmol/L MβCD. Longer time exposure to MβCD may be toxic and this was confirmed for RBMVECS given 10 mmol/L MβCD for 4.5 hr. After the treatments, RBMVECs were washed once with HBB and fresh 100 µl of HBB was added to each

well. Cell titer blue was added to each well and RBMVECs were incubated at 37°C for 3 hr with cell titer blue before cells were excited at 560 nm and fluorescence was measured at 590 nm. Results are expressed as relative fluorescence units (RFU). This experiment was repeated 3 times. Within each experiment, each condition had 8 technical replicates.

2.3.5 Insulin ELISA

Blood was collected from ND and HFD rats immediately prior to sacrifice. Insulin was measured with a rat-specific insulin ELISA (Mercodia, Uppsala, Sweden) or an ultrasensitive ELISA (Alpco, Salem, NH).

2.3.6 Real time RT-PCR

RNA was extracted from iBECs and real-time quantitative RT-PCR was used to determine expression levels of IR-β (*Insr* β) and IDE (*Ide*).

RNA extraction was performed with TRIzol® reagent (Invitrogen, Carlsbad, CA, USA). Genomic DNA was removed by treatment with 2 U RNase Free DNase I/10µg RNA (New England Biolabs, Ipswich, MA, USA) at 37°C for 20 min. DNA-free RNA (1 µg) was reverse transcribed using SuperScript® III First-Strand Synthesis System (Invitrogen) with random hexamers, according to manufactures protocol. The resulting cDNA was used in real time PCR assay.

IR (*Insr*) β subunit and IDE (*Ide*) mRNA were measured by real time RT-PCR using an iCycler IQ (Bio-Rad, Hercules, CA, USA) and ABsolute Blue QPCR Mix,

SYBR Green, fluorescein (Thermo Fisher). Assay conditions were optimized to generate a single PCR product, confirmed by melt curves. All PCR reactions were further optimized for primer annealing temperature to obtain PCR efficiencies of 95-100%. The primers for *Insr* β subunit were forward (FWD) 5' CTGGACAGAACCCACCTATTT 3', reverse (REV) 5' CTGAAGAGGAAGACGAAGATGAG 3'; *Ide* forward (FWD) 5' GGAGGAACGAAGTCCACAATAA 3', reverse (REV) 5' GTTGAAGCAAGGCTCAGAGATA 3' (Integrated DNA Technologies, Coralville, IA). Primer concentration for real time PCR was 100 nmol/l. Unknown samples were measured using 100 ng reverse-transcribed RNA against an external standard curve. All samples, including standards, were measured in triplicate, in the same assay.

2.3.7 *Immunoblotting*

IR expression and downstream insulin signaling was assessed by immunoblot. Cells were placed on ice and washed twice with ice-cold PBS before lysis with M-PER and phosphatase and protease inhibitors (Thermo Fisher). Lysate protein was quantified with Bradford reagent and samples prepared for western blot. hBEC lysates were concentrated using a polyethersulfone membrane microcentrifuge spin column with a 10 kD molecular-weight cut off (Thermo Fisher) prior to addition of SDS and then equal volumes were loaded on gels. RBMVEC and hBEC lysates were run on 4-20% gradient gels and iBEC lysate samples on 10% Criterion gels (Bio-Rad). Gels were transferred onto nitrocellulose membranes, blocked in 5% BSA or milk and incubated with primary antibodies overnight at 4^{o}C (see Table 2-2). Blots probed for phosphorylated proteins

were stripped (BP-98, Boston Bioproducts, Boston, MA, USA) before reprobing for total protein concentrations. All primary antibodies were used at 1:1000 dilution during an overnight incubation at 4^{o}C. Secondary antibodies (Cell Signaling anti-mouse 7076, anti-rabbit 7074) were used at 1:2000 before imaging. Quantification of densitometry was performed using ImageJ software. For insulin-stimulated responses, phosphorylated protein was normalized to total protein. Insulin receptor was normalized to GAPDH expression.

For pharmacologic experiments, drugs were added 30 min prior to incubation with 10 nmol/l insulin.

2.3.8 NFκB binding activity

Nuclei were isolated from cultured ND and HFD iBECs using a nuclear extraction kit (Active Motif, Carlsbad, CA) and were positive for Lamin A/C (see Table 2-2) nuclear marker upon western blot. Nuclear NFκB p65 binding activity was measured using a TransAM® Transcription Factor ELISA (Active Motif), normalized to protein, and compared to a standard curve of recombinant NFκB p65 protein (Active Motif) per manufacturer's instructions.

2.3.9 In vitro blood-brain barrier co-culture and transcytosis

For transcytosis assays, co-cultures of isolated astrocytes and iBECs were used as *in vitro* BBB (Figure 2-3, Figure 2-4)[178,179]. Two days prior to co-culture, astrocytes were thawed and seeded (80,000 cells/well) on poly-L-lysine-coated 6-well plates[180]. One day

before co-culture, iBECs from 3-4 wk old Sprague Dawley rats were passaged onto transwell inserts (90,000 cells/cm^2, 1.0 μm, PET, EMD Millipore, Billerica, MA, USA) and fresh media was provided to astrocytes. On day 0 of co-culture, iBEC transwell inserts were placed over astrocytes and the apical chamber was given fresh DMEM/F12 with hydrocortisone (550 nmol/l), Anti-Anti (1X) and insulin/transferrin/selenium growth supplement (1X, ITS-G, Thermo Fisher). On day 3 of co-culture, insulin was removed from culture media and iBECs were given DMEM/F12 with hydrocortisone (550 nmol/l, Sigma-Aldrich), RO-20-1724 (17.4 μmol/l, EMD Millipore), CPT-cAMP (250 μmol/l, Abcam, Cambridge, MA), IGF-1 (20 nmol/l, PeproTech, Rocky Hill, NJ, USA), holo-transferrin (68.75 nmol/l, R&D Systems), sodium selenite (38.7 nmol/l, Sigma-Aldrich), and Anti-Anti (1X). This medium maintained barrier integrity. On day 3, astrocytes were fed with an equivolume mixture of DMEM/F12 with IGF-1-media and conditioned media. On day 5 of co-culture, iBEC monolayer and astrocytes were washed 1x in HBB. Basolateral chamber received equivolume mixture of DMEM/F12 with IGF-1 and conditioned media.

Barrier integrity was assessed by measuring trans-endothelial resistance (TEER) (End Ohm, WPI, Sarasota, FL) and expressed as $\Omega \times cm^2$. Peak TEER (reported as mean ± SD) was achieved on day 5 when transcytosis experiments were performed. Prior to the experiment, iBEC monolayer and astrocytes were washed once in HBB. Then, basolateral chamber received equivolume mixture of DMEM/F12 with IGF-1 and astrocyte-conditioned media and apical chamber received HBB.

In transcytosis experiments, either native or heat-denatured (70^oC for 90 min) ^{125}I-TyrA14-insulin (200 pmol/l) was added to the apical or basolateral chamber. Heat-

denatured (HD-^{125}I-TyrA14-insulin) insulin is a control for paracellular leak[140]. Following insulin incubation, the total fluid volume from the apical and basolateral chambers was collected and quantified on a gamma counter. To estimate insulin transcytosis, HD-^{125}I-TyrA14-insulin was subtracted from ^{125}I-TyrA14-insulin.

To investigate iBEC regulation of transcytosis, apical chambers were pretreated for 15 min (S-961) or 30 min (all other drugs) before addition of native or HD-^{125}I-TyrA14-insulin (200 pmol/l) for 30 min. To investigate astrocyte-mediated regulation of insulin transcytosis, glutamate was added to basolateral chamber 30 min before addition of insulin. Thapsigargin was added 30 min before glutamate.

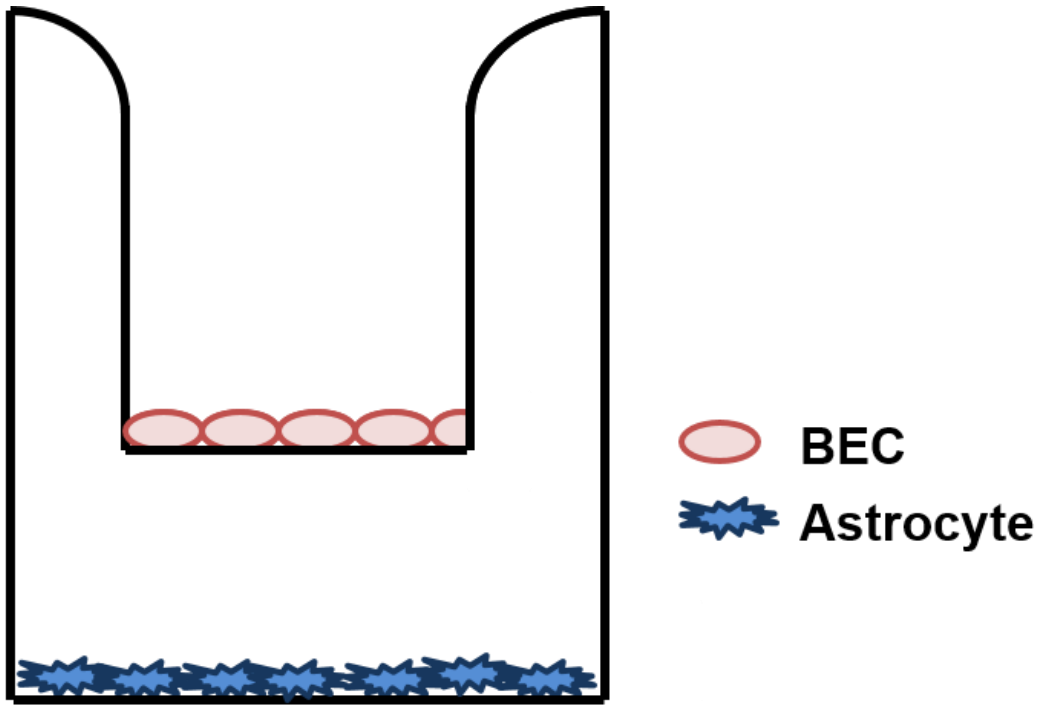

Figure 2-3 Diagram of *in vitro* blood—brain barrier

Astrocytes were seeding on 6-well plates. Isolated BECs were seeded on a transwell filter and co-cultured with astrocytes.

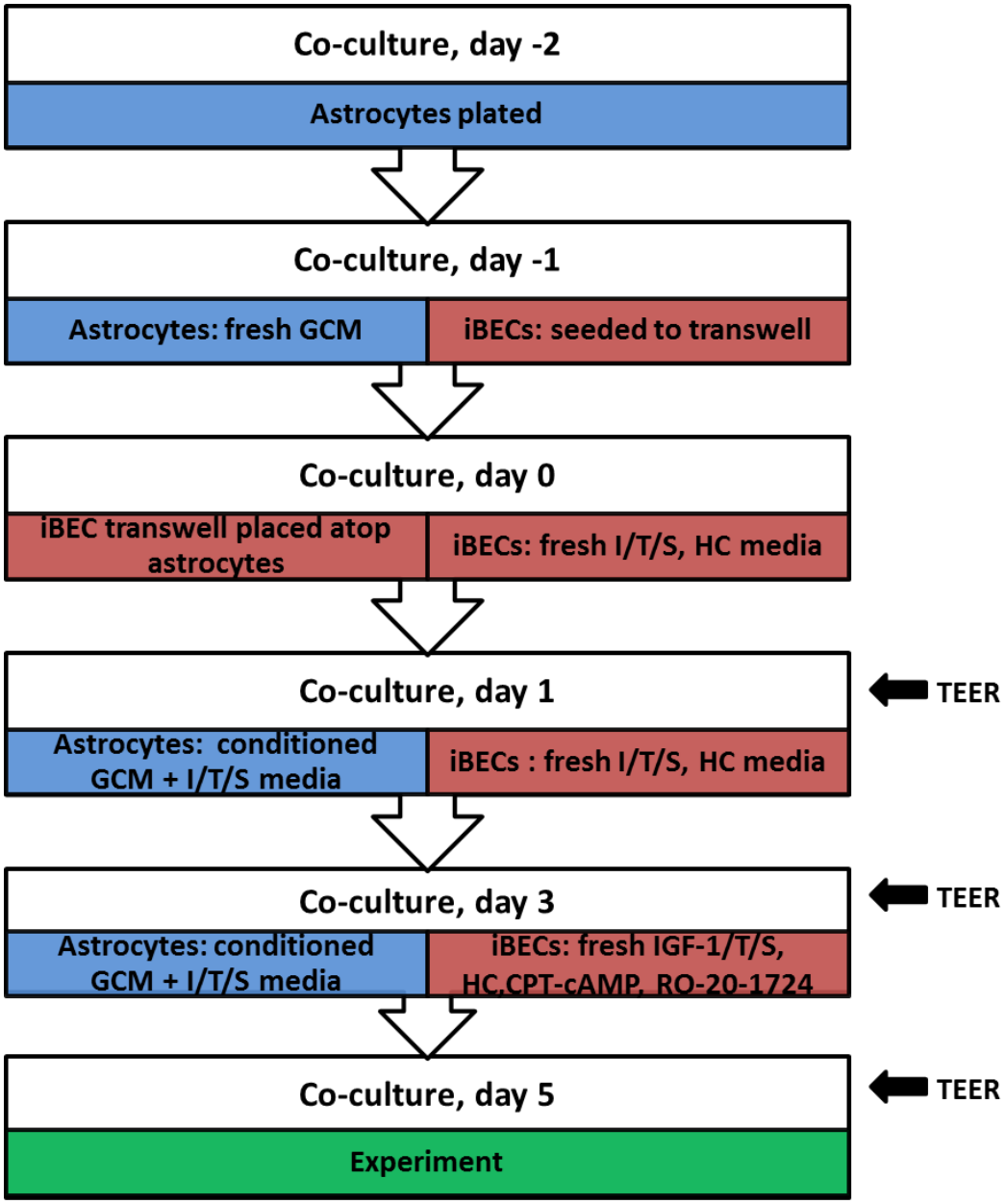

Figure 2-4 Time course of co-culture conditions for *in vitro* BBB

Cell seeding and media changes are depicted in the time course above, along with time points for TEER measurement. Day 0 of co-culture indicates date when iBECs and astrocytes were placed in the same well (see Figure 2-3). GCM: glial culture media (DMEM/F12, 10% FBS, 1X Anti-Anti).

2.3.10 Pharmacological reagents

Drug manufacturers are listed in Table 2-1.

2.3.11 *Insulin degradation*

Insulin degradation was determined by elution profile from a Sephadex G-50 (medium, Sigma-Aldrich) column as previously established [181]. Briefly, samples were loaded onto a 50-cm column and eluted with 0.15 M ammonium bicarbonate buffer, 0.02% BSA, and 5% sodium azide, pH 8.0. To verify the column elution profile discriminates intact from degraded insulin, ^{125}I-TyrA14-insulin (200 pmol/l) was incubated with or without HepG2 cells overnight at 37^{o}C. ^{125}I-TyrA14-insulin samples collected after transcytosis assays were compared to native and HepG2-degraded insulin elution peaks.

2.4 Statistics

Experimental replicates and individual rats are shown as dot plots in each figure. ^{125}I-TyrA14-insulin uptake data were log-transformed and analyzed with a 1-way ANOVA or hierarchical linear mixed model if there were missing values. Normality was assessed using the Shapiro-Wilk normality test. Non-normally distributed groups were compared with Mann-Whitney *U*-test. Normally distributed groups were compared using unpaired t-test, paired t-test, or 1-way ANOVA. Post hoc testing is specified where employed. Significance was declared at $p<0.05$ and a trend toward significance at $p\leq0.10$.

Table 2-1. Pharmacological agents and manufacturers

Drug	Product #	Manufacturer	Location
Ab-3	GR31L	Calbiochem	San Diego, CA, USA
Dynasore	2897	Tocris	Minneapolis, MN, USA
Filipin	70440	Cayman Chemical	Ann Arbor, MI, USA
Genistein	G6649	Sigma-Aldrich	St. Louis, MO, USA
L-glutamate	0218	Tocris	Minneapolis, MN, USA
N^{ω}-nitro-L-arginine methyl ester (L-NAME)	N5751	Sigma-Aldrich	St. Louis, MO, USA
Methyl-β-cyclodextrin (MβCD)	C4555	Sigma-Aldrich	St. Louis, MO, USA
PD98059	1213	Tocris	Minneapolis, MN, USA
PP1	14244	Cayman Chemical	Ann Arbor, MI, USA
PP2	13198	Cayman Chemical	Ann Arbor, MI, USA
S-961		Novo Nordisk	Copenhagen, Denmark
(*S*)-Nitroso-*N*-acetylpenicillamine (SNAP)	0598	Tocris	Minneapolis, MN, USA
Sodium nitroprusside (SNP)	567538	Calbiochem	San Diego, CA,USA
Thapsigargin	1138	Tocris	Minneapolis, MN, USA
Wortmannin	W1628	Sigma-Aldrich	St. Louis, MO, USA

Table 2-2 Antibody manufacturers

Antibody	Product #	Manufacturer	Location
Akt	9272	Cell Signaling Technology	Danvers, MA
Akt^{Ser473}	4060	Cell Signaling Technology	Danvers, MA
α-tubulin	2144	Cell Signaling Technology	Danvers, MA
β-actin	4967	Cell Signaling Technology	Danvers, MA
eNOS	9572	Cell Signaling Technology	Danvers, MA
$eNOS^{Ser117}$	4967	Cell Signaling Technology	Danvers, MA
ERK	4695	Cell Signaling Technology	Danvers, MA
$ERK^{Thr202/Tyr204}$	4376	Cell Signaling Technology	Danvers, MA
GAPDH	2118	Cell Signaling Technology	Danvers, MA
IR-β	711	Santa Cruz	Dallas, TX
Lamin A/C	2032	Cell Signaling Technology	Danvers, MA
MEK 1/2	8727	Cell Signaling Technology	Danvers, MA
MEK 1/2 $Ser^{217/221}$	9154	Cell Signaling Technology	Danvers, MA

CHAPTER 3 UNRAVELING THE REGULATION OF INSULIN TRANSPORT ACROSS THE BRAIN ENDOTHELIAL CELL

3.1 Introduction

Insulin's actions on the central nervous system (CNS) have been well documented. Insulin administration ICV robustly decreased food intake and body weight in rats[90] and baboons[79]. This effect was decreased in insulin-resistant Zucker rats or rats fed a moderate- or high-fat diet (HFD)[82,83,95], but was restored by weight loss[94]. In humans, insulin resistance is associated with increased rates of dementia and Alzheimer's disease[182]. Despite important CNS actions, how (or whether) circulating insulin accesses the brain interstitial fluid (BISF) or neuronal tissues remains uncertain. Using autoradiographic methods, van Houten et al.[64-66,183] and others[158,159] demonstrated saturable binding of labelled insulin to brain blood vessels, consistent with a receptor-dependent process. Isolated human and bovine brain capillaries also bound radiolabeled insulin and released it in a time-dependent manner[156,157]. However, these studies did not resolve whether intact insulin was bound to the vessel exterior, internalized by brain endothelial cells (BECs), transported across vessels, or degraded by insulin degrading enzyme (IDE) or other proteases either on the BECs[184] or in brain tissue[185].

Recent imaging studies have delineated the 'glymphatic' circulation of cerebrospinal fluid (CSF)[25,27,28], whereby ventricular CSF flows to the subarachnoid space before entering the Virchow–Robin space (VRS) that parallels penetrating pial arterioles into brain tissue. Compounds crossing the BECs, the first layer of the blood–brain barrier (BBB), mix with CSF in the VRS and must then cross astrocyte endfeet that

form the VRS's lateral boundary to reach the BISF. CSF within the BISF may flow into the VRS along venules and function to clear waste from the brain to the lymphatics along dural veins or to the venous circulation via arachnoid granulations (reviewed[28]).

Numerous studies have reported low insulin concentrations in CSF, as well as a slow transport of circulating insulin into CSF[149,151,186]. Mathematical modeling of circulating insulin entry into CSF suggested a three-compartment model in which BISF was predicted to be an unsampled 'intermediate' compartment with plasma insulin crossing the BBB, then passing through BISF and eventually entering CSF[148]. The frequent use of CSF in multiple studies as a BISF 'surrogate' assumes some validity to this model. However, no study has validated this model of intact insulin entry into CSF by transport across the BBB. This is understandable as neither BISF nor the VRS compartment is accessible to sampling without tissue damage.

We recently compared the rate of ^{125}I-TyrA14-insulin transport into brain tissue with its movement into CSF and found its appearance in brain tissue preceded its appearance in CSF and that this was mediated by the IR and blunted by HFD feeding[177]. However, these studies were unable to differentiate insulin appearance in brain tissue from its binding and potential uptake into the BECs. To date, no work has elucidated the path by which BECs internalize insulin or clarified whether ^{125}I-TyrA14-insulin crosses the brain endothelium without degradation.

Given the importance of brain insulin action and paucity of information on BBB insulin transport, we undertook a detailed study of the mechanisms that regulate insulin uptake by, action upon, and transcytosis across BECs using human and rat BECs and an *in vitro* BBB model. The rat provides a historical model for examining brain insulin

transport and sufficient tissue to compare dietary effects between individual animals. We hypothesized that, similar to the peripheral endothelium[142], insulin transport would be mediated by its receptor and downstream signaling through phosphoinositide-3-kinase (PI3K) and NO generation, and that transport would be decreased in rats fed an HFD. Additionally, we hypothesized that astrocyte stimulation would increase BEC insulin transcytosis.

3.2 Results

3.2.1 RBMVECs and hBECs take up insulin and signal through Akt

RBMVECs exposed to physiological concentrations of ^{125}I-TyrA14-insulin (200 pmol/l) internalized the tracer within 5 min and uptake continued for 60 min (Figure 3-1). Uptake was rapid and approximately linear between 0 and 15 min; therefore 15 min incubations were used for subsequent experiments. We previously reported that the IR-specific antagonist S-961 blocked ^{125}I-TyrA14-insulin uptake by RBMVECs, while IGF-I receptor blockade did not[177].

Figure 3-2 shows this (panel a) and similar findings in hBECs (panel b). Excess unlabeled insulin (2 µmol/l) and S-961 pretreatment (10 nmol/l or 20 nmol/l) blunted ^{125}I-TyrA14-insulin uptake. Pretreatment with an IGF-1 receptor antibody, Ab-3 (1 µg/ml), did not decrease hBEC insulin uptake.

Insulin (10 nmol/l) treatment for 15 min increased Akt^{Ser473} phosphorylation in hBECs and RBMVECs, which was blocked by pretreatment with 10 nmol/l or 20 nmol/l

S-961 in both human and rat cells (Figure 3-2 c, d). Importantly, IGF-1 receptor blockade did not decrease insulin-stimulated Akt phosphorylation. These results confirm our earlier rodent studies and identify a role for the IR in hBEC insulin transport.

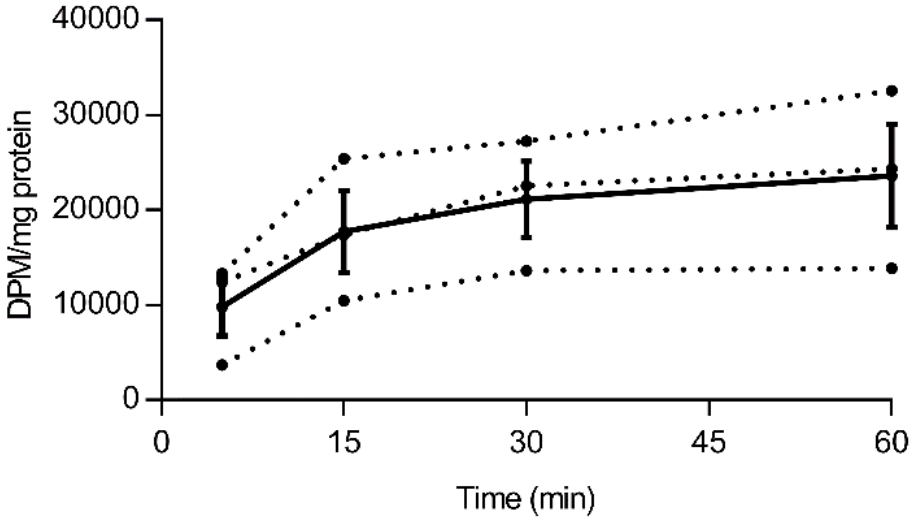

Figure 3-1 ^{125}I-TyrA14-insulin uptake is most rapid between 5-15 min and continues over 60 min.

RBMVEC were serum starved for 4 hr before addition of 200 pmol/l ^{125}I-TyrA14-insulin for 5-60 min at 37°C. Radioactivity (DPM) was measured and normalized to protein content. Dotted line indicates individual replicates, solid line indicates mean ± SEM.

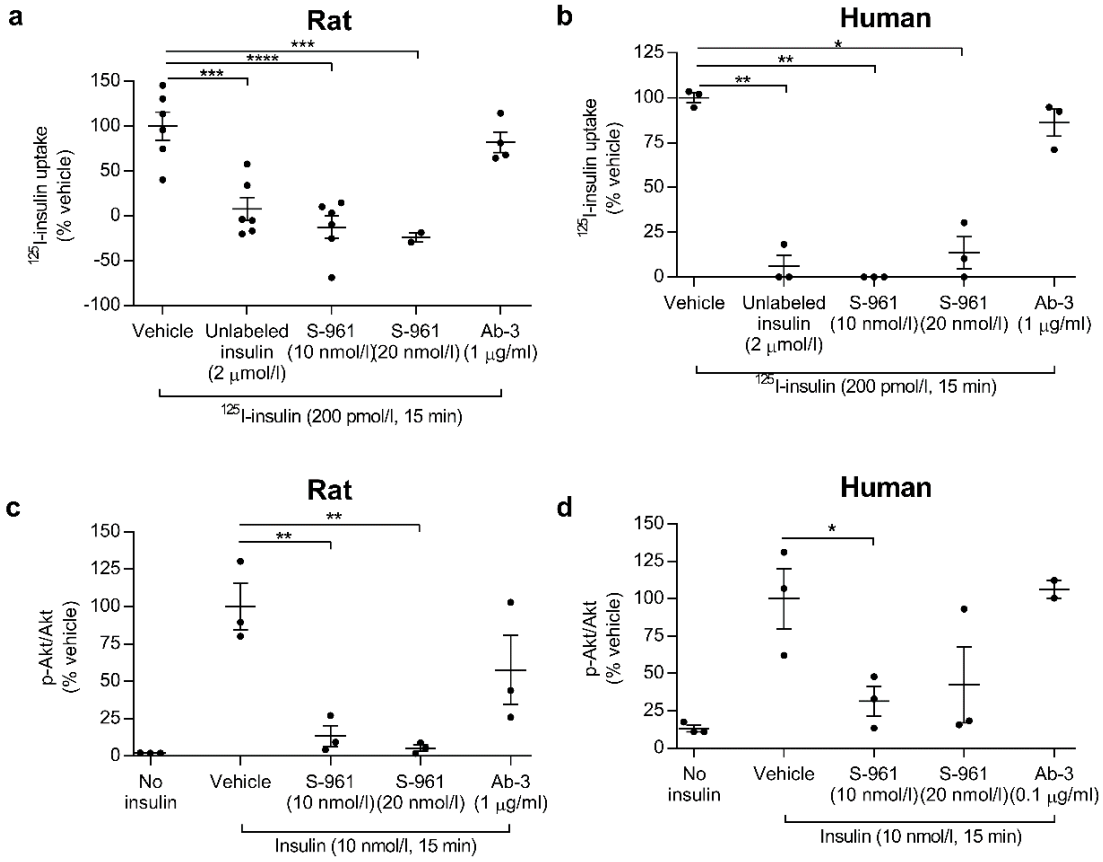

Figure 3-2 IR blockade blunts insulin uptake and signaling in human and rat BECs.

IR blockade by S-961 blunts ^{125}I-TyrA14-insulin (^{125}I-insulin) uptake (200 pmol/l, 15 min) in RBMVECs (**a**) and hBECs (**b**) and Akt^{Ser473} phosphorylation in RBMVECs (**c**) and hBECs (vehicle vs 20 nmol/l S-961, p=0.08) (**d**), while the IGF-1 receptor antibody Ab-3 did not significantly decrease uptake. Data presented are means ± SEM. One-way ANOVA with Dunnett's (**a**, **b**) or Sidak (**c**, **d**) post hoc test. *p<0.05, **p<0.01 vs vehicle.

3.2.2 Insulin uptake is not affected by PI3K or MEK signaling but requires intact lipid rafts

In bovine aortic endothelial cells, blocking insulin signaling with wortmannin, genistein or PD98059 decreased FITC-insulin endocytosis[142]. Treating RBMVECs with these agents did not affect ^{125}I-TyrA14-insulin uptake (Figure 3-3). The brain endothelium is highly restrictive because of its tight junctions and multiple efflux pumps, with the latter preventing BEC accumulation of numerous compounds and lipophilic pharmacological agents [38]. Therefore, we confirmed that wortmannin (100 nmol/l) and genistein (50 μmol/l) inhibited insulin-induced Akt^{Ser473} phosphorylation in RBMVECs (Figure 3-4 a, b). Insulin did not consistently increase extracellular signal-regulated kinase (ERK) phosphorylation and PD98059 (25 μmol/l) inhibited basal ERK$^{Thr202/Tyr204}$ phosphorylation (Figure 3-4, c). In aggregate, these findings suggest insulin uptake by RBMVECs does not require insulin-stimulated signaling.

Next, we tested whether inhibiting lipid rafts or vesicle endocytosis affected insulin uptake. Pretreating RBMVECs with filipin (5 μg/ml) or methyl-β-cyclodextrin (MβCD, 10 mmol/l) prior to ^{125}I-TyrA14-insulin exposure decreased tracer uptake Figure 3-5. MβCD had a greater effect than filipin (p=0.004, Tukey's post hoc). Given that MβCD can be detrimental for cells at high concentrations or during long incubations, we determined cell viability following 30 min MβCD treatment. After 30 min, MβCD (10 mmol/L) did not affect cell viability compared to vehicle control; however, longer

incubations with MβCD (4.5 h) clearly decreased cell viability (Figure 3-6). MβCD depletes and filipin binds cholesterol in lipid rafts, suggesting that intact raft formation/function is necessary for insulin endocytosis. Neither pretreatment with dynasore (40 µmol/l), which inhibits dynamin-mediated scission of internalized endocytic vesicles from the plasma membrane, nor with PP1 or PP2 (10 µmol/l), inhibitors of Src-kinase, which is implicated in facilitating caveolae- and clathrin-mediated endocytosis, decreased ^{125}I-TyrA14-insulin uptake.

Since NO regulates insulin uptake in aortic endothelial cells[137,143], we tested whether eNOS inhibition would affect insulin uptake in RBMVECs. Pretreatment with N^{ω}-nitro-L-arginine methyl ester (L-NAME, 200 µmol/l) did not significantly decrease ^{125}I-TyrA14-insulin uptake. Pretreatment of RBMVECs with NO donors, (*S*)-nitroso-*N*-acetylpenicillamine (SNAP) or sodium nitroprusside (SNP), at several concentrations did not affect ^{125}I-TyrA14-insulin uptake (Figure 3-7). These results suggest that the brain endothelium regulates insulin uptake differently from peripheral vasculature.

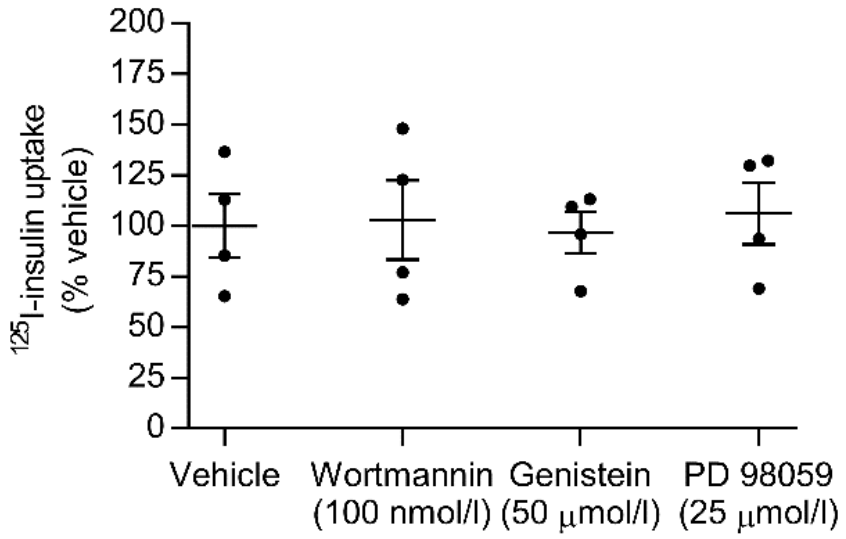

Figure 3-3 Wortmannin, genistein, and PD98059 do not inhibit ^{125}I-TyrA14-insulin uptake.

RBMVECs were serum starved for 2 hr before 30 min pretreatment with drugs and subsequent 15 min incubation with ^{125}I-TyrA14-insulin (^{125}I-insulin, 200 pmol/l) for 15 min at 37^{o}C. Each circle denotes individual replicate. Data is shown as mean ± SEM, n=4 per condition.

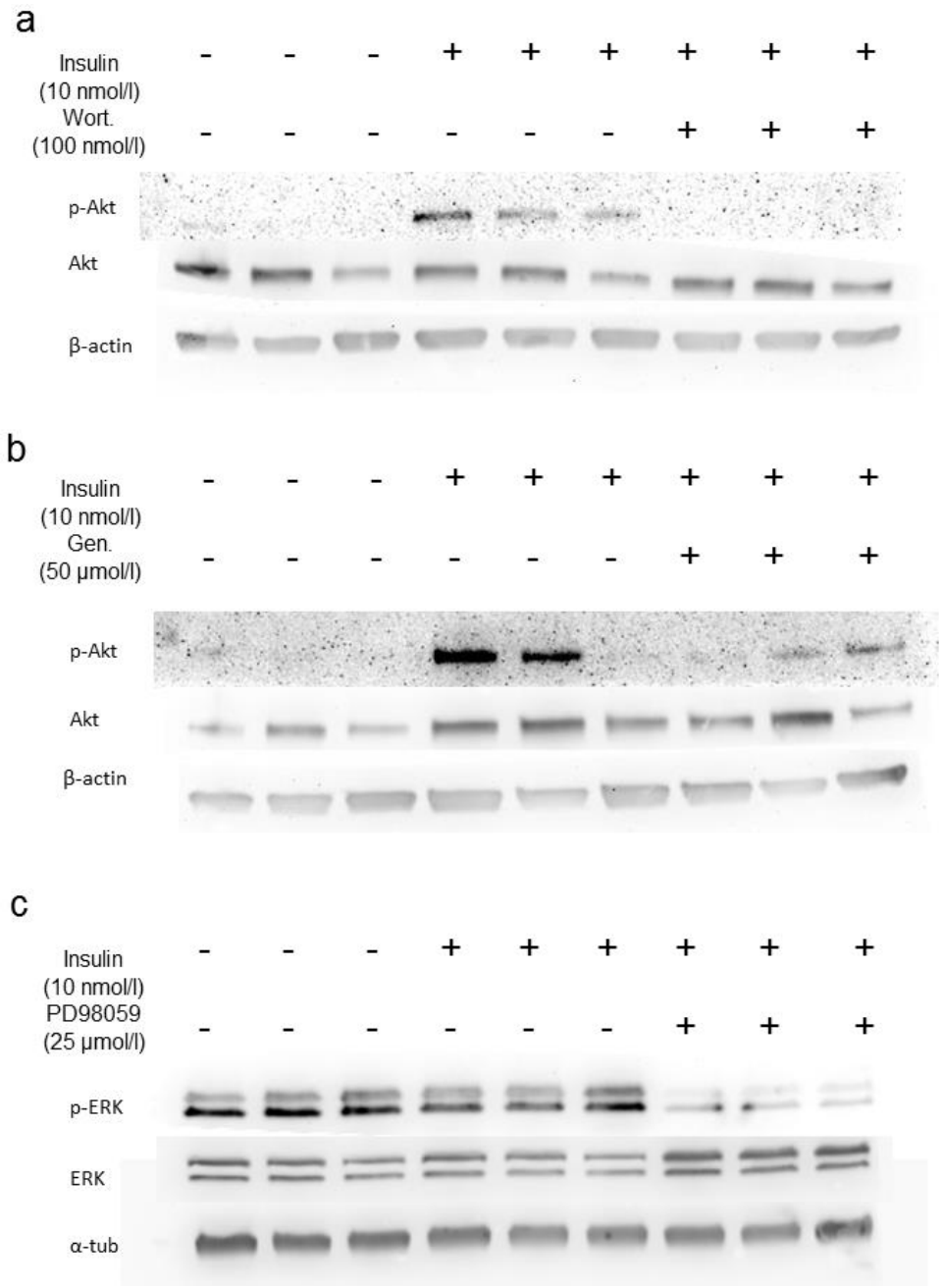

Figure 3-4 Wortmannin, genistein, and PD98059 inhibited insulin-stimulated signaling in RBMVEC.

RBMVECs were serum starved for 2 hr before 30 min pretreatment with wortmannin (wort, a), Genistein (Gen, b), PD98059 (c) and subsequent 15 min incubation with insulin (10 nmol/l) at 37°C. Three individual experiments were run on the same gel.

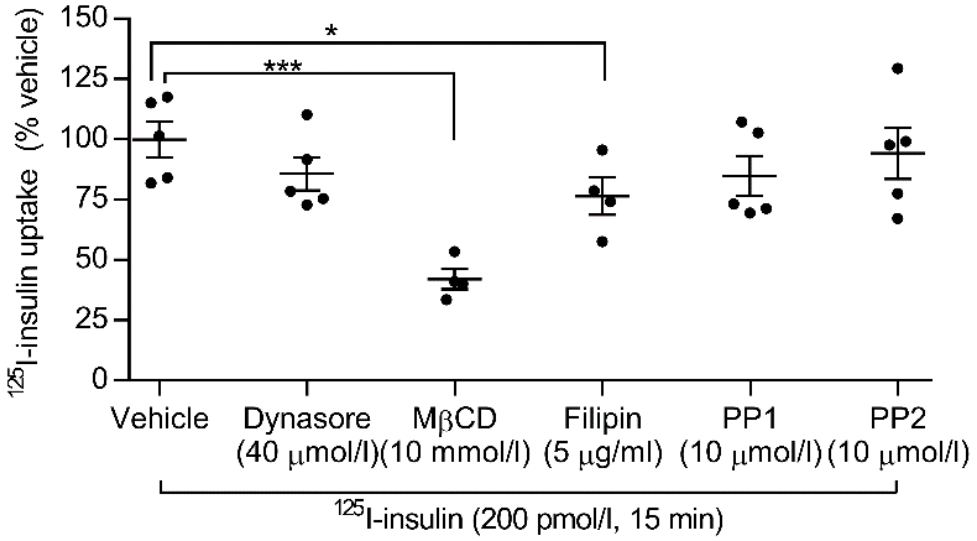

Figure 3-5 Insulin uptake requires lipid rafts.

^{125}I-TyrA14-insulin (^{125}I-insulin) uptake decreased in RBMVECs pretreated with MβCD and filipin. Dynasore, PP1 and PP2 did not decrease uptake. Data presented are means ± SEM, compared using Dunnett's test. *p<0.05, ***p<0.001 vs vehicle.

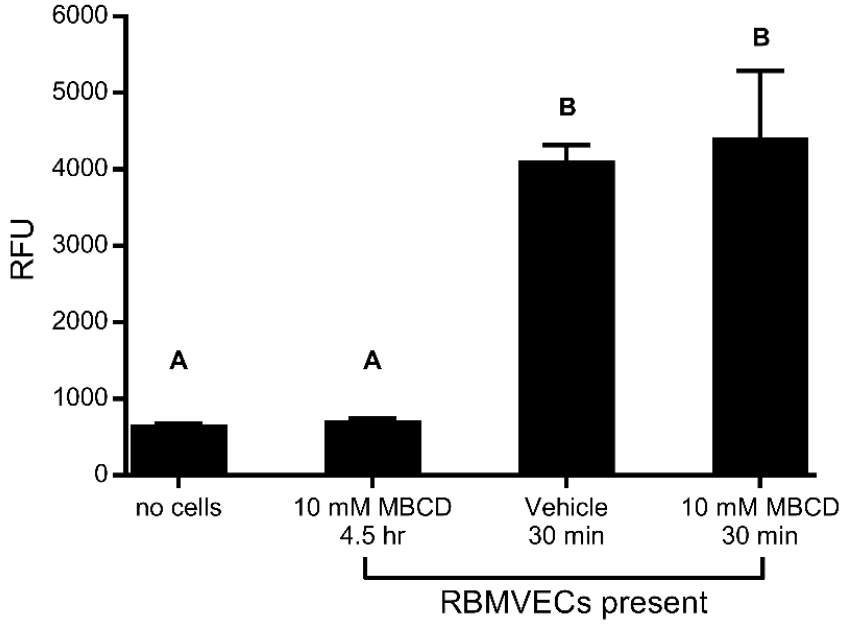

Figure 3-6 MβCD does not decrease RBMVEC viability after 30 min

Cell viability, as quantified by cell titer blue RFU, did not differ between MβCD (10 mmol/L) and vehicle treatment for 30 min. Longer incubations with MβCD caused significant decrease in RFU, comparable to wells without RBMVECs present. Groups were compared by 1-way ANOVA, with Tukey's post hoc comparison between groups. Means ± SEM of RFU from these experiments are shown below. Different letters above groups indicate significant differences ($p<0.01$).

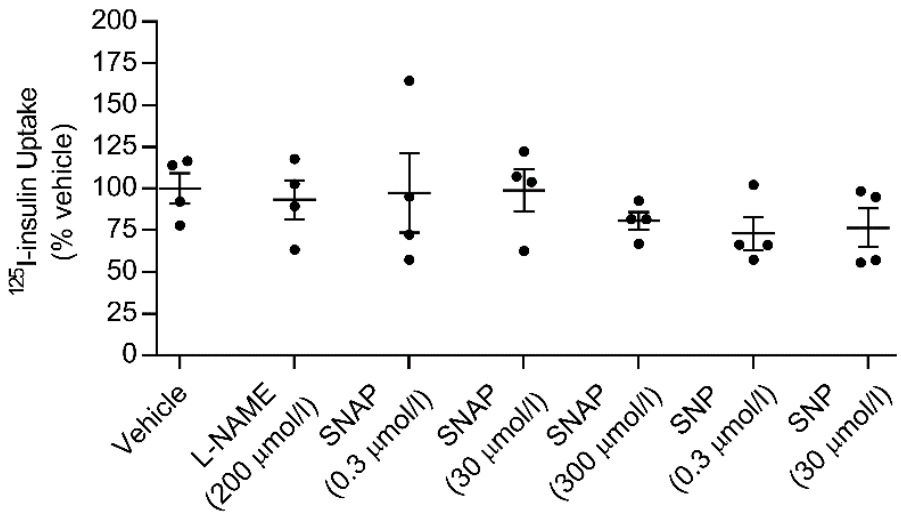

Figure 3-7 ^{125}I-TyrA14-insulin uptake was not affected by nitric oxide (NO) inhibitor (L-NAME) or NO donors (SNAP, SNP).

RBMVECs were serum starved for 2 hr before 30 min pretreatment with drugs and subsequent 15 min incubation with ^{125}I-TyrA14-insulin (^{125}I-insulin, 200 pmol/l) at 37°C. Each circle denotes individual replicate. Data is shown as mean ± SEM and were compared using Dunnett's test. n=4 per condition.

3.2.3 HFD decreases iBEC insulin uptake and increases NFκB binding

In vivo, 4 wk of HFD feeding decreased brain insulin clearance[177], so we purified iBECs from male Sprague Dawley rats fed a ND or an HFD (60% lipid) ad lib for 4 wk. iBECs were cultured for 5–7 days before experiments. HFD rats weighed more than ND rats (479 ± 10 vs 430 ± 9 g, $p<0.01$, $n=17$ per diet). Non-fasting insulin concentrations (HFD = 1.53 ± 0.31 ng/ml, ND = 0.94 ± 0.23 ng/ml, $n=17$ per diet) did not differ (Mann–Whitney test, $p=0.14$**).**

iBECs from HFD rats had 30% lower ^{125}I-TyrA14-insulin (200 pmol/l) uptake compared with ND rats ($p<0.01$,Figure 3-8). In aortic tissues, HFD feeding can increase NFκB p65 activity [187]. Nuclei from HFD iBECs had increased NFκB p65 binding activity compared with ND iBEC nuclei ($p<0.05$, Figure 3-8). Insulin (10 nmol/l, 15 min) increased Akt^{Ser473} (Figure 3-8 c, d) and eNOS^{Ser1177} (Figure 3-9, a) phosphorylation comparably in iBECs from ND and HFD rats ($n=4$ per diet). Insulin did not affect ERK$^{Thr202/Tyr204}$ phosphorylation in either group (Figure 3-9, b). Expression of endocytotic proteins caveolin-1 and clathrin heavy chain did not differ between diet groups and insulin did not increase caveolin-1^{Tyr14} phosphorylation in either group (data not shown). We also compared IR and IDE expression to assess whether this might be driving differences in insulin uptake. We did not detect differences in IR mRNA, IDE mRNA or IR-β protein between iBECs from ND and HFD rats (Figure 3-8 e, f, g).

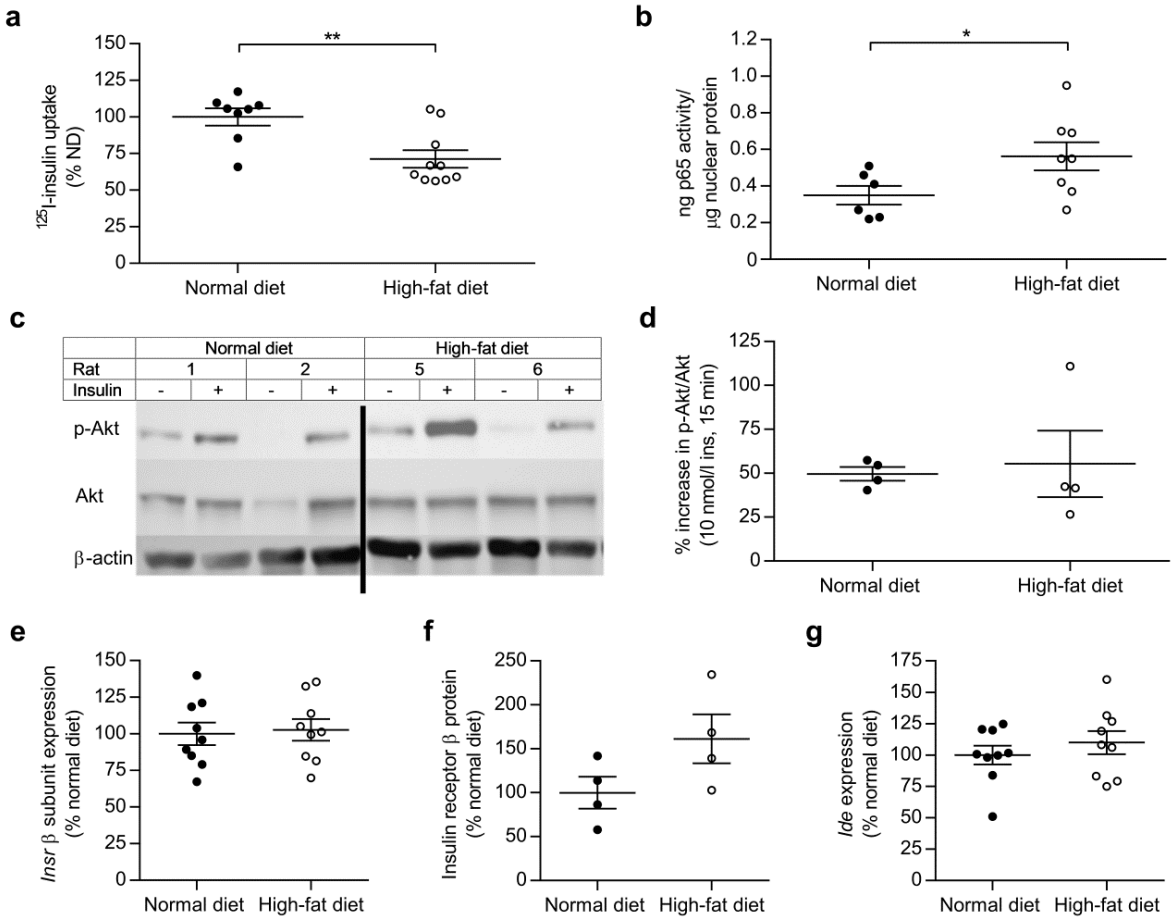

Figure 3-8 HFD feeding decreases insulin uptake and increases NFκB nuclear binding activity in iBECs despite intact IR expression and signaling.

HFD feeding decreased ^{125}I-TyrA14-insulin (^{125}I-insulin) uptake (a) and increased NFκB p65 nuclear binding activity (b) in iBECs. Representative blot (line denotes crop) (c) and quantification (d) of insulin-stimulated (10 nmol/l, 15 min) Akt phosphorylation (p-Akt, normalized to total Akt) did not differ between ND and HFD rats. IR-β (e, f) and IDE expression (g) did not differ between diet groups. White circles, rats fed an HFD for 4 wk; black circles, rats fed an ND for 4 wk. Mann–Whitney *U* test (a, b), Welch's *t* test for non-equal variance (d) and *t* tests (e, f, g) were used to analyze data. Data presented are means ± SEM. *p<0.05, **p<0.01.

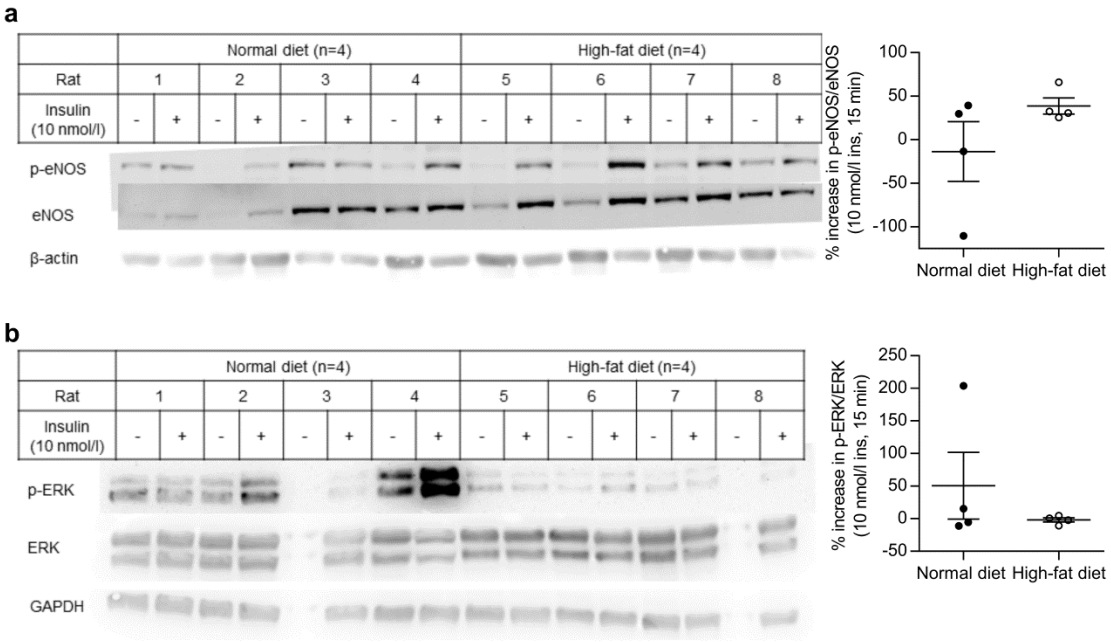

Figure 3-9 Insulin-stimulated eNOS and ERK signaling in iBECs is not significantly affected by HFD.

iBECs from normal diet and high-fat diet fed rats showed signaling following 15 min insulin (10 nmol/l) treatment for p-eNOS ($eNOS^{Ser1177}$, a) and p-ERK ($ERK^{Thr202/Tyr204}$, b). Quantification is phosphorylated protein normalized to total protein.

3.2.4 iBECs transcytose intact insulin

Using our *in vitro* BBB, we first measured the time course for transcytosis of 200 pmol/l ^{125}I-TyrA14-insulin or HD-^{125}I-TyrA14-insulin added to the apical chamber (TEER 362 ± 38 Ω × cm^2). Transcytosis of ^{125}I-TyrA14-insulin (corrected for paracellular leak) increased linearly, with 0.4% of the added ^{125}I-TyrA14-insulin (132 ± 33 fmol) transcytosed at 15 min to 2.4% (728 ± 241 fmol) at 60 min (Figure 3-10, a). Using linear regression (R^2=0.99), we estimated this transport rate at 13.1 fmol/min. To assess the symmetry of this transport, we measured insulin transcytosis 30 min after adding ^{125}I-TyrA14-insulin to the apical or basolateral chamber (TEER 439 ± 55 Ω × cm^2). We found insulin's movement from apical to basolateral or from basolateral to apical was comparable (Figure 3-10, b), indicating that transport is bidirectional.

The brain expresses IDE[185,188], some of which is localized to the BEC[184], and previous reports hypothesize the BEC lysosome degrades insulin[154]. We confirmed that ^{125}I-TyrA14-insulin incubated with HepG2 cells was rapidly degraded [181], giving an elution peak distinctly different from intact ^{125}I-TyrA14-insulin (Figure 3-10, insert). By contrast, media collected from basolateral chambers 30 min after adding ^{125}I-TyrA14-insulin to the apical transwell chamber eluted similar to ^{125}I-TyrA14-insulin that was not exposed to BECs (Figure 3-10, c). Similar results were observed in the apical chamber from these same experiments (Figure 3-11). Thus, we conclude that insulin is transported across iBECs without being degraded.

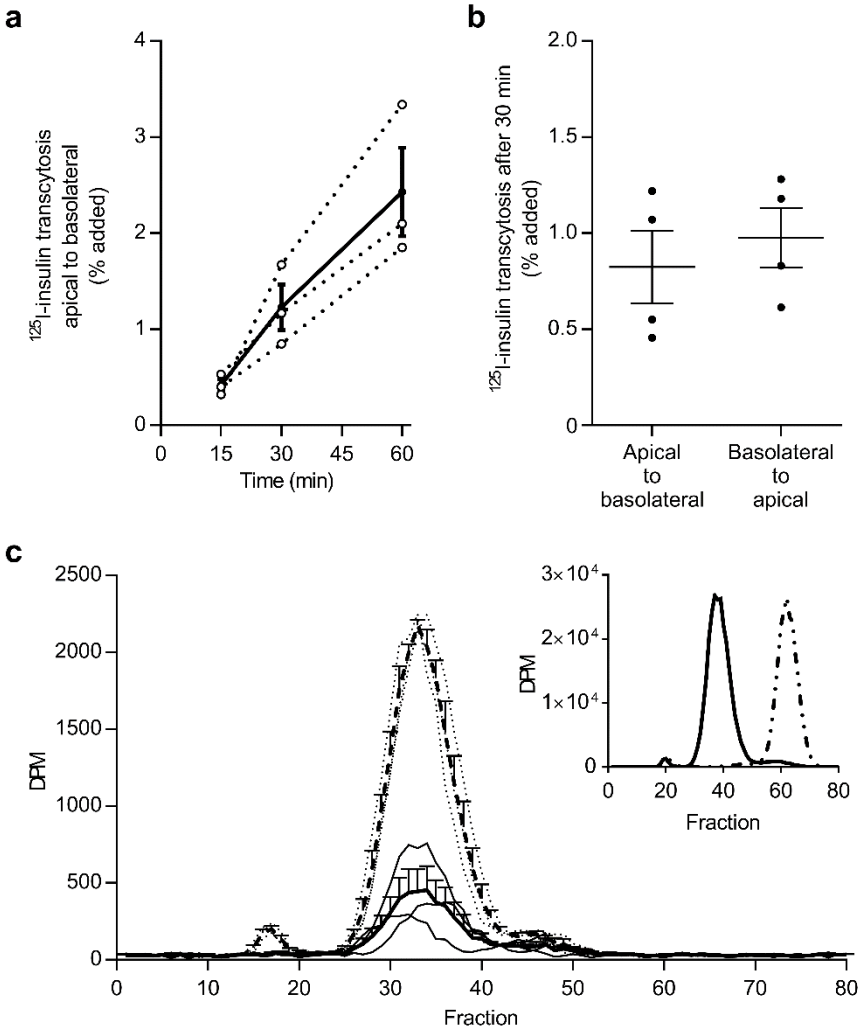

Figure 3-10 ^{125}I-TyrA14-insulin (^{125}I-insulin) is transported across iBECs and remains intact.

^{125}I-TyrA14-insulin transcytosis over 60 min (a). Dotted lines are individual experiments (*n*=3) and solid line is mean ± SEM. Transport of ^{125}I-TyrA14-insulin transcytosis after 30 min is bidirectional and directions did not differ significantly (b). Data are presented as means ± SEM, paired *t* test. Basolateral media radioactivity (DPM) from transwell experiments sampled 30 min after apical ^{125}I-TyrA14-insulin addition eluted from a Sephadex G-50 column in the same fractions in presence (solid line) or absence (dashed

line) of iBECs (c). Thin dotted lines represent individual experiments without iBECs and thin solid lines represent individual experiments with iBECs (*n*=3). These peaks corresponded to intact insulin (insert, solid line) and did not appear in the same fraction as HepG2-degraded insulin (insert, dotted line).

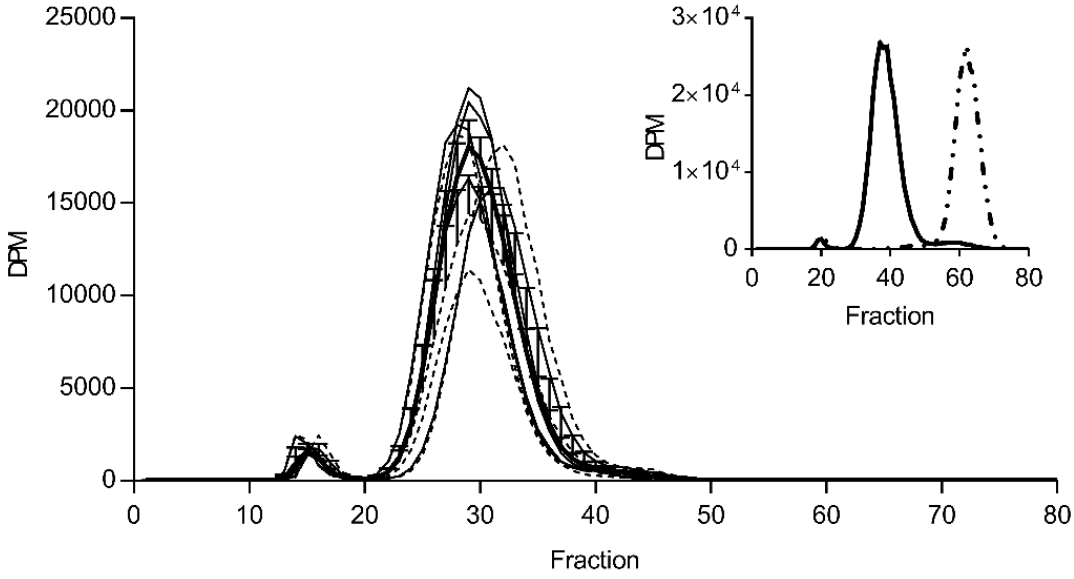

Figure 3-11 Degraded ^{125}I-TyrA14-insulin was not present in the apical transwell chamber.

^{125}I-TyrA14-insulin incubated with or without iBEC for 30 min was collected from the apical chamber (luminal aspect of iBEC), eluted from Sephadex column, and radioactivity in column fractions were quantified (DPM). Dotted line indicates no iBECs present, solid line indicates iBECs were present. Thin lines represent individual experiments and thick lines represent means ± SEM; n=3 without iBEC; n=5 with iBECs. ^{125}I-TyrA14-insulin incubated with iBECs eluted in same fraction as ^{125}I-TyrA14-insulin that was not exposed to iBEC. ^{125}I-TyrA14-insulin degraded by HepG2 cells eluted much later, for reference (insert).

3.2.5 IR and endocytosis machinery regulate transcytosis

To test IR's role in transcytosis, iBECs were pretreated with 10 nmol/l S-961 for 30 min before adding either 200 pmol/l ^{125}I-TyrA14-insulin or HD-^{125}I-TyrA14-insulin to the apical side of the transwell insert (TEER 284 ± 72 Ω × cm^2). S-961 specifically decreased insulin transcytosis (p<0.05, Figure 3-12, a), affirming IR's role in insulin uptake and transcytosis. Dynasore decreased transcytosis by 40% (p<0.05), while filipin did not decrease transcytosis significantly (Figure 3-12, b, TEER 440 ± 84 Ω × cm^2). MβCD greatly increased paracellular leak (>200%) and therefore was not investigated further.

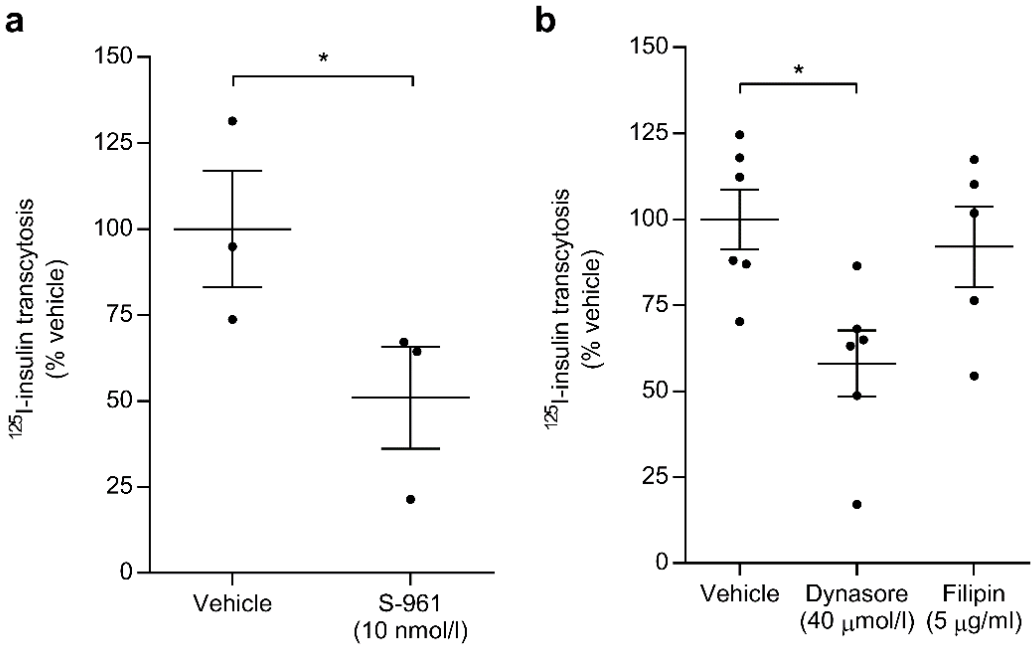

Figure 3-12 ^{125}I-TyrA14-insulin (^{125}I-insulin) is transported across iBECs by IR and dynamin-mediated vesicles.

IR antagonist S-961 blunted ^{125}I-TyrA14-insulin transcytosis across iBECs (a). ^{125}I-TyrA14-insulin transcytosis was decreased by pretreatment with dynasore, but the effect of filipin was not significant (b). Data presented are means ± SEM, paired *t* test vs vehicle control. *p<0.05 vs vehicle.

3.2.6 Neurovascular coupling can affect insulin transcytosis

Knowing neurovascular coupling regulates IGF-1 transcytosis[22], we investigated whether astrocyte stimulation affected insulin transcytosis. Using our BBB model, we treated the astrocytes in the basolateral ('brain') chamber with L-glutamate (100 μM) before adding 200 pmol/l ^{125}I-TyrA14-insulin to iBECs in the apical ('blood') chamber. Glutamate increased insulin transcytosis across the iBEC monolayer by 30% (p<0.05, TEER 473 ± 182 Ω × cm^2, Figure 3-13, a), without affecting HD-^{125}I-TyrA14-insulin transport. Apical pretreatment with L-NAME for 30 min decreased ^{125}I-TyrA14-insulin transcytosis (p<0.001, TEER 429 ± 115 Ω × cm^2, Figure 3-13, b) and adding glutamate (basolateral) with L-NAME (apical) restored insulin transcytosis to control rates (TEER 534 ± 42 Ω × cm^2, Figure 3-13, c). L-NAME and glutamate treatment did not affect HD-^{125}I-TyrA14-insulin transcytosis. Glutamate can increase calcium signaling in astrocytes[189]. We pretreated astrocytes with thapsigargin (1 μmol/l) to increase cytosolic calcium 30 min prior to glutamate or vehicle treatment for an additional 30 min (TEER 476 ± 45 Ω × cm^2). Thapsigargin alone trended towards increasing ^{125}I-TyrA14-insulin transcytosis (p=0.07, Figure 3-13, d). Thapsigargin and glutamate co-treatment increased transcytosis vs vehicle (p<0.05, Fig. Figure 3-13, d) but the effect was not additive with glutamate, consistent with glutamate acting by increasing astrocyte cytosolic calcium. Thapsigargin increased HD-^{125}I-TyrA14-insulin transcytosis, but increased transcytosis persisted after correcting for this.

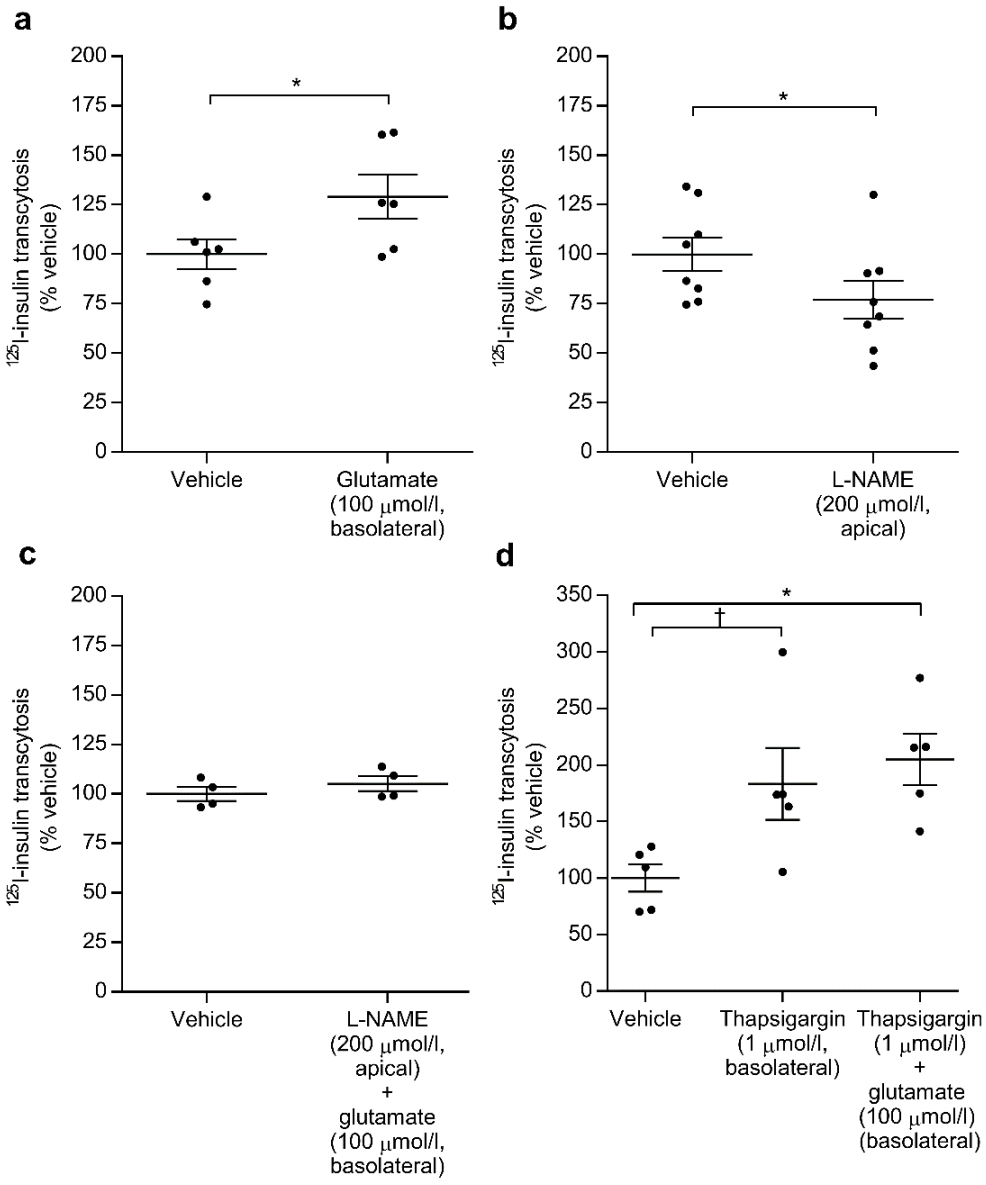

Figure 3-13 ^{125}I-TyrA14-insulin (^{125}I-insulin) transcytosis is increased by glutamate stimulation and cytosolic calcium at the astrocyte and inhibited by NO blockade.

^{125}I-TyrA14-insulin transcytosis was stimulated by basolateral glutamate pretreatment (a) and decreased by apical L-NAME pretreatment (b). Combined basolateral glutamate and apical L-NAME restored L-NAME-induced decreases in transcytosis (c). Basolateral

thapsigargin pretreatment tended to increase transcytosis (p=0.07), and combination of basolateral thapsigargin and subsequent glutamate increased transcytosis (d). Thapsigargin treatment did not differ significantly from thapsigargin and glutamate treatments combined. Data presented are means ± SEM, paired t test vs vehicle (a–c), one-way ANOVA with Tukey's post hoc (d). $^{\dagger}p$=0.07, $*p$<0.05.

3.3 Discussion

The results presented here demonstrate that BEC insulin transport is IR-dependent, but does not require intact insulin signaling through PI3K. Second, insulin transport requires lipid raft functionality, consistent with a vesicular endocytotic process. Third, despite the presence of proteases, such as IDE, insulin remains intact during BEC transcytosis. Fourth, insulin transport can be regulated by astrocyte stimulation, as evidenced by glutamate-induced increases in transport. Finally, *in vivo*, HFD feeding has sustained effects to diminish insulin uptake and increase basal NFκB binding activity in cultured iBECs.

Multiple studies have demonstrated saturable insulin binding to brain microvessels or retention by brain tissue, consistent with IR-mediated transport. However, these studies did not eliminate a role for IGF-1R or IGF-1R/IR hybrid receptors present on endothelial cells[190]. Our use of the specific IR-blocker S-961 and physiological insulin concentrations strongly support IR-facilitated insulin transport at physiological insulin concentrations. Inhibition of insulin-stimulated PI3K signaling did not decrease insulin uptake, suggesting BECs regulate insulin transport differently from aortic endothelial cells[142]. Insulin stimulates ERK phosphorylation within 15 min in bovine aortic endothelial cells. We did not detect ERK phosphorylation and cannot implicate any role for this in BEC insulin transport. However, vesicular transport of insulin appears to be conserved between peripheral and brain ECs. Our studies emphasize

the importance of lipid raft formation and dynamin-mediated vesicle budding for insulin uptake and transcytosis. Filipin did not decrease insulin transcytosis despite inhibiting uptake. This may be due to residual serum in the conditioned media in the basolateral chamber, which may have reversed filipin action[191].

We are unaware of prior studies of insulin transport across an intact *in vitro* BBB. Miller et al preloaded bovine BECs for 30 min with ^{125}I-TyrA14-insulin before measuring an additional 90 min of tracer efflux. After 30 min efflux, they found <5% of insulin was degraded as assessed by trichloroacetic acid precipitation[154]. Unfortunately, neither TEER nor permeability markers were measured, making it difficult to resolve whether the luminal or abluminal membrane mediated efflux. In our studies, TEER and HD-^{125}I-TyrA14-insulin measurements indicated tight iBEC monolayers and insulin degradation was not detected in the apical or basolateral media of iBECs.

Glutamate's action to increase insulin BEC transcytosis suggests astrocytes can regulate BBB insulin transport. Neuronal activation and subsequent downstream release of astrocyte-derived factors facilitates IGF-1 BBB transcytosis [22]. In response to glutamate, astrocytes increase cytosolic calcium and secrete factors such as PGE_2 or EET, which may influence BEC transcytosis[22,52]. While NOS blockade reduces astrocyte glutamate uptake[192], we observed that glutamate stimulation of astrocytes rescued L-NAME-induced decreases in insulin transcytosis. It is possible that these are acting through unrelated mechanisms and that the glutamate action on astrocytes induces the secretion of factors that counteract the eNOS inhibition in iBECs. L-NAME and NO donors did not affect insulin uptake, which may be due to methodological differences or may suggest a role for NO in regulating either intracellular vesicle trafficking or

exocytosis (i.e. steps beyond uptake). Thapsigargin treatment of astrocytes tended to increase transcytosis, yet did not differ significantly from combination of thapsigargin and glutamate. This suggests elevated cytosolic calcium may mediate glutamate-stimulated increases in insulin transcytosis across the BEC layer. Elucidating the regulation of BEC transcytosis merits further investigation.

The decrease in ^{125}I-TyrA14-insulin uptake by iBECs from rats fed an HFD for 4 wk is particularly intriguing. Mechanistically, we did not find evidence for altered canonical insulin signaling to Akt or eNOS. However, increased oxidative stress, acting via increased NFκB binding activity, may contribute. While we[177] and others[82,83,91,94] found a delay of insulin entry into or action in the brains of HFD-fed animals, this is the first study to our knowledge to report impaired insulin transport at the level of the BEC. Our co-culture findings, as well as recent work regarding insulin signaling in astrocytes[170,171], may suggest a role for astrocytes in the effect of an HFD on BBB insulin transport. Given the clinical importance of brain insulin resistance, the latter possibly warrants further investigation.

We previously reported that insulin brain uptake *in vivo* is ~40-fold greater than its transfer to CSF[177] While production of insulin within brain tissue has been reported[121], our studies strongly indicate that insulin detected in the brain can originate from plasma. Insulin's transport across the BBB occurs first at the BEC, involves IR (not IGF-1R or IGF-1R/IR hybrids) and lipid rafts, and there is no detectable degradation of insulin during transcytosis despite the presence of IDE and other proteases. Finally, the ability of HFD feeding and astrocyte activation to affect insulin transport highlights the complex and multifaceted regulation of insulin's entry into brain. These results materially advance

our understanding of the pathways involved in brain insulin transport, highlight the previously unrecognized role of the astrocyte in BBB insulin transport, and offer potential pathways for ameliorating central insulin resistance.

CHAPTER 4 CONCLUSIONS AND FUTURE DIRECTIONS

Brain insulin may regulate feeding behavior, hepatic metabolism, and cognition, yet prior to this work it was not understood neither how physiological insulin concentrations may cross the BBB nor how diet may affect this process. The work described in this thesis, as well as another recent publication from our lab[177], has begun to elucidate how insulin is transported across the BBB.

In vivo studies demonstrated that intravenously-administered physiological concentrations of radiolabeled insulin were detected the brain before appearing in the CSF. This transport is dependent on the IR and decreased in rats fed 4 wk of HFD[177]. These studies used brain tissue samples and were unable to resolve insulin's exact location, i.e. whether insulin was bound to the luminal aspect of the endothelium, within the endothelial cell, or within the BISF after crossing the BBB. The studies were the foundation for those presented in this dissertation, which have begun to elucidate the cellular machinery that regulates insulin transport across the BBB.

The work presented here demonstrates that insulin transport is: 1) dependent on IR, 2) not dependent on insulin-stimulated signaling through PI3K or MEK, 3) requires intact lipid rafts, 4) increased by astrocyte stimulation, 5) decreased following four wk of HFD. Based on work in the periphery, we hypothesized that insulin transport across the BEC would be dependent on IR and downstream signaling through PI3K and/or MEK. To our surprise, this was only partially conserved in the brain endothelium. This highlights differences in the peripheral vasculature compared to the brain. Additionally, these data support the notion that different cell types within the BBB, e.g. astrocytes, may work in concert to facilitate transport of circulating substances into the brain. These

findings suggest neurovascular coupling may facilitate the transport of insulin across the BBB. Lastly, the finding that HFD feeding can decrease insulin uptake in iBECs is the first to describe insulin resistance at the level of the brain vasculature. This suggests that the brain endothelium is sensitive to changes in diet and diet may influence the transport of other hormones, nutrients, and substances across the BBB.

These findings are exciting and only begin to elucidate the complex regulation of blood-brain barrier transport and the effect of high-fat diet. Thus, there are many opportunities for continued study to improve our understanding of basic physiology as well as diet-induced changes in these mechanisms.

Intravenously-injected radiolabeled insulin appears in brain tissue within five minutes and is undetectable in cerebrospinal fluid at this time, indicating that insulin transport through the cerebrospinal fluid circulation is likely not the pool through which insulin exerts its main effects in the CNS[177]. In these studies, the vasculature was flushed with saline; however, in the brain tissue samples, we were unable to resolve whether insulin was bound to the exterior of the BEC, within the BEC, or had crossed the BEC and entered the Virchow-Robin/perivascular space or the brain interstitial fluid. The work presented in this thesis clarifies the first step of this transport process, as we have accumulated substantial evidence that BECs take up and transcytose insulin in an *in vitro* BBB system. Going forward, confirming these findings *in vivo* is necessary. Imaging radiolabeled insulin by autoradiography is not sufficiently precise to determine the relative distribution of insulin between the VRS, BISF, or the various cells of the BBB. Fluorescently-tagged insulin is less biologically active than radiolabeled insulin, necessitating higher dosages. Numerous fluorescently-tagged insulins are commercially

available; however, evidence that these products are bioactive is either unavailable or nonexistent. In our hands, FITC-labeled insulin (FITC-insulin) is biologically active, though the fluorophore is sensitive to bleaching and can require the use of a subsequent anti-FITC primary antibody with a fluorescent secondary. Our preliminary work using live isolated capillaries supports use of FITC-insulin in this capacity (Figure B-1). Improving the image collection could potentially help determine whether insulin is being transported from the abluminal aspect of the capillary

The combined use of fluorescently-tagged insulin and antibodies against the cell types of the BBB could perhaps clarify the location of transported insulin in brain sections as suggested by pilot experiments (Figure B-2, Figure B-3,Figure B-4). Moreover, these experiments could examine whether insulin moves differently at various levels of the vasculature (e.g., arteriole versus capillary) or in different areas of the brain (e.g., the fenestrated median eminence as compared to the BBB in the cerebellum).

The work detailed in this thesis is the first to suggest neurovascular coupling as a mechanism for increasing insulin transport across the brain endothelium. Neurovascular coupling serves principally to increase blood flow to supply increased oxygen and nutrients to areas of neuronal activation[48], but has also been implicated in the transcytosis of IGF-1 across the BBB[22]. Stimuli such as exercise[193], environmental enrichment[194], and whisker stimulation[22] increase IGF-1 transcytosis across the BBB. We have yet to explore what stimuli promote insulin movement across the BBB. Postprandial increases in circulating insulin concentrations provide an increased pool of insulin to travel across the BBB. Future work could explore the potential role of glucose or amino acid-mediated

neuronal stimulation in increasing insulin transcytosis across the BBB. These questions could be explored using an *in vitro* system or, perhaps, in an *in vivo* model.

In vivo imaging of neurovascular coupling is possible and it is likely that techniques will advance in the upcoming years to increase resolution. Intravenously-injected AlexaFluor 633 binds to the elastin in arteries and arterioles, allowing for real-time, 2-photon imaging of vasodilation and vasoconstriction, which can be combined with measurements of neuronal calcium changes via Oregon Green 488 Bapta-1 acetoxymethyl ester[195]. While this may be difficult to combine with FITC-insulin imaging, exploring potential changes in neurovascular coupling in animals fed HFD. Use of fluorescent dextrans to label the blood vessels or Virchow Robin/perivascular space or AlexaFluor 633 labeling of arteries and arterioles could be combined with intravenous FITC-insulin injections in attempts to localize FITC-insulin movement across the BBB in fixed or live sections. Live *in vivo* 2 photon imaging is limited as to how deep into the brain imaging can go, and at this point, resolution at the capillary level has not been reported. Indeed, undertaking of the study of *in vivo* insulin movement across the BBB in concert with imaging neurovascular coupling is a technically-challenging endeavor.

At the level of the BEC, there is much that remains to be uncovered regarding the mechanisms of insulin transport and the role HFD feeding has in decreasing this process. As presented in this dissertation, insulin signaling through PI3K or MEK does not mediate insulin uptake in the BEC, which is in contrast to the periphery. However, the importance of NO in insulin transcytosis appears conserved between the BEC and the peripheral endothelium. Peripherally, insulin signaling increases eNOS activity, generating NO and causing vasodilation[141,196,197]. While this mechanism does not appear

to be conserved in the BEC, NO appears to play a role in either transcytosis or exocytosis. In our *in vitro* co-culture setting, it is likely that NO is produced from eNOS activity; however, *in vivo*, NO may potentially be generated from neurons via neuronal nitric oxide synthase (nNOS). In HFD-fed mice, decreased NO production in the endothelium preceded the development of insulin resistance[198]. Whether HFD feeding induces similar changes in the brain endothelium or in neurons to reduce NO generation remains unknown. Importantly, NO is also known to affect caveolae function in endothelial cells[199]. Whether this is conserved in the BEC and whether this relationship is altered by HFD remains to be discovered.

Lipid rafts are critical for endocytosis and transcytosis in the peripheral endothelium and BECs. Given our findings that lipid rafts are critical for insulin transport in the BEC, further investigation into the regulation of lipid raft-mediated transport is warranted. Recent work has investigated the interactions between lipid raft-mediated endocytosis and lipid transporters in the brain endothelium. Major facilitator superfamily domain-containing protein 2 (Mfsd2a), a lipid flippase in the plasma membrane of BECs, transports docosahexaenoic acid and other lipids[200,201] and regulates caveolae-mediated transcytosis[202]. When knocked out, Mfsd2a mice have BBB development defects, including increased caveolae vesicles and leaky barriers, despite intact tight junctions[202,203]. Thus, lipids transported Mfsd2a serve to inhibit cav-1 function[202]. Given our findings regarding the importance of lipid rafts in facilitating insulin uptake and dynamin in regulating insulin transcytosis, this newfound regulation of caveolae-mediated transport by a lipid flippase provides a potential new regulatory mechanism for transport of numerous substances, potentially including insulin. Moreover, given our

findings, it may be helpful to explore the effect of HFD feeding on lipid composition in the BEC. Dietary fat may affect membrane lipid composition and function[204]. Whether high-fat diet induces changes in the lipid composition of the BEC plasma membrane that may impact uptake of insulin, and other hormones, is an area that deserves attention.

Beyond further investigation into insulin uptake and transcytosis, whether insulin is degraded following transcytosis across the BEC remains an open question. Insulin is generally degraded intracellularly in the lysosome, though there is some evidence that IDE can degrade circulating insulin[205]. Despite its name, IDE degrades numerous peptides and hormones[206]. Its ability to degrade amyloid-β protein[206,207], has made it an attractive target for Alzheimer's disease research. Insulin degrading enzyme is present in the BEC[184,208] and within brain tissue[185]. Additionally, it may be secreted from many cell types[209], including astrocytes[210]. Insulin degrading enzyme has been detected in CSF of healthy controls and individuals with dementia[211]. Whether IDE in brain tissue or CSF serves to regulate insulin degradation in the brain is unknown. Additionally, the role of this protease in both type 2 diabetes and Alzheimer's disease progression is complicated[206]. Going forward, insulin degradation in the brain could be addressed in multiple ways. Continuing with the imaging of intravenously-injected insulin (Appendix B), addition of markers for intact insulin would be beneficial. For example, use of both an anti-FITC antibody and an anti-insulin antibody may allow detection of intact FITC-insulin, as opposed to detection of the FITC tag, which may be cleaved from insulin during degradation. Additionally, use of immunofluorescence and/or immunohistochemistry could examine co-localization of FITC-insulin with downstream

signaling markers, such as phosphorylated Akt. Successful colocalization would indicate biological activity of the FITC-insulin and suggest the peptide remains intact.

While we did not detect differences in *Ide* expression between iBECs from ND and HFD animals, it is curious whether diet could have an effect on IDE production. We did not measure protein concentrations or activity levels. Perhaps iBECs from HFD rats have increased IDE activity, which then results in decreased insulin uptake. It is also curious whether HFD could affect IDE content in whole brain tissue, CSF, or other cell types of the BBB. These pursuits may enhance our understanding of insulin transport and metabolism in the brain and, potentially, link type 2 diabetes to Alzheimer's disease.

In conclusion, while we have begun to elucidate insulin transport across the brain vasculature and the effect that high-fat diet may have on this process, much remains to be discovered. The opportunities for continuing this research forward are many and continued investigation has the potential to impact our understanding of how diet, insulin resistance, and type 2 diabetes may affect the brain. This has implications not only for diabetes, but also for dementia and Alzheimer's disease.

APPENDIX A CALCULATED CSF INSULIN CONCENTRATIONS

Table A-1 Studies infusing insulin into third ventricle of rat

Authors	Insulin dose (mU/d)	CSF volume (mL)[9]	Total Dose (µU/mL/d)	Conversion factor to pmol/L	CSF insulin (pmol/L)	CSF insulin (nmol/L)
Brief & Davis[89]	5	0.156	32051	7.174	229936	230
Brief & Davis[89]	7.5	0.156	48077	7.174	344904	345
Brief & Davis[89]	10	0.156	64103	7.174	459872	460
Ikeda et al.[95]	2	0.156	12821	7.174	91974	92
Arase et al. [93]	20	0.156	64103	7.174	459872	460
Chavez et al. [90]	6	0.156	64103	7.174	275923	276
Chavez et al. [91]	6	0.156	64103	7.174	459872	460
Chavez et al. [91]	10	0.156	38462	7.174	275923	276
Obici et al. [99]	0.03	0.156	192	7.174	1380	1
Clegg et al. [82]	8	0.156	25641	7.174	367897	368
Pocai et al. [98]	0.03	0.156	192	7.174	1380	1
Pocai et al. [98] *	0.002					
Clegg et al. [83]	4	0.156	192308	7.174	183949	184
Clegg et al. [83]	8	0.156	25641	7.174	367897	368
Begg et al. [94]	8	0.156	51282	7.174	367897	368

*Intrahypothalamic infusion, no estimate on CSF volume

Table A-2 Studies infusing insulin into CSF of large animals

Authors	Species	Dose (mU/kg)	Weight (kg)	Insulin dose (mU/d)	CSF volume (mL)	Total Dose (µU/mL/d)	Conversion factor to pmol/L	CSF insulin (pmol/L)	CSF insulin (nmol/L)
Woods et al.[79]	Baboon	0.001	15	0.015	1 *	15	7.174	108	0.1
Woods et al.[79]	Baboon	0.01	15	0.15	1 *	150	7.174	1076	1.1
Woods et al.[79]	Baboon	0.1	15	1.5	1 *	1500	7.174	10761	10.8
Foster et al.[92]	Sheep	––	––	––	––	255 †	7.174	1829	1.8
Ramnanan et al.[102]	Dog	––	––	––	––	69.5 ‡	7.174	499	0.5

* Woods et al. estimated CSF volume at 1 ml in the baboon[79]
† Foster et al. measured and reported in study[92]
‡ Ramnanan et al. measured and reported in study[102]

APPENDIX B DETERMINING INSULIN TRANSPORT ACROSS INTACT BRAIN VASCULATURE

This appendix depicts preliminary attempts to examine the movement of fluorescently-tagged (FITC) insulin in isolated brain capillaries and brain sections. The goal of these studies is to determine whether FITC-insulin is transported across the BBB and refine these techniques with the ultimate goal of confirming our *in vitro* studies and further investigating the regulation of insulin transport across the BBB.

B.1 FITC-insulin binds to brain capillaries

Brain capillaries were isolated from retired male breeder Sprague Dawley rats per established techniques[212]. Live, freshly-isolated brain capillaries were incubated with 50 nmol/L FITC-insulin or vehicle control and live imaged for 30 min. Differential interference contrast images and fluorescent images were taken to co-localize FITC-insulin within the isolated capillaries. FITC-insulin treated capillaries had detectable fluorescence in the 488 channel colocalized with capillaries, indicating FITC-insulin binding (Figure B-1). In contrast, vehicle-treated live capillaries did not exhibit background fluorescence in the 488 channel, indicating that FITC-insulin movement was detectable in live isolated capillaries.

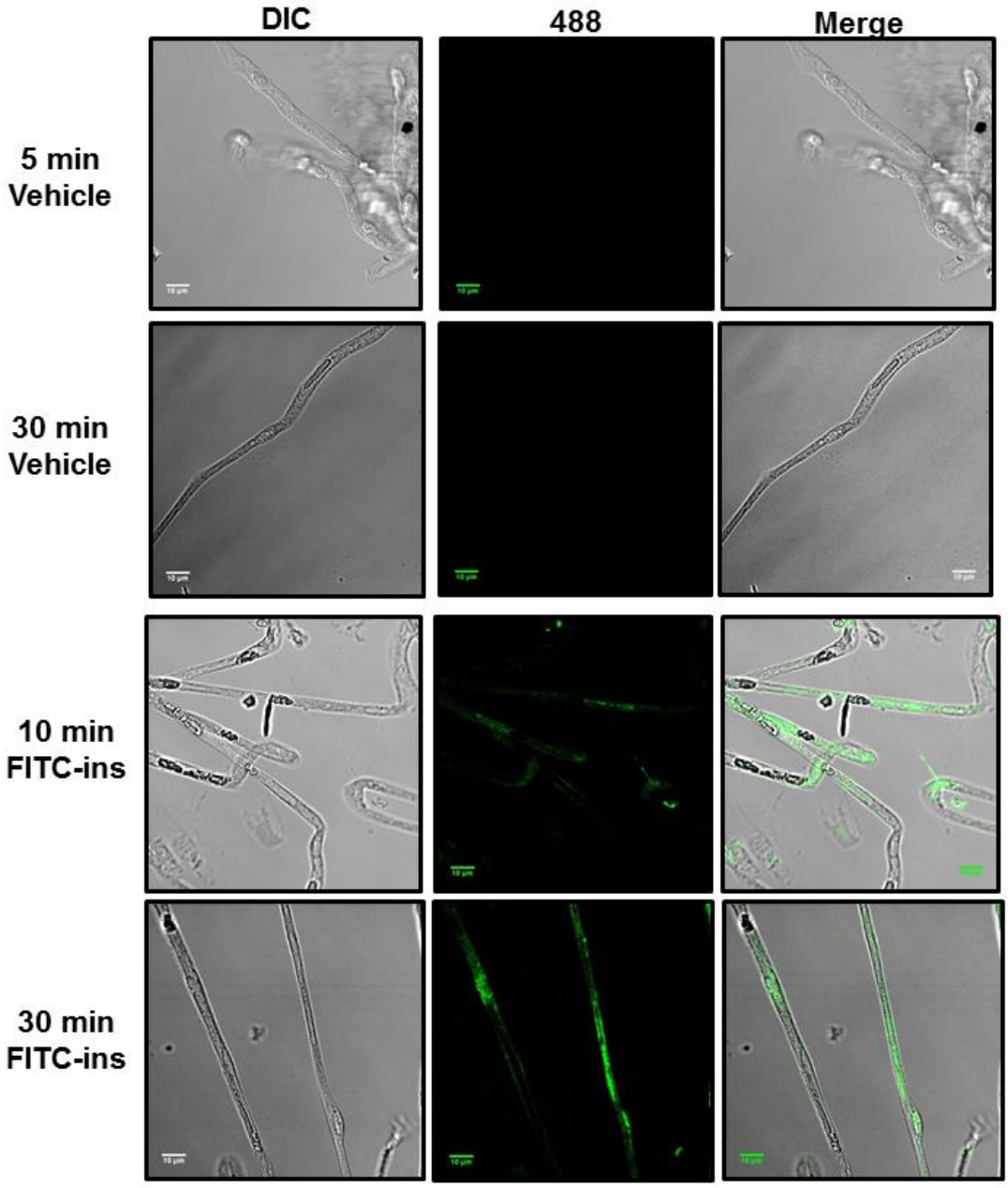

Figure B-1 FITC-insulin binds to isolated brain capillaries.

Isolated brain capillaries incubated with vehicle did not emit in the 488 channel. Capillaries incubated with 50 nmol/L FITC-insulin (FITC-ins) showed fluorescence throughout a 30 min incubation. Representative images are shown with differential interference contrast (DIC) indicating capillary location, 488 depicting fluorescence, and merge depicting the FITC-ins location within capillary. Scale bar is 10 μm.

B.2 Intravenously-injected insulin exits the vasculature

Adult (>8 wk) Sprague Dawley rats received carotid catheters and were infused with 100 mU/kg/min of FITC-insulin for 15 min. Then, rats received a bolus infusion of Texas Red-labeled dextran (70 kD, TR-d70) at 7.5 mg/kg to label the vasculature. This size dextran is unable to cross the endothelium. Rats were perfused with 4% paraformaldehyde and brain tissue was post fixed for 72 hr. Brains were sectioned into thick sections (300 µm) imaged using a Zeiss 780 system with a pulse multiphoton laser. Texas Red and FITC-insulin were excited at 780 nm, with FITC emitting at 520 nm and Texas Red emitting at 615 nm with the goal of detecting FITC-ins outside of the brain vasculature. These experiments suggested some colocalization of FITC-insulin within and just beyond the labeled vasculature. However, no vehicle control was successfully imaged and these results should be interpreted with caution.

Later experiments employed an anti-FITC antibody (Invitrogen, ANZ0202) and fluorescently-tagged secondary to improve the detection signal of the infused insulin. Brain sections from the same animals described above were used to determine whether anti-FITC antibody was useful. Preliminary images suggested that anti-FITC antibody may be useful for visualizing FITC-insulin movement in brain sections (Figure B-3).

In a separate experiment, FITC-insulin infused rats were infused for 15 min (100 mU/kg/min) and then the vasculature was flushed with saline before fixation with paraformaldehyde. Aquaporin 4 antibodies were used to depict astrocytic endfeet and

isolectin staining was used to show the endothelium. This pilot experiment showed small amounts of staining between the endothelium and the astrocyte endfeet (Figure B-4).

Collectively, these studies show promise at detecting FITC-insulin movement across the brain endothelium. However, much remains to be done. Of note, more controls need to be added. Ideally, infusion of a FITC-labeled dextran or inulin, which would not be expected to cross the BBB, would serve as a vehicle control.

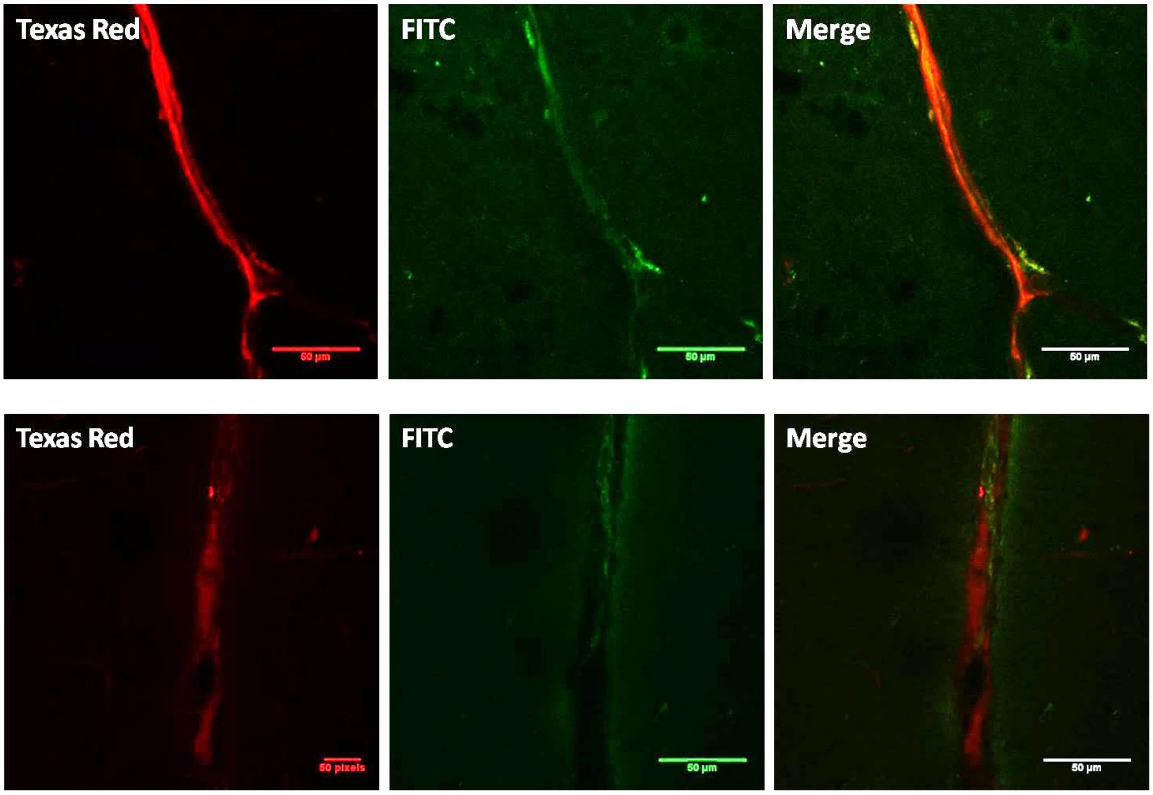

Figure B-2 FITC-insulin and Texas Red dextran fluorescence

Two vessels from a rat infused with FITC-insulin was infused intravenously (100 mU/min/kg) and subsequent bolus infusion of TR-d70 (7.5 mg/kg). Scale bar is 50 µm.

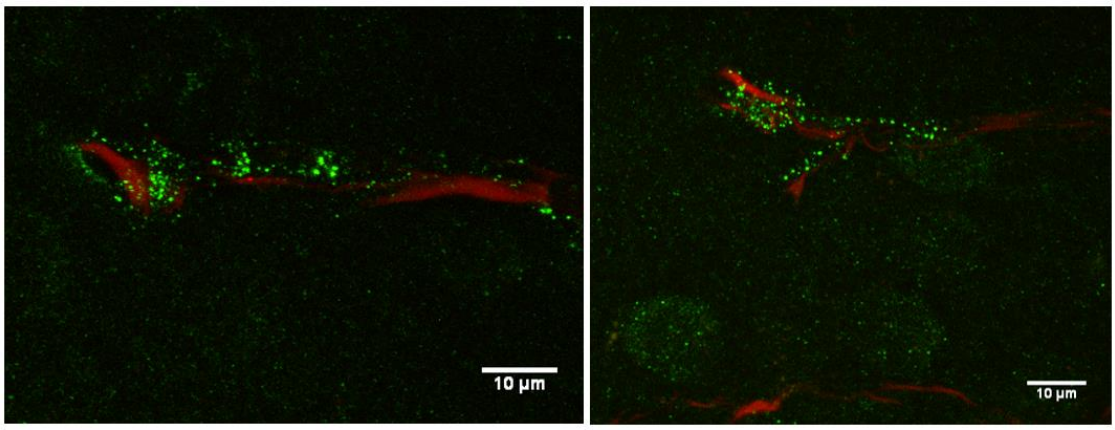

Figure B-3 FITC-insulin and Texas Red dextran immunofluorescence

Two vessels from a rat receiving intravenous infusion of FITC-insulin (100 mU/min/kg) and subsequent bolus infusion of TR-d70 (7.5 mg/kg). Anti-FITC antibody and fluorescent secondary (green) was used to enhance FITC signal. Scale bar is 10 µm.

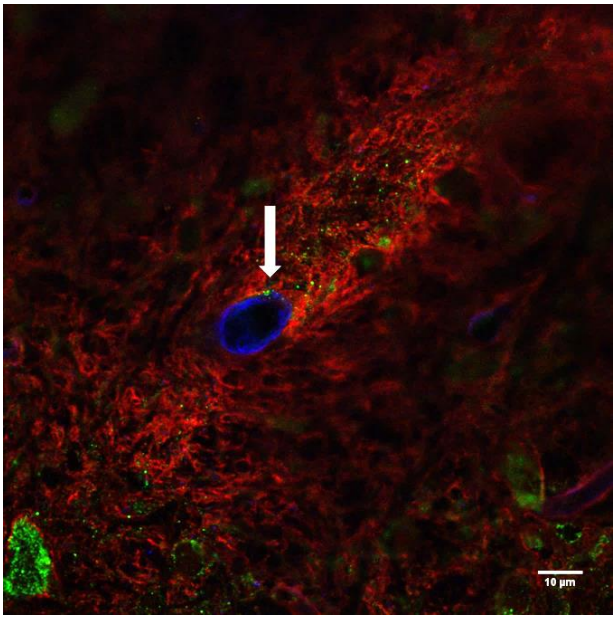

Figure B-4 Intravenously-injected FITC-insulin appears in the perivascular space

FITC-insulin (green) insulin was infused intravenously (100 mU/min/kg) and its appearance was detected in brain sections. Isolectin (blue) staining for the endothelium and aquaporin 4 (red) staining for the astrocyte endfeet indicates that FITC-insulin may localize to the perivascular space (indicated by white arrow). Scale bar is 10 µm.

PUBLICATIONS RESULTING FROM THIS WORK

Gray SM, Aylor KW, Barrett EJ. 2017. Unravelling the regulation of insulin transport across the brain endothelial cell. *Diabetologia*. DOI: 10.1007/s00125-017-4285-4 (In press).

Meijer RI, **Gray SM**, Aylor KW, Barrett EJ. 2016. Pathways for insulin access to the brain: the role of the microvascular endothelial cell. *American Journal of Physiology-Heart and Circulatory Physiology.* 311(5): H1132-H1138.

ADDITIONAL PUBLICATIONS

Gray SM, Barrett EJ. 2017. "Blood brain barrier dysfunction, diabetes and dementia" in Type 2 Diabetes and Dementia edited by V. Srikanth and Z. Arvanitakis, Elsevier. In Press.

Gray SM, Thorner, MO. 2017. Spatiotemporal regulation of insulin-like growth factor-1 and its receptor in the brain: is there a role for growth hormone? *Endocrinology*. 158 (2): 229-232.

Gray SM, Meijer RI, Barrett EJ. 2014. Insulin regulates brain function, but how does it get there? *Diabetes*. 63 (12): 3992-3997.

REFERENCES

1. Brown P, Davies S, Speake T, Millar I. Molecular mechanisms of cerebrospinal fluid production. *Neuroscience*. 2004;129(4):955-968.

2. Bouldin TW, Krigman MR. Differential permeability of cerebral capillary and choroid plexus to lanthanum ion. *Brain Res*. 1975;99(2):444-448.

3. Wolburg H, Paulus W. Choroid plexus: Biology and pathology. *Acta Neuropathol*. 2010;119(1):75-88.

4. Cserr HF. Physiology of the choroid plexus. *Physiol Rev*. 1971;51(2):273-311.

5. Welch K. The principles of physiology of the cerebrospinal fluid in relation to hydrocephalus including normal pressure hydrocephalus. *Adv Neurol*. 1975;13:247-332.

6. Spector R, Keep RF, Snodgrass SR, Smith QR, Johanson CE. A balanced view of choroid plexus structure and function: Focus on adult humans. *Exp Neurol*. 2015;267:78-86.

7. Rubin RC, Henderson ES, Ommaya AK, Walker MD, Rall DP. The production of cerebrospinal fluid in man and its modification by acetazolamide. *J Neurosurg*. 1966;25(4):430-436.

8. Brinker T, Stopa E, Morrison J, Klinge P. A new look at cerebrospinal fluid circulation. *Fluids and Barriers of the CNS*. 2014;11(1):10.

9. Johanson CE, Duncan JA, Klinge PM, Brinker T, Stopa EG, Silverberg GD. Multiplicity of cerebrospinal fluid functions: New challenges in health and disease. *Cerebrospinal fluid research*. 2008;5(1):10.

10. Owler BK, Pitham T, Wang D. Aquaporins: Relevance to cerebrospinal fluid physiology and therapeutic potential in hydrocephalus. *Cerebrospinal fluid research*. 2010;7(1):15.

11. Damkier HH, Brown PD, Praetorius J. Cerebrospinal fluid secretion by the choroid plexus. *Physiol Rev*. 2013;93(4):1847-1892. doi: 10.1152/physrev.00004.2013 [doi].

12. Tietz S, Engelhardt B. Brain barriers: Crosstalk between complex tight junctions and adherens junctions. *J Cell Biol*. 2015;209(4):493-506. doi: 10.1083/jcb.201412147 [doi].

13. Carro E, Trejo JL, Gomez-Isla T, LeRoith D, Torres-Aleman I. Serum insulin-like growth factor I regulates brain amyloid-β levels. *Nat Med*. 2002;8(12):1390-1397.

14. Liddelow SA, Dzięgielewska KM, Møllgård K, et al. Cellular specificity of the blood–CSF barrier for albumin transfer across the choroid plexus epithelium. *PLoS One*. 2014;9(9):e106592.

15. Seyfert S, Ehlen F, Klostermann F. Receptor-mediated transfer of IgG and albumin at cerebrospinal fluid interfaces. *J Neural Transm*. 2015;122(9):1249-1251.

16. Deane R, Zheng W, Zlokovic BV. Brain capillary endothelium and choroid plexus epithelium regulate transport of transferrin-bound and free iron into the rat brain. *J Neurochem*. 2004;88(4):813-820.

17. Carro E, Nunez A, Busiguina S, Torres-Aleman I. Circulating insulin-like growth factor I mediates effects of exercise on the brain. *J Neurosci*. 2000;20(8):2926-2933.

18. Carro E, Spuch C, Trejo JL, Antequera D, Torres-Aleman I. Choroid plexus megalin is involved in neuroprotection by serum insulin-like growth factor I. *J Neurosci*. 2005;25(47):10884-10893. doi: 25/47/10884 [pii].

19. Devos R, Richards JG, Campfield LA, et al. OB protein binds specifically to the choroid plexus of mice and rats. *Proc Natl Acad Sci U S A*. 1996;93(11):5668-5673.

20. Zlokovic BV, Jovanovic S, Miao W, Samara S, Verma S, Farrell CL. Differential regulation of leptin transport by the choroid plexus and blood-brain barrier and high affinity transport systems for entry into hypothalamus and across the blood-cerebrospinal fluid barrier 1. *Endocrinology*. 2000;141(4):1434-1441.

21. Dietrich MO, Spuch C, Antequera D, et al. Megalin mediates the transport of leptin across the blood-CSF barrier. *Neurobiol Aging*. 2008;29(6):902-912.

22. Nishijima T, Piriz J, Duflot S, et al. Neuronal activity drives localized blood-brain-barrier transport of serum insulin-like growth factor-I into the CNS. *Neuron*. 2010;67(5):834-846.

23. Orlando RA, Rader K, Authier F, et al. Megalin is an endocytic receptor for insulin. *J Am Soc Nephrol*. 1998;9(10):1759-1766.

24. Dandy WE. Experimental hydrocephalus. *Ann Surg*. 1919;70(2):129-142.

25. Iliff JJ, Wang M, Liao Y, et al. A paravascular pathway facilitates CSF flow through the brain parenchyma and the clearance of interstitial solutes, including amyloid beta. *Sci Transl Med*. 2012;4(147):147ra111. doi: 10.1126/scitranslmed.3003748; 10.1126/scitranslmed.3003748.

26. Xie L, Kang H, Xu Q, et al. Sleep drives metabolite clearance from the adult brain. *Science*. 2013;342(6156):373-377. doi: 10.1126/science.1241224 [doi].

27. Yang L, Kress BT, Weber HJ, et al. Evaluating glymphatic pathway function utilizing clinically relevant intrathecal infusion of CSF tracer. *J Transl Med*. 2013;11(1):107. doi: 1479-5876-11-107 [pii].

28. Jessen N, Munk A, Lundgaard I, Nedergaard M. The glymphatic system: A beginner's guide. *Neurochem Res*. 2015;40(12):2583-2599.

29. Zhang ET, Inman CB, Weller RO. Interrelationships of the pia mater and the perivascular (virchow-robin) spaces in the human cerebrum. *J Anat*. 1990;170:111-123.

30. Morris AW, Carare RO, Schreiber S, Hawkes CA. The cerebrovascular basement membrane: Role in the clearance of β-amyloid and cerebral amyloid angiopathy. *Frontiers in aging neuroscience*. 2014;6:251.

31. Bakker EN, Bacskai BJ, Arbel-Ornath M, et al. Lymphatic clearance of the brain: Perivascular, paravascular and significance for neurodegenerative diseases. *Cell Mol Neurobiol*. 2016;36(2):181-194.

32. Bedussi B, van der Wel NN, de Vos J, et al. Paravascular channels, cisterns, and the subarachnoid space in the rat brain: A single compartment with preferential pathways. *J Cereb Blood Flow Metab*. 2017;37(4):1374-1385. doi: 10.1177/0271678X16655550 [doi].

33. McCaslin AF, Chen BR, Radosevich AJ, Cauli B, Hillman EM. In vivo 3D morphology of Astrocyte—Vasculature interactions in the somatosensory cortex: Implications for neurovascular coupling. *Journal of cerebral blood flow & metabolism*. 2011;31(3):795-806.

34. Crone C, Thompson AM. Comparative studies of capillary permeability in brain and muscle. *Acta Physiol Scand*. 1973;87(2):252-260. doi: 10.1111/j.1748-1716.1973.tb05388.x.

35. Crone C, Olesen S. Electrical resistance of brain microvascular endothelium. *Brain Res*. 1982;241(1):49-55.

36. Olesen S, Crone C. Electrical resistance of muscle capillary endothelium. *Biophys J*. 1983;42(1):31-41.

37. Iwamoto N, Higashi T, Furuse M. Localization of angulin-1/LSR and tricellulin at tricellular contacts of brain and retinal endothelial cells in vivo. *Cell Struct Funct*. 2014;39(1):1-8.

38. Löscher W, Potschka H. Drug resistance in brain diseases and the role of drug efflux transporters. *Nature Rev Neurosci*. 2005;6(8):591-602.

39. Miller DS, Bauer B, Hartz AM. Modulation of P-glycoprotein at the blood-brain barrier: Opportunities to improve central nervous system pharmacotherapy. *Pharmacol Rev*. 2008;60(2):196-209. doi: 10.1124/pr.107.07109 [doi].

40. Mathiisen TM, Lehre KP, Danbolt NC, Ottersen OP. The perivascular astroglial sheath provides a complete covering of the brain microvessels: An electron microscopic 3D reconstruction. *Glia*. 2010;58(9):1094-1103. doi: 10.1002/glia.20990 [doi].

41. Peppiatt CM, Howarth C, Mobbs P, Attwell D. Bidirectional control of CNS capillary diameter by pericytes. *Nature*. 2006;443(7112):700-704.

42. Hall CN, Reynell C, Gesslein B, et al. Capillary pericytes regulate cerebral blood flow in health and disease. *Nature*. 2014;508(7494):55-60.

43. Sweeney MD, Ayyadurai S, Zlokovic BV. Pericytes of the neurovascular unit: Key functions and signaling pathways. *Nat Neurosci*. 2016;19(6):771-783.

44. Hartmann DA, Underly RG, Grant RI, Watson AN, Lindner V, Shih AY. Pericyte structure and distribution in the cerebral cortex revealed by high-resolution imaging of transgenic mice. *Neurophotonics*. 2015;2(4):041402-041402.

45. Attwell D, Mishra A, Hall CN, O'Farrell FM, Dalkara T. What is a pericyte? *Journal of Cerebral Blood Flow & Metabolism*. 2016;36(2):451-455.

46. Kisler K, Nelson AR, Rege SV, et al. Pericyte degeneration leads to neurovascular uncoupling and limits oxygen supply to brain. *Nat Neurosci*. 2017.

47. Iliff JJ, Lee H, Yu M, et al. Brain-wide pathway for waste clearance captured by contrast-enhanced MRI. *J Clin Invest*. 2013;123(3):1299-1309.

48. Attwell D, Buchan AM, Charpak S, Lauritzen M, MacVicar BA, Newman EA. Glial and neuronal control of brain blood flow. *Nature*. 2010;468(7321):232-243.

49. Pellerin L, Magistretti PJ. Glutamate uptake into astrocytes stimulates aerobic glycolysis: A mechanism coupling neuronal activity to glucose utilization. *Proc Natl Acad Sci U S A*. 1994;91(22):10625-10629.

50. Lundgaard I, Li B, Xie L, et al. Direct neuronal glucose uptake heralds activity-dependent increases in cerebral metabolism. *Nature communications*. 2015;6.

51. Mächler P, Wyss MT, Elsayed M, et al. In vivo evidence for a lactate gradient from astrocytes to neurons. *Cell metabolism*. 2016;23(1):94-102.

52. Iadecola C, Nedergaard M. Glial regulation of the cerebral microvasculature. *Nat Neurosci*. 2007;10(11):1369-1376.

53. Bazargani N, Attwell D. Astrocyte calcium signaling: The third wave. *Nat Neurosci*. 2016;19(2):182-189.

54. Harada K, Kamiya T, Tsuboi T. Gliotransmitter release from astrocytes: Functional, developmental and pathological implications in the brain. *Frontiers in neuroscience*. 2016;9:499.

55. Bezzi P, Gundersen V, Galbete JL, et al. Astrocytes contain a vesicular compartment that is competent for regulated exocytosis of glutamate. *Nat Neurosci*. 2004;7(6):613-620.

56. Perea G, Araque A. Astrocytes potentiate transmitter release at single hippocampal synapses. *Science*. 2007;317(5841):1083-1086. doi: 317/5841/1083 [pii].

57. Hamilton NB, Attwell D. Do astrocytes really exocytose neurotransmitters? *Nature Reviews Neuroscience*. 2010;11(4):227-238.

58. Mulligan SJ, MacVicar BA. Calcium transients in astrocyte endfeet cause cerebrovascular constrictions. *Nature*. 2004;431(7005):195-199.

59. Grima G, Benz B, Do KQ. Glutamate-induced release of the nitric oxide precursor, arginine, from glial cells. *Eur J Neurosci*. 1997;9(11):2248-2258.

60. Coco S, Calegari F, Pravettoni E, et al. Storage and release of ATP from astrocytes in culture. *J Biol Chem*. 2003;278(2):1354-1362. doi: 10.1074/jbc.M209454200 [doi].

61. Pascual O, Casper KB, Kubera C, et al. Astrocytic purinergic signaling coordinates synaptic networks. *Science*. 2005;310(5745):113-116. doi: 310/5745/113 [pii].

62. Lovick T, Brown L, Key B. Neurovascular relationships in hippocampal slices: Physiological and anatomical studies of mechanisms underlying flow-metabolism coupling in intraparenchymal microvessels. *Neuroscience*. 1999;92(1):47-60.

63. Duvernoy HM, Risold P. The circumventricular organs: An atlas of comparative anatomy and vascularization. *Brain Res Rev*. 2007;56(1):119-147.

64. van Houten M, Posner B, Kopriwa B, Brawer J. Insulin-binding sites in the rat brain: In vivo localization to the circumventricular organs by quantitative radioautography. *Endocrinology*. 1979;105(3):666-673.

65. van Houten M, Posner BI, Kopriwa BM, Brawer JR. Insulin binding sites localized to nerve terminals in rat median eminence and arcuate nucleus. *Science*. 1980;207(4435):1081-1083.

66. van Houten M, Posner B. Specific binding and internalization of blood-borne [^{125}I]-iodoinsulin by neurons of the rat area postrema. *Endocrinology*. 1981;109(3):853-859.

67. Ciofi P, Garret M, Lapirot O, et al. Brain-endocrine interactions: A microvascular route in the mediobasal hypothalamus. *Endocrinology*. 2009;150(12):5509-5519. doi: 10.1210/en.2009-0584 [doi].

68. Ciofi P. The arcuate nucleus as a circumventricular organ in the mouse. *Neurosci Lett*. 2011;487(2):187-190. doi: 10.1016/j.neulet.2010.10.019 [doi].

69. Ambach G, Palkovits M, Szentagothai J. Blood supply of the rat hypothalamus. IV. retrochiasmatic area, median eminence, arcuate nucleus. *Acta Morphol Acad Sci Hung*. 1976;24(1-2):93-119.

70. Mullier A, Bouret SG, Prevot V, Dehouck B. Differential distribution of tight junction proteins suggests a role for tanycytes in blood-hypothalamus barrier regulation in the adult mouse brain. *J Comp Neurol*. 2010;518(7):943-962.

71. Rodriguez EM, Blazquez JL, Guerra M. The design of barriers in the hypothalamus allows the median eminence and the arcuate nucleus to enjoy private milieus: The former opens to the portal blood and the latter to the cerebrospinal fluid. *Peptides*. 2010;31(4):757-776. doi: 10.1016/j.peptides.2010.01.003 [doi].

72. Langlet F, Mullier A, Bouret SG, Prevot V, Dehouck B. Tanycyte-like cells form a blood–cerebrospinal fluid barrier in the circumventricular organs of the mouse brain. *J Comp Neurol*. 2013;521(15):3389-3405.

73. Rodríguez EM, Blázquez JL, Pastor FE, et al. Hypothalamic tanycytes: A key component of brain–endocrine interaction. *Int Rev Cytol*. 2005;247:89-164.

74. Langlet F, Levin BE, Luquet S, et al. Tanycytic VEGF-A boosts blood-hypothalamus barrier plasticity and access of metabolic signals to the arcuate nucleus in response to fasting. *Cell metabolism*. 2013;17(4):607-617.

75. Kleinridders A, Ferris HA, Cai W, Kahn CR. Insulin action in brain regulates systemic metabolism and brain function. *Diabetes*. 2014;63(7):2232-2243. doi: 10.2337/db14-0568 [doi].

76. Morton GJ, Cummings DE, Baskin DG, Barsh GS, Schwartz MW. Central nervous system control of food intake and body weight. *Nature*. 2006;443(7109):289-295. doi: 10.1038/nature05026.

77. Benedict C, Kern W, Schultes B, Born J, Hallschmid M. Differential sensitivity of men and women to anorexigenic and memory-improving effects of intranasal insulin. *J Clin Endocrinol Metab*. 2008;93(4):1339-1344. doi: 10.1210/jc.2007-2606; 10.1210/jc.2007-2606.

78. Hallschmid M, Higgs S, Thienel M, Ott V, Lehnert H. Postprandial administration of intranasal insulin intensifies satiety and reduces intake of palatable snacks in women. *Diabetes*. 2012;61(4):782-789. doi: 10.2337/db11-1390; 10.2337/db11-1390.

79. Woods SC, Lotter EC, McKay LD, Porte D,Jr. Chronic intracerebroventricular infusion of insulin reduces food intake and body weight of baboons. *Nature*. 1979;282(5738):503-505.

80. Bruning JC, Gautam D, Burks DJ, et al. Role of brain insulin receptor in control of body weight and reproduction. *Science*. 2000;289(5487):2122-2125.

81. Obici S, Feng Z, Karkanias G, Baskin DG, Rossetti L. Decreasing hypothalamic insulin receptors causes hyperphagia and insulin resistance in rats. *Nat Neurosci*. 2002;5(6):566-572.

82. Clegg DJ, Benoit SC, Reed JA, Woods SC, Dunn-Meynell A, Levin BE. Reduced anorexic effects of insulin in obesity-prone rats fed a moderate-fat diet. *Am J Physiol Regul Integr Comp Physiol*. 2005;288(4):R981-6. doi: 10.1152/ajpregu.00675.2004.

83. Clegg DJ, Gotoh K, Kemp C, et al. Consumption of a high-fat diet induces central insulin resistance independent of adiposity. *Physiol Behav*. 2011;103(1):10-16. doi: 10.1016/j.physbeh.2011.01.010; 10.1016/j.physbeh.2011.01.010.

84. Craft S, Baker LD, Montine TJ, et al. Intranasal insulin therapy for alzheimer disease and amnestic mild cognitive impairment: A pilot clinical trial. *Arch Neurol*. 2012;69(1):29-38. doi: 10.1001/archneurol.2011.233; 10.1001/archneurol.2011.233.

85. Vandal M, White PJ, Tremblay C, et al. Insulin reverses the high-fat diet-induced increase in brain abeta and improves memory in an animal model of alzheimer disease. *Diabetes*. 2014;63(12):4291-4301. doi: 10.2337/db14-0375 [doi].

86. Craft S, Claxton A, Baker LD, et al. Effects of regular and long-acting insulin on cognition and alzheimer's disease biomarkers: A pilot clinical trial. *J Alzheimer's Dis*. 2017(Preprint):1-10.

87. Schwartz MW, Woods SC, Porte D, Seeley RJ, Baskin DG. Central nervous system control of food intake. *Nature*. 2000;404(6778):661-671.

88. Williams KW, Margatho LO, Lee CE, et al. Segregation of acute leptin and insulin effects in distinct populations of arcuate proopiomelanocortin neurons. *J Neurosci*. 2010;30(7):2472-2479. doi: 10.1523/JNEUROSCI.3118-09.2010 [doi].

89. Brief DJ, Davis JD. Reduction of food intake and body weight by chronic intraventricular insulin infusion. *Brain Res Bull*. 1984;12(5):571-575.

90. Chavez M, Kaiyala K, Madden LJ, Schwartz MW, Woods SC. Intraventricular insulin and the level of maintained body weight in rats. *Behav Neurosci*. 1995;109(3):528-531.

91. Chavez M, Riedy CA, Van Dijk G, Woods SC. Central insulin and macronutrient intake in the rat. *Am J Physiol*. 1996;271(3 Pt 2):R727-31.

92. Foster L, Ames N, Emery R. Food intake and serum insulin responses to intraventricular infusions of insulin and IGF-I. *Physiol Behav*. 1991;50(4):745-749.

93. Arase K, Fisler JS, Shargill NS, York DA, Bray GA. Intracerebroventricular infusions of 3-OHB and insulin in a rat model of dietary obesity. *Am J Physiol*. 1988;255(6 Pt 2):R974-81.

94. Begg DP, Mul JD, Liu M, et al. Reversal of diet-induced obesity increases insulin transport into cerebrospinal fluid and restores sensitivity to the anorexic action of central

insulin in male rats. *Endocrinology*. 2013;154(3):1047-1054. doi: 10.1210/en.2012-1929; 10.1210/en.2012-1929.

95. Ikeda H, West DB, Pustek JJ, et al. Intraventricular insulin reduces food intake and body weight of lean but not obese zucker rats. *Appetite*. 1986;7(4):381-386.

96. Ramnanan CJ, Edgerton DS, Cherrington AD. Evidence against a physiologic role for acute changes in CNS insulin action in the rapid regulation of hepatic glucose production. *Cell metabolism*. 2012;15(5):656-664.

97. Heni M, Kullmann S, Preissl H, Fritsche A, Häring H. Impaired insulin action in the human brain: Causes and metabolic consequences. *Nature reviews Endocrinology*. 2015.

98. Pocai A, Lam TK, Gutierrez-Juarez R, et al. Hypothalamic KATP channels control hepatic glucose production. *Nature*. 2005;434(7036):1026-1031.

99. Obici S, Zhang BB, Karkanias G, Rossetti L. Hypothalamic insulin signaling is required for inhibition of glucose production. *Nat Med*. 2002;8(12):1376-1382.

100. Lin HV, Plum L, Ono H, et al. Divergent regulation of energy expenditure and hepatic glucose production by insulin receptor in agouti-related protein and POMC neurons. *Diabetes*. 2010;59(2):337-346. doi: 10.2337/db09-1303 [doi].

101. Edgerton DS, Lautz M, Scott M, et al. Insulin's direct effects on the liver dominate the control of hepatic glucose production. *J Clin Invest*. 2006;116(2):521-527. doi: 10.1172/JCI27073 [doi].

102. Ramnanan CJ, Saraswathi V, Smith MS, et al. Brain insulin action augments hepatic glycogen synthesis without suppressing glucose production or gluconeogenesis in dogs. *J Clin Invest*. 2011;121(9).

103. Ramnanan CJ, Kraft G, Smith MS, et al. Interaction between the central and peripheral effects of insulin in controlling hepatic glucose metabolism in the conscious dog. *Diabetes*. 2013;62(1):74-84. doi: 10.2337/db12-0148 [doi].

104. Lochhead JJ, Thorne RG. Intranasal delivery of biologics to the central nervous system. *Adv Drug Deliv Rev*. 2012;64(7):614-628.

105. Heni M, Kullmann S, Ketterer C, et al. Nasal insulin changes peripheral insulin sensitivity simultaneously with altered activity in homeostatic and reward-related human brain regions. *Diabetologia*. 2012;55(6):1773-1782.

106. Heni M, Wagner R, Kullmann S, et al. Hypothalamic and striatal insulin action suppresses endogenous glucose production and may stimulate glucose uptake during hyperinsulinemia in lean but not in overweight men. *Diabetes*. 2017. doi: db161380 [pii].

107. Heni M, Wagner R, Kullmann S, et al. Central insulin administration improves whole-body insulin sensitivity via hypothalamus and parasympathetic outputs in men. *Diabetes*. 2014;63(12):4083-4088. doi: 10.2337/db14-0477 [doi].

108. Dash S, Xiao C, Morgantini C, Koulajian K, Lewis GF. Intranasal insulin suppresses endogenous glucose production in humans compared with placebo in the presence of

similar venous insulin concentrations. *Diabetes*. 2015;64(3):766-774. doi: 10.2337/db14-0685 [doi].

109. Gancheva S, Koliaki C, Bierwagen A, et al. Effects of intranasal insulin on hepatic fat accumulation and energy metabolism in humans. *Diabetes*. 2015;64(6):1966-1975. doi: 10.2337/db14-0892 [doi].

110. Ott A, Stolk RP, Hofman A, van Harskamp F, Grobbee DE, Breteler MM. Association of diabetes mellitus and dementia: The rotterdam study. *Diabetologia*. 1996;39(11):1392-1397.

111. Willette AA, Xu G, Johnson SC, et al. Insulin resistance, brain atrophy, and cognitive performance in late middle-aged adults. *Diabetes Care*. 2013;36(2):443-449. doi: 10.2337/dc12-0922; 10.2337/dc12-0922.

112. Chatterjee S, Peters SA, Woodward M, et al. Type 2 diabetes as a risk factor for dementia in women compared with men: A pooled analysis of 2.3 million people comprising more than 100,000 cases of dementia. *Diabetes Care*. 2016;39(2):300-307. doi: 10.2337/dc15-1588 [doi].

113. Novak V, Milberg W, Hao Y, et al. Enhancement of vasoreactivity and cognition by intranasal insulin in type 2 diabetes. *Diabetes Care*. 2014;37(3):751-759. doi: 10.2337/dc13-1672; 10.2337/dc13-1672.

114. Talbot K, Wang HY, Kazi H, et al. Demonstrated brain insulin resistance in alzheimer's disease patients is associated with IGF-1 resistance, IRS-1 dysregulation, and

cognitive decline. *J Clin Invest*. 2012;122(4):1316-1338. doi: 10.1172/JCI59903; 10.1172/JCI59903.

115. Arnold SE, Lucki I, Brookshire BR, et al. High fat diet produces brain insulin resistance, synaptodendritic abnormalities and altered behavior in mice. *Neurobiol Dis*. 2014;67:79-87.

116. Stranahan AM, Norman ED, Lee K, et al. Diet-induced insulin resistance impairs hippocampal synaptic plasticity and cognition in middle-aged rats. *Hippocampus*. 2008;18(11):1085-1088.

117. Sutherland GT, Lim J, Srikanth V, Bruce DG. Epidemiological approaches to understanding the link between type 2 diabetes and dementia. *J Alzheimer's Dis*. 2017(Preprint):-1-11.

118. Havrankova J, Schmechel D, Roth J, Brownstein M. Identification of insulin in rat brain. *Proc Natl Acad Sci U S A*. 1978;75(11):5737-5741.

119. Baskin DG, Stein LJ, Ikeda H, et al. Genetically obese zucker rats have abnormally low brain insulin content. *Life Sci*. 1985;36(7):627-633.

120. Banks WA. The source of cerebral insulin. *Eur J Pharmacol*. 2004;490(1):5-12.

121. Molnar G, Farago N, Kocsis AK, et al. GABAergic neurogliaform cells represent local sources of insulin in the cerebral cortex. *J Neurosci*. 2014;34(4):1133-1137. doi: 10.1523/JNEUROSCI.4082-13.2014 [doi].

122. Aird WC. Phenotypic heterogeneity of the endothelium. *Circ Res*. 2007;100(2):158--173.

123. Mayor S, Pagano RE. Pathways of clathrin-independent endocytosis. *Nature reviews Molecular cell biology*. 2007;8(8):603-612.

124. Johannes L, Parton RG, Bassereau P, Mayor S. Building endocytic pits without clathrin. *Nature Reviews Molecular Cell Biology*. 2015;16(5):311-321.

125. Kirchhausen T, Owen D, Harrison SC. Molecular structure, function, and dynamics of clathrin-mediated membrane traffic. *Cold Spring Harb Perspect Biol*. 2014;6(5):a016725. doi: 10.1101/cshperspect.a016725 [doi].

126. Maib H, Smythe E, Ayscough K. Forty years on: Clathrin-coated pits continue to fascinate. *Mol Biol Cell*. 2017;28(7):843-847. doi: 10.1091/mbc.E16-04-0213 [doi].

127. Predescu SA, Predescu DN, Malik AB. Molecular determinants of endothelial transcytosis and their role in endothelial permeability. *Am J Physiol Lung Cell Mol Physiol*. 2007;293(4):L823-42. doi: 00436.2006 [pii].

128. Chen Z, Bakhshi FR, Shajahan AN, et al. Nitric oxide-dependent src activation and resultant caveolin-1 phosphorylation promote eNOS/caveolin-1 binding and eNOS inhibition. *Mol Biol Cell*. 2012;23(7):1388-1398. doi: 10.1091/mbc.E11-09-0811 [doi].

129. Oh P, McIntosh DP, Schnitzer JE. Dynamin at the neck of caveolae mediates their budding to form transport vesicles by GTP-driven fission from the plasma membrane of endothelium. *J Cell Biol*. 1998;141(1):101-114.

130. Shaul PW, Smart EJ, Robinson LJ, et al. Acylation targets emdothelial nitric-oxide synthase to plasmalemmal caveolae. *J Biol Chem*. 1996;271(11):6518-6522.

131. Wang H, Wang AX, Liu Z, Chai W, Barrett EJ. The trafficking/interaction of eNOS and caveolin-1 induced by insulin modulates endothelial nitric oxide production. *Mol Endocrinol*. 2009;23(10):1613-1623. doi: 10.1210/me.2009-0115; 10.1210/me.2009-0115.

132. Wang H, Wang AX, Barrett EJ. Caveolin-1 is required for vascular endothelial insulin uptake. *Am J Physiol Endocrinol Metab*. 2011;300(1):E134-44. doi: 10.1152/ajpendo.00498.2010; 10.1152/ajpendo.00498.2010.

133. Dutta D, Donaldson JG. Search for inhibitors of endocytosis: Intended specificity and unintended consequences. *Cellular logistics*. 2012;2(4):203-208.

134. Schubert W, Frank PG, Razani B, Park DS, Chow CW, Lisanti MP. Caveolae-deficient endothelial cells show defects in the uptake and transport of albumin in vivo. *J Biol Chem*. 2001;276(52):48619-48622. doi: 10.1074/jbc.C100613200 [doi].

135. Razani B, Engelman JA, Wang XB, et al. Caveolin-1 null mice are viable but show evidence of hyperproliferative and vascular abnormalities. *J Biol Chem*. 2001;276(41):38121-38138. doi: 10.1074/jbc.M105408200 [doi].

136. Yang YJ, Hope ID, Ader M, Bergman RN. Insulin transport across capillaries is rate limiting for insulin action in dogs. *J Clin Invest*. 1989;84(5):1620-1628. doi: 10.1172/JCI114339.

137. Barrett EJ, Wang H, Upchurch CT, Liu Z. Insulin regulates its own delivery to skeletal muscle by feed-forward actions on the vasculature. *Am J Physiol Endocrinol Metab*. 2011;301(2):E252-63. doi: 10.1152/ajpendo.00186.2011; 10.1152/ajpendo.00186.2011.

138. Majumdar S, Genders AJ, Inyard AC, Frison V, Barrett EJ. Insulin entry into muscle involves a saturable process in the vascular endothelium. *Diabetologia*. 2012;55(2):450-456. doi: 10.1007/s00125-011-2343-x; 10.1007/s00125-011-2343-x.

139. King GL, Johnson SM. Receptor-mediated transport of insulin across endothelial cells. *Science*. 1985;227:1583-1587.

140. Genders AJ, Frison V, Abramson SR, Barrett EJ. Endothelial cells actively concentrate insulin during its transendothelial transport. *Microcirculation*. 2013;20(5):434-439. doi: 10.1111/micc.12044; 10.1111/micc.12044.

141. Zeng G, Nystrom FH, Ravichandran LV, et al. Roles for insulin receptor, PI3-kinase, and akt in insulin-signaling pathways related to production of nitric oxide in human vascular endothelial cells. *Circulation*. 2000;101(13):1539-1545.

142. Wang H, Wang AX, Liu Z, Barrett EJ. Insulin signaling stimulates insulin transport by bovine aortic endothelial cells. *Diabetes*. 2008;57(3):540-547. doi: 10.2337/db07-0967.

143. Wang H, Wang AX, Aylor K, Barrett EJ. Nitric oxide directly promotes vascular endothelial insulin transport. *Diabetes*. 2013;62(12):4030-4042. doi: 10.2337/db13-0627; 10.2337/db13-0627.

144. Wang H, Wang AX, Aylor K, Barrett EJ. Caveolin-1 phosphorylation is required for vascular endothelial insulin uptake and impaired by insulin resistance. *Under review*. 2013.

145. Kubota T, Kubota N, Kumagai H, et al. Impaired insulin signaling in endothelial cells reduces insulin-induced glucose uptake by skeletal muscle. *Cell metabolism*. 2011;13(3):294-307.

146. Azizi PM, Zyla RE, Guan S, et al. Clathrin-dependent entry and vesicle-mediated exocytosis define insulin transcytosis across microvascular endothelial cells. *Mol Biol Cell*. 2015;26(4):740-750. doi: 10.1091/mbc.E14-08-1307 [doi].

147. Margolis RU, Altszuler N. Insulin in the cerebrospinal fluid. *Nature*. 1967;215:1375-1376.

148. Baura GD, Foster DM, Porte D,Jr, et al. Saturable transport of insulin from plasma into the central nervous system of dogs in vivo. A mechanism for regulated insulin delivery to the brain. *J Clin Invest*. 1993;92(4):1824-1830. doi: 10.1172/JCI116773.

149. Heni M, Schopfer P, Peter A, et al. Evidence for altered transport of insulin across the blood-brain barrier in insulin-resistant humans. *Acta Diabetol*. 2013. doi: 10.1007/s00592-013-0546-y.

150. Kern W, Benedict C, Schultes B, et al. Low cerebrospinal fluid insulin levels in obese humans. *Diabetologia*. 2006;49(11):2790-2792. doi: 10.1007/s00125-006-0409-y.

151. Schwartz MW, Sipols A, Kahn SE, et al. Kinetics and specificity of insulin uptake from plasma into cerebrospinal fluid. *Am J Physiol*. 1990;259(3 Pt 1):E378-83.

152. Wallum B, Taborsky Jr G, Porte Jr D, et al. Cerebrospinal fluid insulin levels increase during intravenous insulin infusions in man. *The Journal of Clinical Endocrinology & Metabolism*. 1987;64(1):190-194.

153. Schwartz MW, Bergman RN, Kahn SE, et al. Evidence for entry of plasma insulin into cerebrospinal fluid through an intermediate compartment in dogs. quantitative aspects and implications for transport. *J Clin Invest*. 1991;88(4):1272-1281. doi: 10.1172/JCI115431.

154. Miller DW, Keller BT, Borchardt RT. Identification and distribution of insulin receptors on cultured bovine brain microvessel endothelial cells: Possible function in insulin processing in the blood–brain barrier. *J Cell Physiol*. 1994;161(2):333-341.

155. Sato H, Tsuji A, Hirai K, Kang YS. Application of HPLC in disposition study of A14-125I-labeled insulin in mice. *Diabetes*. 1990;39(5):563-569.

156. Pardridge WM, Eisenberg J, Yang J. Human blood-brain barrier insulin receptor. *J Neurochem*. 1985;44(6):1771-1778.

157. Frank HJ, Pardridge WM, Morris WL, Rosenfeld RG, Choi TB. Binding and internalization of insulin and insulin-like growth factors by isolated brain microvessels. *Diabetes*. 1986;35(6):654-661.

158. Duffy KR, Pardridge WM. Blood-brain barrier transcytosis of insulin in developing rabbits. *Brain Res*. 1987;420(1):32-38.

159. Banks WA, Kastin AJ. Differential permeability of the blood–brain barrier to two pancreatic peptides: Insulin and amylin. *Peptides*. 1998;19(5):883-889.

160. Huber JD, Egleton RD, Davis TP. Molecular physiology and pathophysiology of tight junctions in the blood–brain barrier. *Trends Neurosci*. 2001;24(12):719-725.

161. Bouchard P, Ghitescu L, Bendayan M. Morpho-functional studies of the blood-brain barrier in streptozotocin-induced diabetic rats. *Diabetologia*. 2002;45(7):1017-1025.

162. Dai J, Vrensen GF, Schlingemann RO. Blood–brain barrier integrity is unaltered in human brain cortex with diabetes mellitus. *Brain Res*. 2002;954(2):311-316.

163. Kanoski SE, Zhang Y, Zheng W, Davidson TL. The effects of a high-energy diet on hippocampal function and blood-brain barrier integrity in the rat. *J Alzheimer's Dis*. 2010;21(1):207-219.

164. Katakam PV, Snipes JA, Steed MM, Busija DW. Insulin-induced generation of reactive oxygen species and uncoupling of nitric oxide synthase underlie the cerebrovascular insulin resistance in obese rats. *Journal of Cerebral Blood Flow & Metabolism*. 2012;32(5):792-804.

165. Pistell PJ, Morrison CD, Gupta S, et al. Cognitive impairment following high fat diet consumption is associated with brain inflammation. *J Neuroimmunol*. 2010;219(1):25-32.

166. Thaler JP, Yi CX, Schur EA, et al. Obesity is associated with hypothalamic injury in rodents and humans. *J Clin Invest*. 2012;122(1):153-162. doi: 10.1172/JCI59660 [doi].

167. Guyenet SJ, Nguyen HT, Hwang BH, Schwartz MW, Baskin DG, Thaler JP. High-fat diet feeding causes rapid, non-apoptotic cleavage of caspase-3 in astrocytes. *Brain Res*. 2013;1512:97-105.

168. Li W, Prakash R, Chawla D, et al. Early effects of high-fat diet on neurovascular function and focal ischemic brain injury. *Am J Physiol Regul Integr Comp Physiol*. 2013;304(11):R1001-8. doi: 10.1152/ajpregu.00523.2012 [doi].

169. Chowen JA, Argente J, Horvath TL. Uncovering novel roles of nonneuronal cells in body weight homeostasis and obesity. *Endocrinology*. 2013;154(9):3001-3007.

170. García-Cáceres C, Quarta C, Varela L, et al. Astrocytic insulin signaling couples brain glucose uptake with nutrient availability. *Cell*. 2016;166(4):867-880.

171. Fernandez AM, Hernandez-Garzón E, Perez-Domper P, et al. Insulin regulates astrocytic glucose handling through cooperation with insulin-like growth factor I. *Diabetes*. 2017;66:64-74. doi: http://dx.doi.org/10.2337/db16-0861.

172. Burek M, Salvador E, Forster CY. Generation of an immortalized murine brain microvascular endothelial cell line as an in vitro blood brain barrier model. *J Vis Exp*. 2012;66:e4022. doi: 10.3791/4022.

173. Perriere N, Demeuse P, Garcia E, et al. Puromycin-based purification of rat brain capillary endothelial cell cultures. effect on the expression of blood-brain barrier-specific properties. *J Neurochem*. 2005;93(2):279-289. doi: 10.1111/j.1471-4159.2004.03020.x.

174. Catravas JD, Snead C, Dimitropoulou C, et al. Harvesting, identification and barrier function of human lung microvascular endothelial cells. *Vascular pharmacology*. 2010;52(5):175-181.

175. Bernas MJ, Cardoso FL, Daley SK, et al. Establishment of primary cultures of human brain microvascular endothelial cells to provide an in vitro cellular model of the blood-brain barrier. *Nature protocols*. 2010;5(7):1265-1272.

176. Schildge S, Bohrer C, Beck K, Schachtrup C. Isolation and culture of mouse cortical astrocytes. *J Vis Exp*. 2013;71:e50079. doi: 10.3791/50079.

177. Meijer RI, Gray SM, Aylor KW, Barrett EJ. Pathways for insulin access to the brain: The role of the microvascular endothelial cell. *Am J Physiol Heart Circ Physiol*. 2016;311(5):H1132-H1138. doi: 10.1152/ajpheart.00081.2016 [doi].

178. Deli M. Blood–brain barrier models. In: Lajtha A, Reith MEA, eds. *Handbook of neurochemistry and molecular neurobiology: Neural membranes and transport.* 3rd ed. New York: Springer; 2007:29-55.

179. Wuest DM, Wing AM, Lee KH. Membrane configuration optimization for a murine in vitro blood–brain barrier model. *J Neurosci Methods*. 2013;212(2):211-221.

180. Molino Y, Jabès F, Lacassagne E, Gaudin N, Khrestchatisky M. Setting-up an in vitro model of rat blood-brain barrier (BBB): A focus on BBB impermeability and receptor-mediated transport. *J Vis Exp*. 2014;88:e51278-e51278.

181. Keller S, Schmid C, Zapf J, Froesch ER. Inhibition of insulin degradation by insulin-like growth factors I and II in human hepatoma (HepG2) cells. *Acta Endocrinol (Copenh)*. 1989;121(2):279-285.

182. Schrijvers EM, Witteman JC, Sijbrands EJ, Hofman A, Koudstaal PJ, Breteler MM. Insulin metabolism and the risk of alzheimer disease: The rotterdam study. *Neurology*. 2010;75(22):1982-1987. doi: 10.1212/WNL.0b013e3181ffe4f6; 10.1212/WNL.0b013e3181ffe4f6.

183. van Houten M, Posner BI. Insulin binds to brain blood vessels in vivo. *Nature*. 1979;282:623-625.

184. Lynch JA, George AM, Eisenhauer PB, et al. Insulin degrading enzyme is localized predominantly at the cell surface of polarized and unpolarized human cerebrovascular endothelial cell cultures. *J Neurosci Res*. 2006;83(7):1262-1270.

185. Miners JS, Kehoe PG, Love S. Immunocapture-based fluorometric assay for the measurement of insulin-degrading enzyme activity in brain tissue homogenates. *J Neurosci Methods*. 2008;169(1):177-181.

186. Porte D. Central regulation of energy homeostasis. *Diabetes*. 2006;55(Supplement 2):S155-S160.

187. Zhao L, Fu Z, Wu J, et al. Inflammation-induced microvascular insulin resistance is an early event in diet-induced obesity. *Clin Sci (Lond)*. 2015;129(12):1025-1036. doi: 10.1042/CS20150143 [doi].

188. Kuo WL, Montag AG, Rosner MR. Insulin-degrading enzyme is differentially expressed and developmentally regulated in various rat tissues. *Endocrinology*. 1993;132(2):604-611. doi: 10.1210/endo.132.2.7678795 [doi].

189. Koehler RC, Gebremedhin D, Harder DR. Role of astrocytes in cerebrovascular regulation. *J Appl Physiol*. 2006;100(1):307-317.

190. Li G, Barrett EJ, Wang H, Chai W, Liu Z. Insulin at physiological concentrations selectively activates insulin but not insulin-like growth factor I (IGF-I) or insulin/IGF-I hybrid receptors in endothelial cells. *Endocrinology*. 2005;146(11):4690-4696.

191. Dehouck B, Fenart L, Dehouck MP, Pierce A, Torpier G, Cecchelli R. A new function for the LDL receptor: Transcytosis of LDL across the blood-brain barrier. *J Cell Biol*. 1997;138(4):877-889.

192. Hu S, Sheng WS, Ehrlich LC, Peterson PK, Chao CC. Cytokine effects on glutamate uptake by human astrocytes. *Neuroimmunomodulation*. 2000;7(3):153-159. doi: 26433 [pii].

193. Munive V, Santi A, Torres-Aleman I. A concerted action of estradiol and insulin like growth factor I underlies sex differences in mood regulation by exercise. *Sci Rep*. 2016;6:25969. doi: 10.1038/srep25969 [doi].

194. Trueba-Saiz Á, Fernandez AM, Nishijima T, et al. Circulating insulin-like growth factor I regulates its receptor in the brain of male mice. *Endocrinology*. 2016:en. 2016-1468.

195. Shen Z, Lu Z, Chhatbar PY, O'herron P, Kara P. An artery-specific fluorescent dye for studying neurovascular coupling. *Nature methods*. 2012;9(3):273-276.

196. Zeng G, Quon MJ. Insulin-stimulated production of nitric oxide is inhibited by wortmannin. direct measurement in vascular endothelial cells. *J Clin Invest*. 1996;98(4):894-898. doi: 10.1172/JCI118871 [doi].

197. Dimmeler S, Fleming I, Fisslthaler B, Hermann C, Busse R, Zeiher AM. Activation of nitric oxide synthase in endothelial cells by akt-dependent phosphorylation. *Nature*. 1999;399(6736):601-605.

198. Kim F, Pham M, Maloney E, et al. Vascular inflammation, insulin resistance, and reduced nitric oxide production precede the onset of peripheral insulin resistance.

Arterioscler Thromb Vasc Biol. 2008;28(11):1982-1988. doi: 10.1161/ATVBAHA.108.169722 [doi].

199. Li H, Brodsky S, Basco M, Romanov V, De Angelis DA, Goligorsky MS. Nitric oxide attenuates signal transduction: Possible role in dissociating caveolin-1 scaffold. *Circ Res*. 2001;88(2):229-236.

200. Nguyen LN, Ma D, Shui G, et al. Mfsd2a is a transporter for the essential omega-3 fatty acid docosahexaenoic acid. *Nature*. 2014;509(7501):503-506.

201. Quek DQ, Nguyen LN, Fan H, Silver DL. Structural insights into the transport mechanism of the human sodium-dependent lysophosphatidylcholine transporter MFSD2A. *J Biol Chem*. 2016;291(18):9383-9394. doi: 10.1074/jbc.M116.721035 [doi].

202. Andreone BJ, Chow BW, Tata A, et al. Blood-brain barrier permeability is regulated by lipid transport-dependent suppression of caveolae-mediated transcytosis. *Neuron*. 2017.

203. Ben-Zvi A, Lacoste B, Kur E, et al. Mfsd2a is critical for the formation and function of the blood-brain barrier. *Nature*. 2014;509(7501):507-511.

204. Clandinin MT, Cheema S, Field CJ, Garg ML, Venkatraman J, Clandinin TR. Dietary fat: Exogenous determination of membrane structure and cell function. *FASEB J*. 1991;5(13):2761-2769.

205. Duckworth WC, Bennett RG, Hamel FG. Insulin degradation: Progress and potential 1. *Endocr Rev*. 1998;19(5):608-624.

206. Tang W. Targeting insulin-degrading enzyme to treat type 2 diabetes mellitus. *Trends in Endocrinology & Metabolism*. 2016;27(1):24-34.

207. Farris W, Mansourian S, Chang Y, et al. Insulin-degrading enzyme regulates the levels of insulin, amyloid beta-protein, and the beta-amyloid precursor protein intracellular domain in vivo. *Proc Natl Acad Sci U S A*. 2003;100(7):4162-4167. doi: 10.1073/pnas.0230450100 [doi].

208. Gao W, Eisenhauer PB, Conn K, et al. Insulin degrading enzyme is expressed in the human cerebrovascular endothelium and in cultured human cerebrovascular endothelial cells. *Neurosci Lett*. 2004;371(1):6-11.

209. Zhao J, Li L, Leissring MA. Insulin-degrading enzyme is exported via an unconventional protein secretion pathway. *Molecular neurodegeneration*. 2009;4(1):4.

210. Son SM, Kang S, Choi H, Mook-Jung I. Statins induce insulin-degrading enzyme secretion from astrocytes via an autophagy-based unconventional secretory pathway. *Molecular neurodegeneration*. 2015;10(1):56.

211. Qiu WQ, Walsh DM, Ye Z, et al. Insulin-degrading enzyme regulates extracellular levels of amyloid beta-protein by degradation. *J Biol Chem*. 1998;273(49):32730-32738.

212. Cannon RE, Peart JC, Hawkins BT, Campos CR, Miller DS. Targeting blood-brain barrier sphingolipid signaling reduces basal P-glycoprotein activity and improves drug delivery to the brain. *Proc Natl Acad Sci U S A*. 2012;109(39):15930-15935. doi: 1203534109 [pii].